

FINAL REPORT

**ACQUISITION OF SH-WAVE SEISMIC REFLECTION AND
REFRACTION DATA IN THE AREA OF THE NORTHEASTWARD
TRENDING CONTAMINANT PLUME AT THE PGDP**

**Christina Langston
Research Assistant**

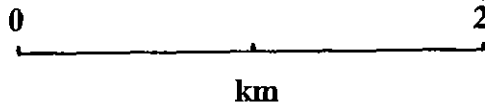
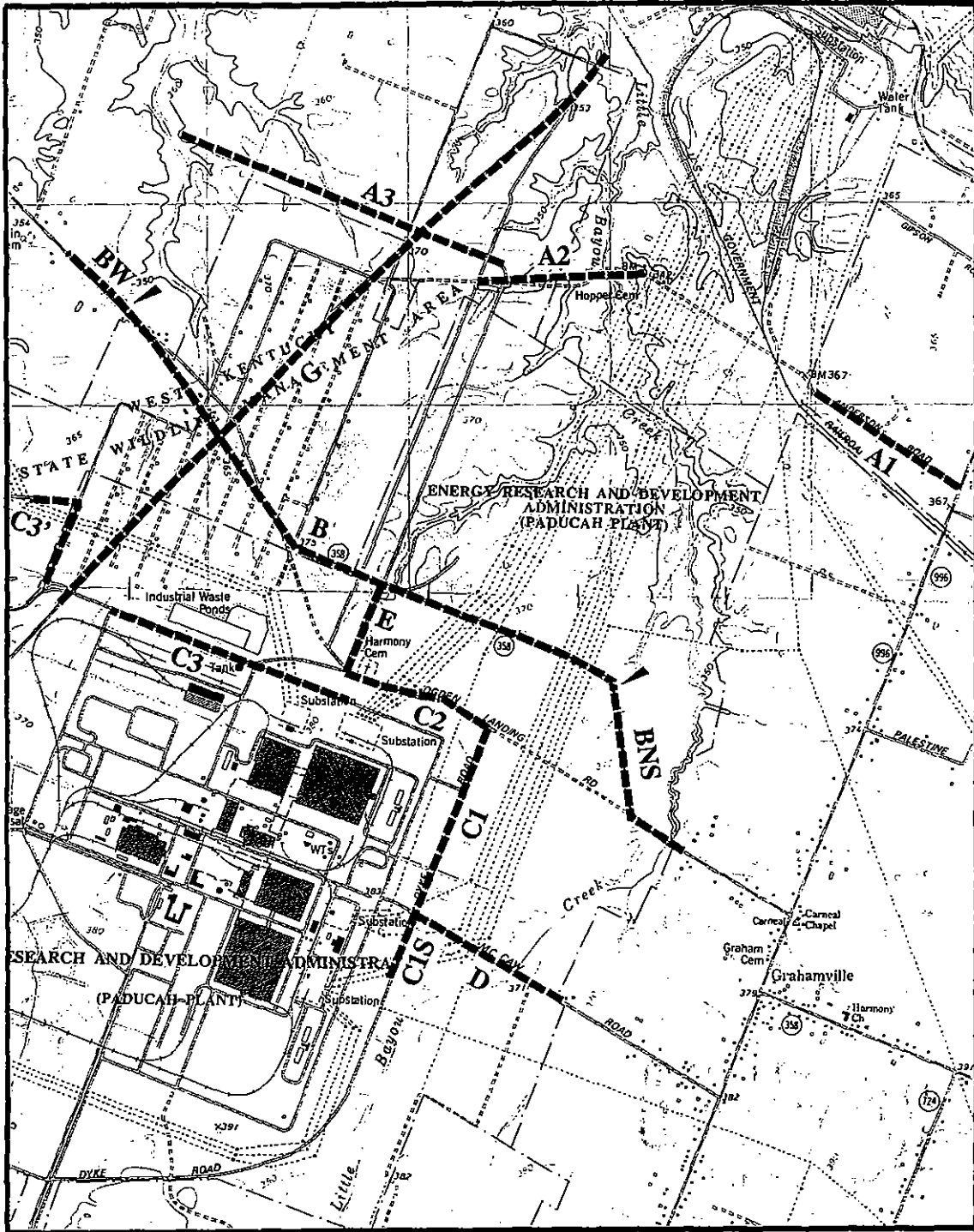
**Ron Street
Principal Investigator
Department of Geological Sciences
University of Kentucky
Lexington, KY 40506**

**Telephone: (606) 257-4777
FAX: (606) 323-1938
email: geo151@ukcc.uky.edu**

RECEIVED
DEC 28 1999

**DIVISION OF WASTE MANAGEMENT
SOLID WASTE BRANCH**

July 31, 1998



CONTENTS

	<u>Page</u>
1.0 INTRODUCTION	1
1.1 BACKGROUND	1
1.2 OBJECTIVES	2
2.0 REGIONAL GEOLOGY	3
2.1 STRATIGRAPHY	3
2.2 DEPOSITIONAL HISTORY	6
2.3 STRUCTURAL FRAMEWORK	9
3.0 SEISMIC DATA ACQUISITION AND PROCESSING	10
4.0 RESULTS	15
4.1 IDENTIFICATION OF REFLECTORS	15
4.2 GENERAL FEATURES	17
4.3 SPECIFIC FEATURES	18
4.3.1 LINE A1	18
4.3.2 LINE A2	19
4.3.3 LINE A3	19
4.3.4 LINE B	20
4.3.5 LINE BNS	22
4.3.6 LINE C1	23
4.3.7 LINE C1S	24
4.3.8 LINE C2	25
4.3.9 LINE C3	26
4.3.10 LINE C3'	27
4.3.11 LINE D	28

4.3.12 LINE E	29
4.3.13 LINE G	30
4.4 CORRELATION OF OBSERVED FEATURES	31
4.5 OTHER FEATURES	32
5.0 SUMMARY	33
REFERENCES	34
TABLE 1 DATA PROCESSING STEPS	12
APPENDICES	
A UNINTERPRETED AND INTERPRETED SEISMIC SECTIONS	
B PROCESSING PROCEDURES, LINES A1-G	
C VELOCITY PICKS, LINES A1-G	
D OPTIMUM OFFSET LINES	
E SOIL BORING LOGS	
F GLOSSARY OF GEOPHYSICAL TERMS	

1.0 INTRODUCTION

The Paducah Gaseous Diffusion Plant (PGDP), a Department of Energy (DOE) facility, is located in the Jackson Purchase area of western Kentucky (Fig. 1). Constructed in 1952, the plant produces uranium enriched in the uranium isotope ^{235}U for nuclear reactors. Procedures involved in everyday plant operations generate wastes and contaminants. Among these are TCE (trichloroethylene) and Tc-99 (technetium-99 isotope). TCE is used at the PGDP as a cleaning agent, while Tc-99 is a byproduct of the reprocessing of nuclear power reactor tails (Clausen et al., 1992).

1.1 BACKGROUND

In 1988, TCE and Tc-99 were discovered in several private wells about 1 mile north of PGDP (Clausen et al., 1992). The source of these contaminants has been linked to the PGDP. These findings led to the initiation of numerous projects designed to characterize the site geology, hydrogeology, and groundwater flow characteristics near the PGDP. Tests showed that two contaminant plumes were emanating from within PGDP. The plumes were found to be traveling through the shallowest aquifer near the PGDP, the regional gravel aquifer (RGA), located at depths ranging from 9 to 25 m. Groundwater flow directions within the RGA are to the north, toward the Ohio River (Clausen et al., 1992). However, the plumes were found to be migrating to the northeast, suggesting that other factors may be involved in the plumes' direction of propagation. J. Drahovzal (pers.

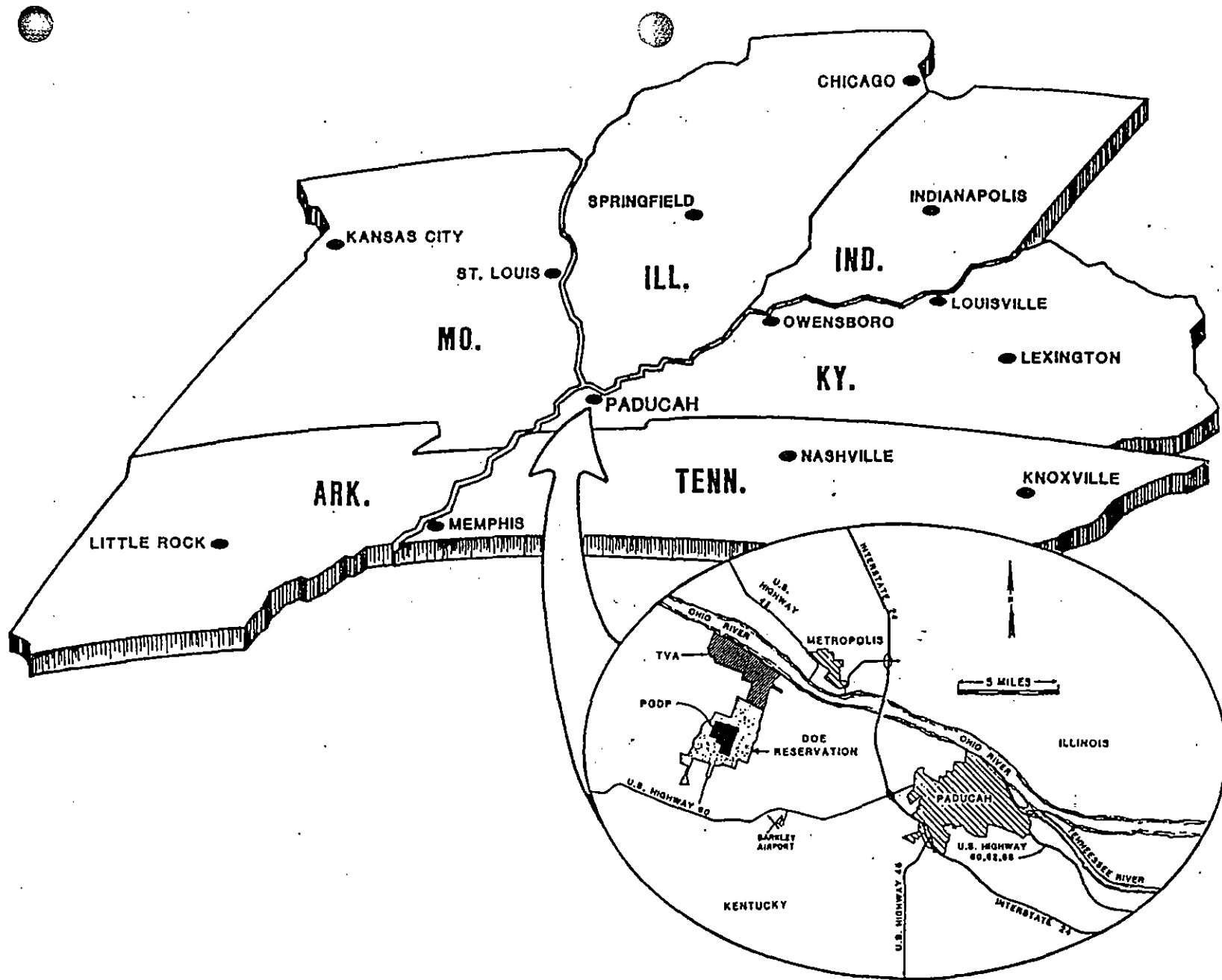


Figure 1. Regional map showing location of PGDP (from Clausen et al., 1992).

comm., 1997) proposed that the migration of the contaminant plumes might be controlled by local geologic structure. A pilot investigation was undertaken to determine data acquisition parameters to be used. Preliminary results indicated the presence of two fault zones near the northwest corner of the plant.

1.2 OBJECTIVES

There were two main objectives of the study. The first was to seismically image the RGA, the top of the Clayton and McNairy Formations, and the top of the limestone bedrock in the area of the contaminant plumes. The second objective was to find evidence of faulting or other aspects of the subsurface that could be controlling migration of the contaminant plumes. The presence of contaminants and their continuing migration indicates a strong need for specific knowledge of the shallow subsurface structure in the vicinity of the PGDP.

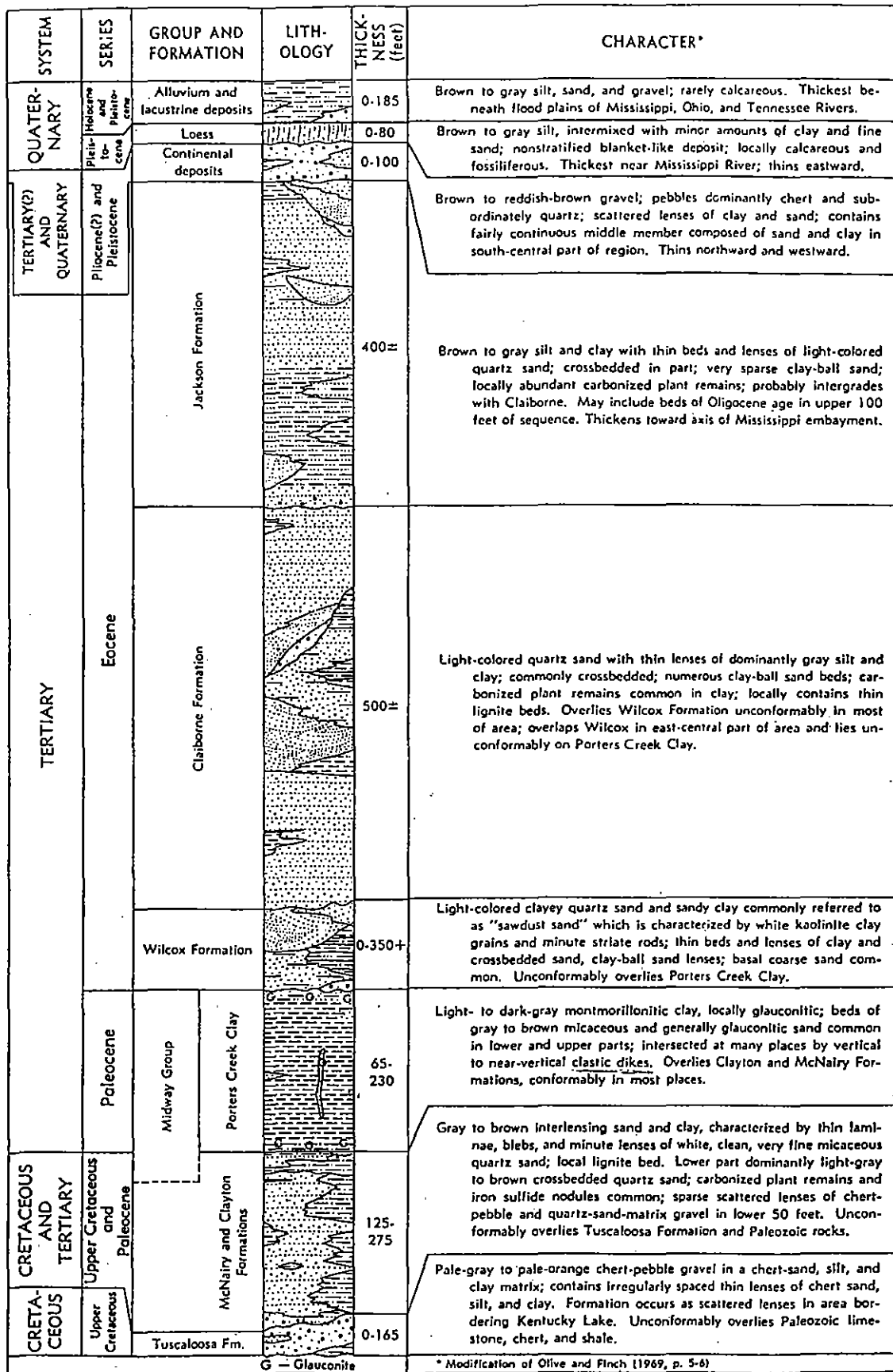
Based on Harris' (1992) study in the area surrounding PGDP, the need to use a nondestructive energy source in the wildlife area surrounding the PGDP, and field tests involving a weight drop for P-waves and a seismic hammer for SH-waves, it was decided that the best results could be achieved by acquiring high-resolution, SH-wave seismic CDP data using a seismic hammer. Results from the field tests were also used to determine the optimum acquisition geometry.

2.0 REGIONAL GEOLOGY

2.1 STRATIGRAPHY

The Jackson Purchase Region of Kentucky is located in the northernmost part of the Mississippi Embayment of the Gulf Coastal Plain Province and encompasses a 2,356-square-mile, eight-county area (Schwalb, 1969). The history of the embayment began in Cambrian time subsequent to the formation of the Reelfoot Rift to the south and the Rough Creek Graben to the east. Paleozoic rocks ranging from Cambrian to Mississippian in age are buried beneath Mesozoic and younger sediments, except on the eastern margin of the embayment, where Mississippian and Devonian strata crop out (Schwalb, 1969).

Cretaceous and younger rocks lie unconformably on this Paleozoic bedrock. A generalized stratigraphic column of the post-Paleozoic stratigraphy of the Jackson Purchase is shown in Figure 2. The oldest post-Paleozoic formation in the Jackson Purchase is the Upper Cretaceous Tuscaloosa Formation. A distinctive unit, this formation is composed of chert and well-rounded or broken chert gravel (Hansen, 1966). The Tuscaloosa is present over a relatively large area. In Kentucky, the formation is age-equivalent to rocks that overlie the Tuscaloosa of Alabama, indicating that the Tuscaloosa is a time-transgressive unit (Olive, 1980). This formation is very similar to another unit present locally, termed the "Little Bear Rubble". Both appear to be derived from similar material; angularity of clasts seems to be the only characteristic that can be



G - Glauconite

* Modification of Olive and Finch (1969, p. 5-6)

Figure 2. Stratigraphic column of the post-Paleozoic succession in the Jackson Purchase (from Olive, 1972).

used to distinguish the two units (Clausen et al., 1992). The Tuscaloosa Formation was encountered by drillhole at only one site in the vicinity of the PGDP, near the Shawnee Steam plant (Sykora and Davis, 1993).

The sediments of the McNairy Formation overlie the Tuscaloosa Formation. First called the McNairy Sand after its type locality, the equivalent strata in the northern Purchase area is referred to as the McNairy Formation because in this location it is principally clay (Olive, 1980). Olive (1972) observed that both formations are lithologically similar and referred to the two formations collectively as the Clayton-McNairy Formation. Sykora and Davis (1993) determined that the elastic properties of the McNairy Formation are likewise similar to those of the Tertiary Clayton Formation in the northern part of the Jackson Purchase. This report will use the nomenclature established by Olive.

The Porters Creek Clay, perhaps the most distinguishable unit in the Tertiary strata, overlies the Clayton-McNairy Formation. Its composition, that of dark-gray montmorillonitic clay that is occasionally glauconitic, is consistent throughout the embayment. Its thickness fluctuates because of erosion preceding deposition of Eocene sediments (Hansen, 1966).

Eocene sediments overlie the Paleocene Porters Creek Clay south of PGDP. Three formations of Eocene age have been identified in the Jackson Purchase: the Wilcox, Claiborne, and Jackson Formations. The sediments of these units are usually distinguished

by means of palynological data (Olive, 1980). The sediments of each unit consist of interbedded and interlensing sand, silt, and clay (Olive, 1966).

During late Tertiary to Quaternary time, a gravel unit was deposited throughout the Jackson Purchase. Common names for this unit include the Lafayette Formation, Lafayette gravel, and Mounds gravel. For the purposes of this study, the unit will be referred to as continental deposits, following the nomenclature of Olive (1980). As indicated by some of the names for this unit, it is composed chiefly of gravel, but it also contains clay lenses, sand, and silty clay (Olive, 1980). The origin and age of these deposits are still controversial; some contend that the deposits are Pleistocene in age and derived from glacial outwash, while others maintain that the gravel is Pliocene-Pleistocene in age and that only the younger gravels of the unit were influenced by glaciation (Olive, 1980). In any case, a southeastern sediment source is likely, as is evidence by a southeastern increase in the altitude of the bedrock surface beneath the deposits, a southeastern increase in the minimum size of the coarsest grains, and a southeastern increase in the size of the modal class (Olive, 1980). The base of the continental deposits is an unconformity and exhibits steps or terraces (Clausen et al., 1992). The continental deposits are overlain by Quaternary loess, lacustrine deposits, and alluvium. Loess deposits are presumably derived from alluvium deposited by glacial meltwaters in the Mississippi and Ohio River valleys (Olive, 1980). Lacustrine sediments are from an ancient lake that once occupied eastern parts of the Purchase; these deposits occur at altitudes lower than 357 feet in areas bordering the Ohio and Tennessee Rivers, as is

suggested by the presence of gravel bars at this altitude (Olive, 1980). Most of the lacustrine sediments were derived from the area surrounding the lake. Pleistocene and Holocene alluvium are derived from the Jackson Purchase Region, although the alluvium of the major rivers bordering the Purchase was likely carried from more distant sources.

2.2 DEPOSITIONAL HISTORY

During the Cretaceous, the Purchase was an upland because of the presumed emergence of the Pascola Arch to the south. Scientists theorize that thermal events in the crust related to reactivation of the faults bounding the Reelfoot Rift contributed to this rise. Streams that flowed across the area emptied into a south-draining trunk stream (Olive, 1980). Eventually, the gradient of this stream was lowered sufficiently so that alluviation of its valley began; this alluviation is represented by the Tuscaloosa Formation (Olive, 1980).

Throughout this time, the Pascola Arch was being eroded and continued to subside. Ultimately, a sea was able to transgress into the northern part of the embayment. The transgression did not extend into the Jackson Purchase; absence of strata that are age-equivalent to those being deposited farther south during this time supports this interpretation (Stearns, 1957). This sea regressed during the Late Cretaceous. Olive (1980) noted that the sea was bordered by bays, lagoons, and saltwater marshes that mixed northward with freshwater swamps of distributaries from the northeast. Sediments

of the McNairy were deposited in this sea. McNairy sediments are thought to have come from an eastern source, as indicated by mineral assemblages (Pryor, 1960). The appearance of clay in the McNairy near PGDP, however, suggests that this area could have been located between two deltas: one to the southeast and one to the north (Olive, 1980).

The Clayton Formation of the Midway Group represents the first Tertiary deposition in the Jackson Purchase. Lithologically very similar to the McNairy Formation, the Clayton probably was deposited in much the same environment as was the McNairy. Interbedded sand and clay indicate that the marine sea, which was present to the south during deposition of the McNairy, may have influenced deposition of the Clayton Formation as well. Following deposition of the Clayton Formation, the Porters Creek Clay was laid down as the marine sea to the south transgressed to its fullest extent in the embayment (Stearns, 1957). Toward the end of the Paleocene, the sea began to regress; Porters Creek Clay continued to be deposited along the embayment axis.

During the Eocene, a sea advanced once more to occupy a large area of the embayment (Stearns, 1957). At this time, the strata of the Wilcox and possibly of the Claiborne Formations were deposited. Presumably, Eocene sediments continued to be deposited even as the sea began to regress. Evidence of this regression is shown by the presence of lignites in the Claiborne Formation (Olive, 1972). The last transgression in the embayment took place during the late Eocene; this advancement went as far north as southwestern

Tennessee (Stearns, 1957). Continued deposition of the Claiborne as well as of the Jackson Formation occurred during this time. The thickness of the combined Eocene section is substantial; some researchers theorize that this thickness is caused by structural movement that resulted in further subsidence of the embayment axis during Eocene time (Olive, 1980).

After deposition of the Jackson Formation, uplift and erosion is inferred to have occurred, based on geomorphic evidence (Clausen et al., 1992). A trunk stream existed on the margins of the Jackson Purchase, occupying roughly the same position of the present-day Tennessee, Ohio, and Mississippi Rivers (Olive, 1980). Along the eastern margin of the Purchase, the stream was confined to a valley bordered by Paleozoic rocks; farther to the west and northwest, the stream's gradient lessened as it passed over much less resistant Cretaceous and Eocene sediments. Olive (1980) theorizes that at this point the river was likely a braided or meandering stream. During the Pliocene, the trunk stream began to dump alluvium and coarser sediments (continental deposits) into the wide valley created. The load of the stream eventually increased so much that the stream could no longer transport sediments; consequently, it began to fill its course, and the alluvial fan that formed at the low-gradient portion of the stream increased in size. Eventually, the fan blanketed most of the Jackson Purchase (Olive, 1980).

In Pleistocene time, glaciation occurred. This caused many rivers throughout the Midcontinent to entrench in response to a lowering of sea level. The trunk stream and its

tributaries began to erode valleys into the alluvial fan deposits. Due to fluctuations in sea level, the streams flowing through the Jackson Purchase in turn alluviated and eroded their channels, so that the continental deposits were heavily reworked and redistributed during this period (Olive, 1980). During and between periods of glaciation, loess was deposited.

As the last stage of glaciation ended, tributaries draining from glaciated areas supplied large amounts of sediment into the ancestral Ohio and Mississippi Rivers. Streams throughout the Purchase area alluviated their valleys as the flood plains of the Ohio and Mississippi rose; however, the gradient of the ancestral Tennessee River was not great enough to keep the river from becoming blocked (Olive, 1980). Subsequently, a lake was formed that existed until the end of the Pleistocene. When it ruptured a northerly divide, the lake drained and caused the Ohio River to take on its present course (Olive, 1980). The sediments derived from this lake and from streams draining out of glaciated areas comprise latest Pleistocene and Holocene sediments.

2.3 STRUCTURAL FRAMEWORK

The main structural influence on the Jackson Purchase Region has been the ancient Reelfoot Rift-Rough Creek Graben rift structure. Despite the large amounts of knowledge gained about these two major intercontinental rift systems during the past 30 years, little is known about the role of the Jackson Purchase in relation to the rift

structures. It is apparent, however, that regional seismicity has affected the area in the past.

Evidence of seismic activity is found throughout the area. For example, the Porters Creek Clay is intersected by vertical to near-vertical clastic dikes in many places (Olive, 1972). Geologic mapping of the Purchase area and southern Illinois has revealed the existence of numerous faults that displace Paleozoic through Quaternary strata (Olive, 1972; Nelson et al., 1997). Other geophysical data, such as proprietary seismic reflection data and gravity and magnetic surveys, indicate that the area is structurally complex (Hildenbrand and Hendricks, 1995; Heigold and Kolata, 1993).

3.0 SEISMIC DATA ACQUISITION AND PROCESSING

Seventeen km of shallow, high-resolution SH-wave reflection and refraction data were acquired in the area of PGDP for this study. Figure 3 shows the locations of the seismic lines discussed in this report; Figures 4 through 8 illustrate the resulting seismic sections.

As previously stated, field tests using a seismic hammer to generate P- and SH-waves, and a vacuum-assisted weight drop to generate P-waves indicated that SH-waves generated by a seismic hammer resulted in the optimum signal-to-noise ratio for imaging the bedrock and unconsolidated sediments in the study area. The energy source used for generating the SH-waves consisted of a 5.4-kg sledgehammer striking a 12-kg section of

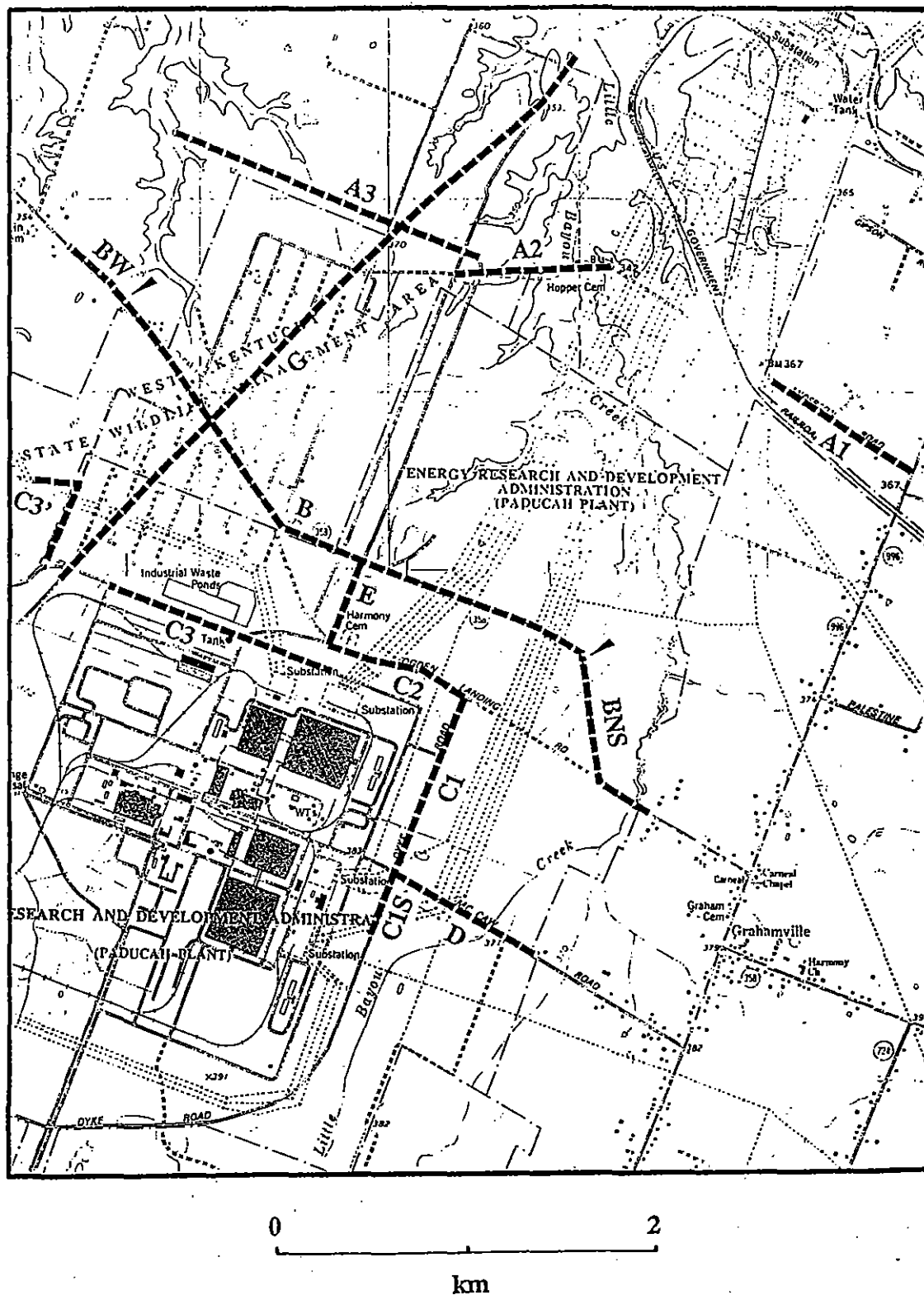


Figure 3. Map showing locations of seismic lines in the vicinity of the Paducah Gaseous Diffusion Plant.

I-beam perpendicular to the geophone spread. The hold-down weight of the I-beam consisted of the weight of the I-beam plus the hammer swinger for a total hold-down weight of approximately 85 kg. Coupling of the energy source to the ground was enhanced by embedding the I-beam against the edge of a blacktop road whenever possible; otherwise, the edge of the I-beam was embedded in a small slit trench. The degree of coupling attained on unpaved surfaces in the PGDP area probably affected the quality of data along certain lines, as is indicated in the discussions of lines A, C3, and G.

An in-line spread of 48, 30-Hz, horizontally polarized geophones spaced at 4 m intervals was used. A zero offset was used with the energy source, and records were generally stacked six times at each shotpoint. To ensure proper identification of SH-wave arrivals, data from each side of the I-beam energy source were recorded. Based on the acquisition parameters, twelve-fold common-depth point (CDP) data were obtainable.

The seismic data used in this study were collected with a 48-channel, 24-bit, IFP Geometrics Strataview RX engineering seismograph. Data were recorded at a sampling rate of 0.5 ms. Acquisition parameters included low-cut and high-cut bandpass filters of 10 and 250 Hz, respectively, and a notch filter of 60 Hz.

Table 1 is a chronological list of the steps followed in processing data. Specific processing procedures for each line can be found in Appendix B. The seismic data were processed using the commercial software package VISTA 7.0 (Seismic Image Software,

Table 1. Data Processing Steps – (using VISTA 7.0)

- 1. Preprocessing**
 - a. band-pass filtering (typically 25–60 Hz)**
 - b. AGC scaling (typically 250 ms)**
 - c. saving .dat files in SEG-Y format**
- 2. Configuration of field geometry into headers**
 - elevation static corrections (where needed)**
- 3. Application of headers to SEG-Y files**
- 4. Velocity Analysis**
 - derived stacking velocities from semblance plots**
- 5. Normal-Moveout Correction**
- 6. CDP Sort**
- 7. CDP Stack (6-fold)**
- 8. Selective Post-Processing**
 - a. AGC scaling**
 - b. F-K filtering**
 - c. weighted 3-trace mixing**

1995). Preprocessing involved first changing the file format from .dat (Geometrics file format) to SEG-Y, a standard file format. Next, a band-pass filter was applied to data in order to reduce the amount of noise encountered during field operations. AGC scaling was also applied. This preprocessing step aided in viewing of data by normalizing data within a specified time window (usually 250 ms) according to the highest wave amplitude within that window. These files were then combined for processing purposes. Geophone spacing, shotpoint spacing, and any elevation corrections were next configured and applied to the combined file. A velocity analysis was subsequently performed on the combined file. Here, a group of traces was selected and a hyperbolic curve fitted to reflections visible in the group. A normal moveout (NMO) correction was applied to correct for differences in reflection travel-times due to source-receiver distance variations. Finally, the combined file was sorted and stacked to produce a profile like those in Appendix A. After preliminary processing with 12-fold data, it was determined that lateral discontinuities and frequency distortions due to wide-angle reflections were affecting the quality of the stacked traces; subsequently, 6-fold data were used for this study. Post-processing steps included additional AGC scaling as well as F-K filtering. This filtering procedure, like band-pass filtering, was used to remove noise. A 3-trace weighted mix was also used on many CDP sections; this procedure introduced an artificial increase in the horizontal coherence, thus making continuity of reflections more apparent (Dobrin and Savit, 1988). A glossary of geophysical terms relating to data processing procedures can be found in Appendix F. Definitions were taken from Sheriff (1973) and Sheriff and Geldart (1982).

As stated in the introduction, the limestone bedrock, the top of the Clayton and McNairy Formations, and the RGA were to be imaged. On all sections, the bedrock was visible at about 500 ms. Imaging the top of the Clayton and McNairy Formations, however, proved to be more difficult; this is due to the negligible velocity contrast between the Clayton-McNairy and the RGA. The top of the RGA was imaged by the refraction interface at roughly 100 ms. Using the method employed by Williams et al. (1995), the traces representing the RGA refraction were stacked and then corrected for linear moveout using the velocity of the refracted wave. The interpretation of the top of the RGA and bedrock was aided by lithologic logs from previous studies in the area (Northeast Plume Preliminary Characterization Summary Report, D.O.E., 1995; Results of the Site Investigation, Phase II at the Paducah Gaseous Diffusion Plant, Paducah, Kentucky, D.O.E., 1992).

A limiting factor in the quality of some of the seismic data acquired was the degree of coupling of the energy source to the ground. Data collected in fields or along gravel or dirt roads, were, in general, of poorer quality than collected along blacktop roads. The most noticeable effect in these instances was a decrease in impulsive amplitude of the seismic reflections. An attempt was made to compensate for this by digging the flanges of the steel beam into the ground, with limited success. Along blacktop roads, one edge of the I-beam was embedded into the shoulder of the road so that it butted up next to the edge of the blacktop. This method provided better coupling of the energy source to the ground.

The nature of deposition of the RGA is a limiting element in the interpretation of the location of the RGA refractor. As discussed before, near PGDP, the continental deposits of the RGA were subject to erosion and reworking by the ancestral Tennessee River during the Pleistocene. This led to the development of an erosional surface at approximately 85 m; this surface varies, however, between 75 m and 95 m. The depositional history of the RGA undoubtedly indicates that the thickness as well as the elevations of the top and bottom of the RGA will be irregular. This variance can be seen on virtually all of the seismic sections presented in this study.

Background noise was also a factor that could affect the quality of data gathered at PGDP. This included noise associated with plant operations, power lines, and automobiles. Pre- and post-processing frequency and F-K filtering was used to remove unwanted noise from the data where possible.

4.0 RESULTS

4.1 IDENTIFICATION OF REFLECTORS

Reflections and refractions were correlated with lithologic units by comparing velocity picks from offset panels to lithologic logs of available monitoring wells at PGDP.

Velocity picks were obtained in VISTA 7.0 (Seismic Image Software, 1995) by entering a set of sorted and stacked traces corresponding to a common depth point (CDP). Next, a

semblance analysis was performed and the velocities and offset times were picked from the semblance output. From these parameters, depths to various horizons could be obtained using the formula

$$d = (V \times T)/2$$

where d is depth (m), V is velocity (m/s), and T is time (s). These depth values for individual reflectors and refractors were then compared with data from the lithologic logs closest to the line upon which the velocity analysis was performed. Appendix C gives a complete list of the velocity picks used for each line presented in Figure 3. Lithologic data referenced in this study are included in Appendix E.

In general, the limestone bedrock reflector was the most identifiable reflector on a velocity pick. The large velocity contrast between the Mississippian limestone and the overlying sediments was likely the reason for this easily observable reflection. Harder to interpret was the refraction for the top of the RGA. Often, this refraction was masked by the direct wave. Muting the top of the CDP section often resulted in erasing the RGA refractor. Depths obtained for the RGA refraction and bedrock reflection were compared to drill hole data (Northeast Plume Preliminary Characterization Summary Report, D.O.E., 1995; Results of the Site Investigation, Phase II at the Paducah Gaseous Diffusion Plant, Paducah, Kentucky, D.O.E., 1992). Other reflectors were picked in much the same way when possible.

The top of the Clayton-McNairy was able to be determined with confidence using the above procedure only along line C2. However, the reflector corresponding to the top of the Clayton-McNairy was generally not visible. This was likely because shear-wave velocity contrasts between the Continental Deposits and the Clayton-McNairy are negligible (Sykora and Davis, 1993).

4.2 GENERAL FEATURES

Several examples of stratigraphic units that have been affected by faulting are indicated on the seismic lines in Appendix A. Fault-related and erosional features are evident on most of the lines in the study area to varying degrees. Specific features will be discussed in greater detail for specific lines in the next section.

The most significant findings of the study are that faulting is observable in areas where edges of the contaminant plumes are located and that the strike of the faults correspond to the direction of migration of the contaminant plumes. This suggests structural control on plum migration. In many instances, the faults can be traced from the limestone bedrock to the top of the RGA, thereby suggesting Quaternary activity in an area where no Quaternary faulting had previously been observed. This finding is not unexpected in light of Nelson et al.'s (1997) study just across the Ohio River in southern Illinois.

4.3 SPECIFIC FEATURES

4.3.1 Line A1

Line A1 runs from the intersection of Anderson Road and Highway 996 to the U.S. government railroad lines (Fig. 4). Throughout much of the section, a prominent reflector, the limestone bedrock, is noticeable at 500 ms. A distinct break in this reflector occurs near shotpoint 36. Further breaks are seen near shotpoints 108 and 145. All of these features have been interpreted as faulting in the bedrock. The refractor imaged at roughly 100 ms is interpreted as the RGA. Here, faulting can be distinguished as well; in many cases, the faults within the RGA appear to be continuations of faults emanating from the bedrock.

The surfaces of both the RGA and the bedrock are noticeably undulatory along much of line A1, presumably because of weathering, which affected each unit subsequent to deposition. However, the depression between shotpoints 108 and 145, evident in both the bedrock and the RGA, is here interpreted as a downdropped area bounded by faulting.

Between shotpoints 1 and 36, the bedrock reflector drops to the east. The RGA refractor does not present a corresponding drop. This is thought to be primarily an erosional feature in the bedrock, or possibly basement faulting. There is no indication that these faults continue into the RGA.

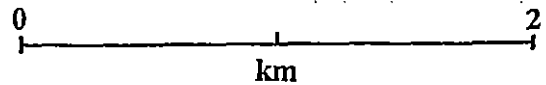
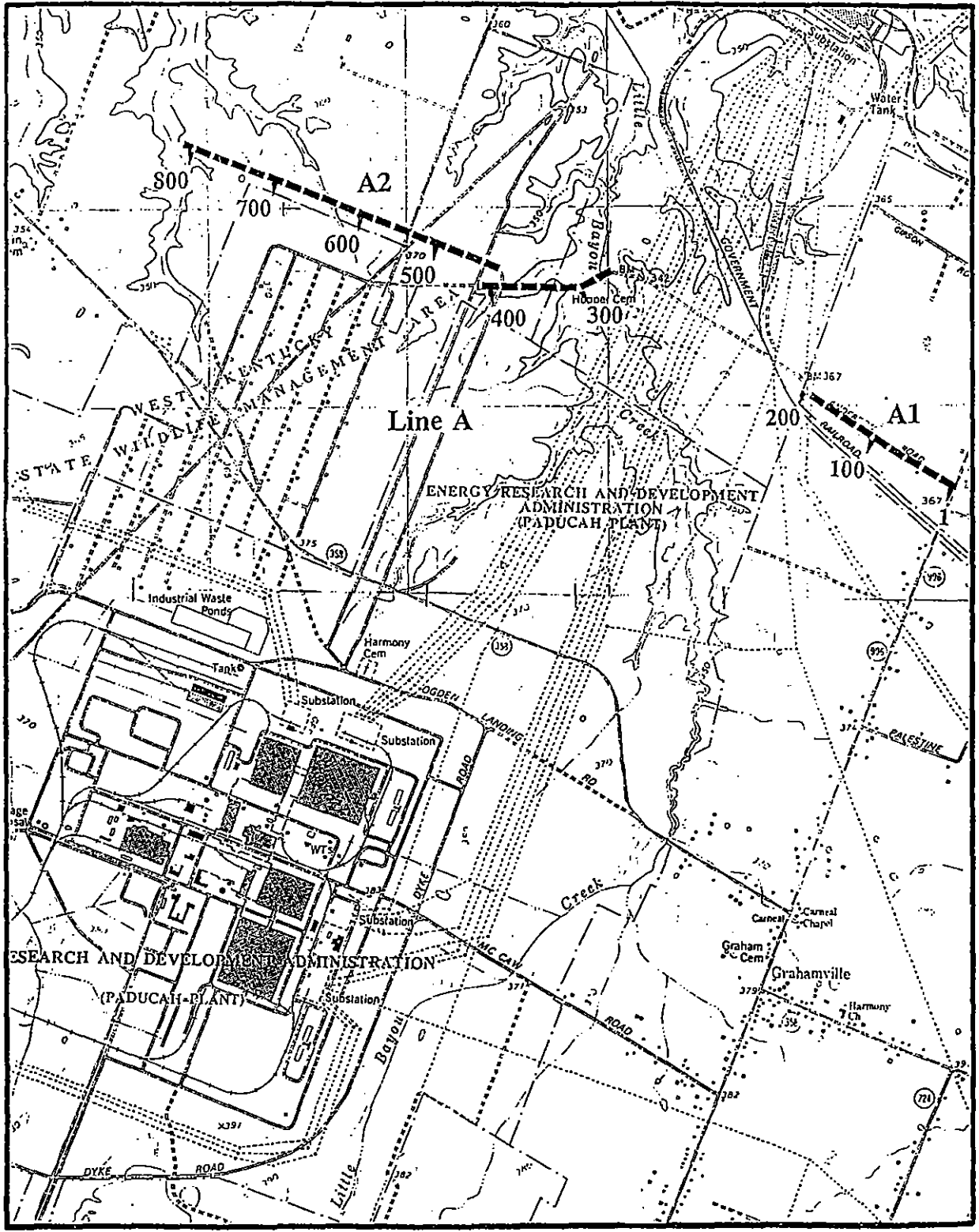


Figure 4. Shotpoint map, lines A1, A2, A3.

4.3.2 Line A2

Line A2 is an east-west section, located to the north of PGDP (Fig. 4). The reflector identified as the top of the bedrock is located at about 500 ms on the time section. However, in some places the bundles of energy are not as strong as in others, making interpretation difficult. The RGA refractor is present at roughly 100 ms on the section; it is noticeably undulatory. Data quality along A2 is average, likely due to differences in the degree of coupling. However, examples of faulting that are visible from the top of the bedrock through the top of the RGA are located near shotpoint 335, 350, and 370.

4.3.3 Line A3

Line A3 is an east-west profile between the Ohio River and the PGDP, paralleling the northern perimeter of PGDP (Fig. 4). The bedrock reflector is present at about 500 ms at the ends of this section. However, in the middle of the section, the bedrock reflections become weaker and occur deeper in the time section. Overlying reflectors within the Clayton-McNairy as well as the refractor identified as the top of RGA also exhibit this downdrop. This feature, located between shotpoints 434 and 745, is interpreted as a graben. Within the graben, the RGA refractor exhibits some topographic relief, attributable to weathering or to tectonism associated with graben formation, or to subsequent movement along faults within or bounding the graben. In any case, the feature is significant, since it affects the RGA, and could therefore exert some control over

migration of contaminants in the area. This feature is discussed in more detail in section 4.5. Faulting is evident in both the bedrock and the RGA reflectors on the bounding margins of the graben. Faults identified near shotpoints 525, 560, and 830 provide good examples of faulting that extends into the RGA refractor.

4.3.4 Line B

Line B runs east-west along Ogden Landing Road (Fig. 5). It is divided into three sections: BW, B, and BNS. Line B is key to the study, for the data gathered along this line serves as a correlator with data from other lines running parallel and perpendicular to it, thus enabling trends of features present in the subsurface to be established.

Line B begins in the western part of the study area. Here, the bedrock reflector, usually seen at 500 ms, is weak and appears to occur deeper in the time section. Near shotpoint 84, the bedrock reflector returns to 500 ms. This drop in the bedrock reflector west of shotpoint 84 is interpreted to be the eastern margin of the graben previously identified on line A3. Other reflectors and the RGA refractor above the graben tend to be disturbed in this location as well. Toward the western end of line B (indicated as BW on Fig. 4), the RGA refractor, located near 150 ms, is noticeably disturbed.

East of shotpoint 84, strong reflections from the bedrock are exhibited. The refraction from the top of the RGA is also seen clearly here at around 100 ms. Between shotpoints

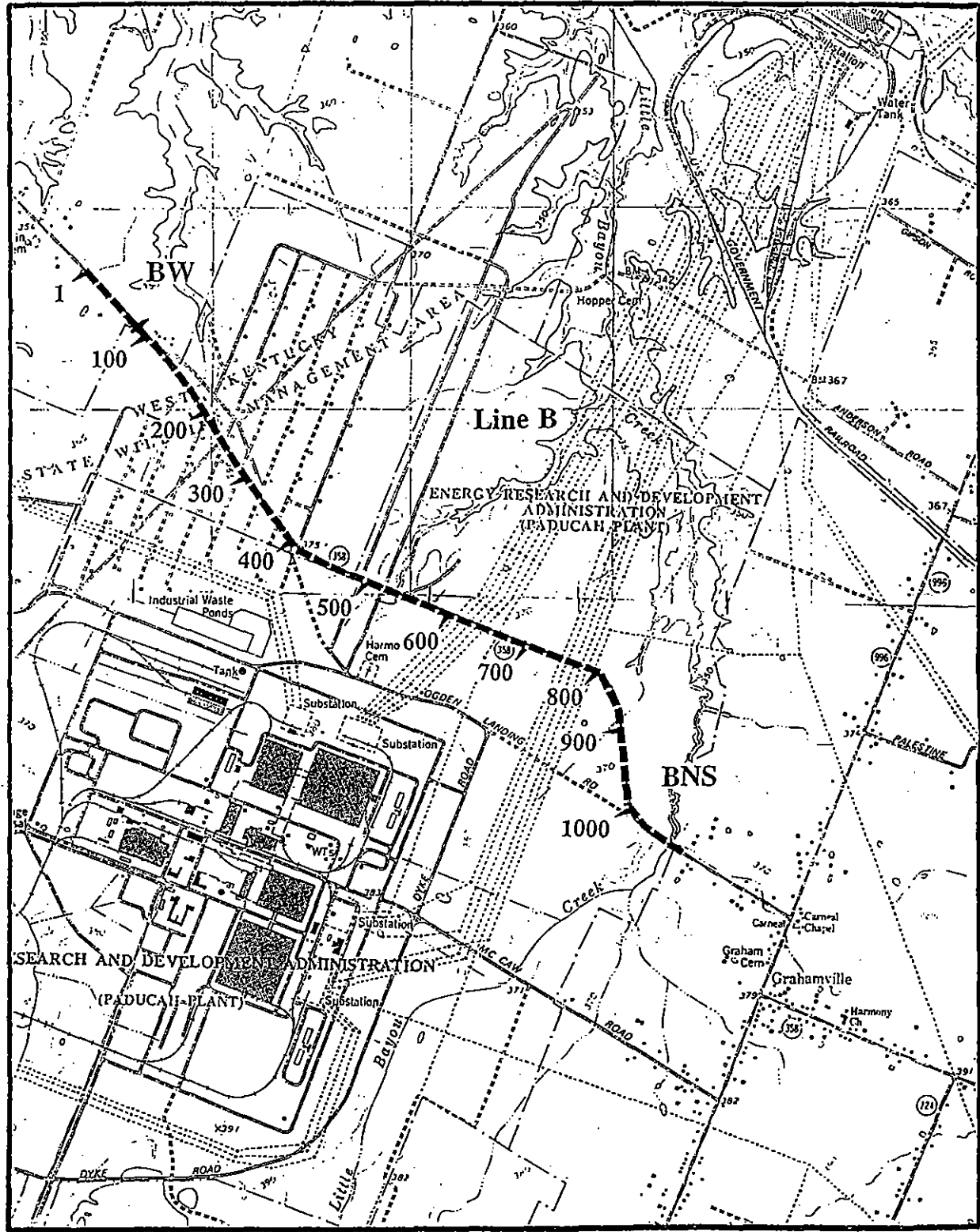


Figure 5. Shotpoint map, line B.

97 and 265, small but distinct breaks are seen in both units, providing further examples of faulting that has penetrated the top of the RGA. Some of these faults are part of a fault zone detected in a pilot study of the PGDP area (Street, personal comm., 1997). Between shotpoints 265 and 337, another zone of faulting is interpreted to intersect the top of the RGA; this group of faults is interpreted to be part of a second zone of faulting also detected in the pilot study.

Between shotpoints 241 and 301, a large dome-like feature is present below the limestone bedrock reflector. This feature appears again farther to the east on line B and on several other lines in the study. The dome-like feature could represent parts of the bedrock that were less resistant to weathering. Correlations to this feature can be found in Hunter et al. (1984).

Past shotpoint 301 and continuing until near shotpoint 505, small breaks occur in the refractor representing the top of the RGA as well as in the bedrock reflector. Notable displacements are located near shotpoints 330 and 460. Near shotpoint 505, both reflectors drop down to the east, returning to their usual locations in the section near shotpoint 575. Just before shotpoint 553, line B intersects line E. In an attempt to correlate features across these two lines, an optimum offset technique was used in the lab with data from lines B, E, and C3. The results obtained through the use of this method will be presented in section 4.4.

Dome-like features are evident in the bedrock again between shotpoints 600 and 649, indicating that these parts of the bedrock were likely less resistant to erosion. A small down-to-the-east displacement is also present in the RGA and bedrock reflectors at this location. After shotpoint 700, the RGA refractor dips down to the east, while the bedrock reflector exhibits an opposing trend. Past this point, no other significant features are observable on line B (shotpoints 1 through 864).

4.3.5 Line BNS

Line BNS is discussed separately because it trends in a different direction than the main part of line B. Reflector and refractor locations are as noted in the earlier discussion of Line B. Line BNS begins at shotpoint 865 of line B.

The most obvious displacement occurring in both reflectors is located near shotpoint 877, where both the RGA and the bedrock reflectors are downdropped to the east. The east-bounding fault that accompanies this feature is located near shotpoint 913, indicating that this could be interpreted as a small graben. Another down-to-the-east drop in both reflectors occurs near the intersection of Line BNS with Old Ogden Landing Road. Here, near shotpoint 1000, the RGA refractor and bedrock reflector show evidence of displacement. Line BNS becomes an east-west profile as it intersects Old Ogden Landing Road near shotpoint 1022. The bedrock reflection becomes very weak at this point, and the RGA reflection becomes hard to follow with certainty. This could indicate the

presence of structure; likewise, the change in data quality might be related to other factors such as background noise. Line BNS ends at the bridge that crosses Little Bayou Creek.

4.3.6 Line C1

Line C1 runs from the intersection of Old Ogden Landing Road and Dyke Road to the intersection of Dyke Road and McCaw Road (Fig. 6). Line C1 is punctuated by at least seven monitoring wells along its length; therefore, good depth control of the RGA and the Clayton-McNairy Formation was maintained along this line.

Quality of data along Line C1 is variable. Extensive processing was necessary in order to image the top of the RGA. A solid image of the top of the limestone bedrock was likewise attained only through the use of considerable filtering. Background noise from PGDP probably affected data quality along line C1.

Examples of interpreted faulting are shown in the interpreted C1 section in Appendix A. Throughout the section, the surfaces of both the RGA and the bedrock undulate significantly; due to data quality constraints, it is not possible to say with certainty where faulting has played a role in the disruption of these units. Near shotpoint 12, the bedrock reflector bends noticeably; however, this is not seen in the top of the RGA at this location. This indicates that the downdip in the bedrock could be representative of weathering.

Alternatively, faulting could occur here that simply does not penetrate the RGA. A

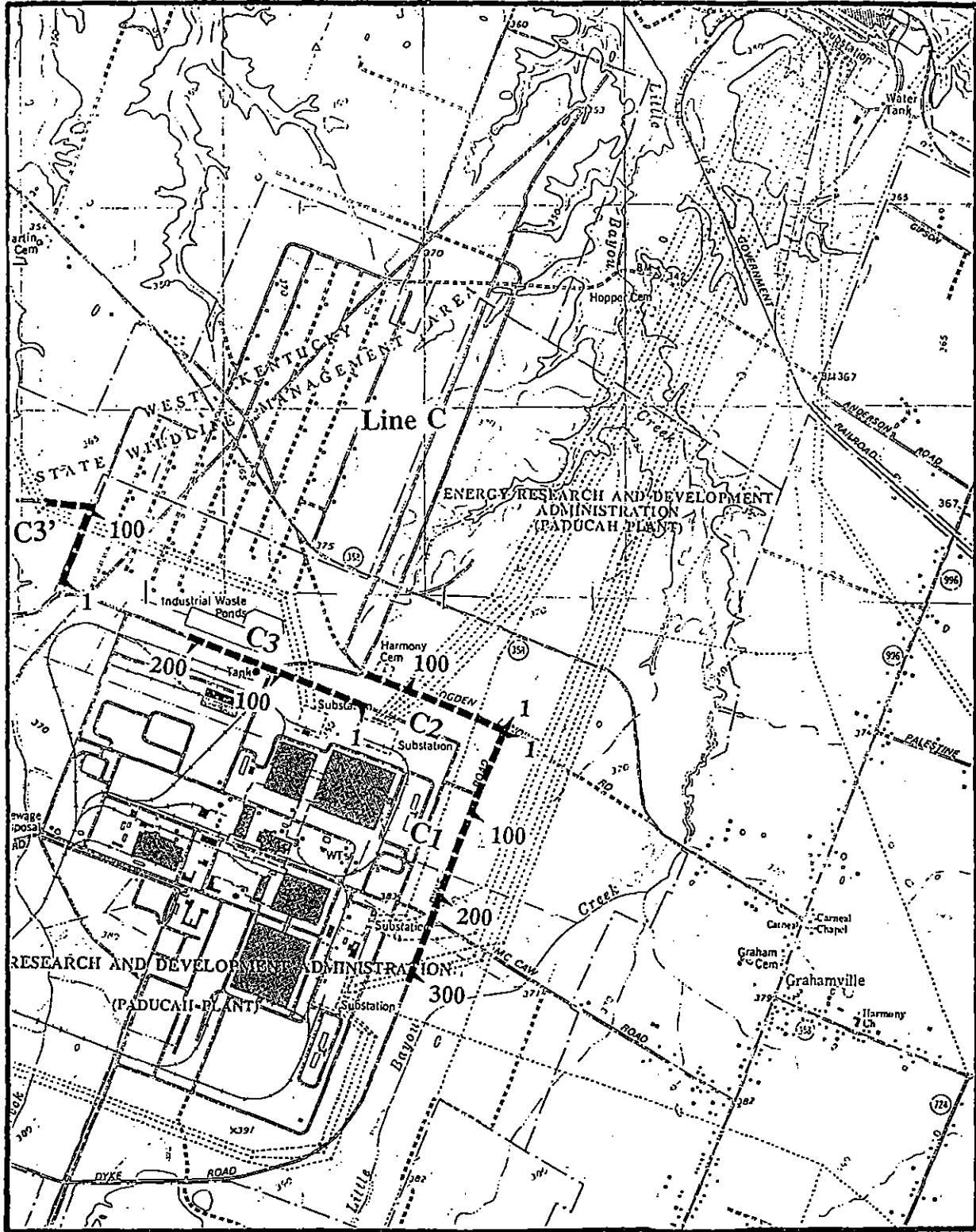


Figure 6. Shotpoint map, lines C1, C2, C3, C3'.

distinct break occurs in an unidentified reflector below the interpreted top of the RGA just past shotpoint 36. This is accompanied by a drop in the bedrock reflector as well, indicating that this displacement is fault-related. Another break occurs in the identified top of the RGA at shotpoint 120, although this displacement is not clearly seen in the reflectors beneath. A likely candidate for faulting is located between shotpoints 136 and 144. Here, the RGA reflector is displaced, as is the somewhat weaker bedrock reflection at about 550 ms.

4.3.7 Line C1S

Although not indicated as such on the shotpoint map, Line C1S is the section of Line C1 that runs south along Dyke Road from the intersection of Dyke Road and McCaw Road. A monitoring well at this intersection provides only approximate control on the extent of the RGA. The depth to the RGA determined from velocity picks closely correlates with the lithologic data in this area.

As is seen in both the uninterpreted and interpreted sections in Appendix A, the surfaces of the RGA and the limestone bedrock are highly variable. Between shotpoints 264 and 276, the RGA surface slopes down to the south and is broken. At this location, the top of the bedrock appears to be displaced, as do other unidentified reflectors in the 200 to 400 ms range. At shotpoint 300, both the RGA refractor and the bedrock reflector are noticeably downdropped, outlining a small graben. The other bounding fault to this

structure occurs near shotpoint 324. This feature, as well as the one between shotpoints 264 and 288, is located in the general vicinity of the lower boundary of the northeast-trending contaminant plume.

Line C1S does not cross the terrace feature present to the south of PGDP. Well data to the west and southwest of C1S show that the terrace is located to the south of the terminus of C1S.

4.3.8 Line C2

Line C2 runs from the intersection of Old Ogden Landing Road and Dyke Road west along Old Ogden Landing Road. It ends at the southern terminus of line E (Fig. 6). At its western end, C2 nears the upper boundary of the northeast-trending contaminant plume, making it potentially important for determination of fault-related control.

Line C2 is one of the few lines in the study area along which the Clayton-McNairy has been identified. Appendix C lists the velocity picks made for this line. The prominent refractor at 100 ms is identified as the top of the RGA; the somewhat fainter reflector at roughly 200 to 235 ms is distinguished as the top of the Clayton-McNairy; and the reflector at 500 ms is labeled as top of bedrock. As noted in descriptions of other sections, the surfaces of the RGA and the bedrock are undulatory and broken in many places. Specific displacements in the RGA can be seen near shotpoints 25, 30, and 55.

Accompanying breaks in the Clayton-McNairy are not as apparent; however, these displacements can be traced down into the bedrock reflector. Dome-like structures are also apparent within the bedrock along this line. A significant feature along line C2 occurs between shotpoints 145 and 150. Here, all three units are displaced in what is interpreted as a zone of faulting.

4.3.9 Line C3

Line C3 runs from a point just east of the guard gate on the northern periphery of the plant west for 812 meters. The RGA and bedrock reflectors have been identified at 120 ms and 550 ms, respectively. Only one monitoring well, P4-F08, provided control on velocity picks made during processing.

In general, the data quality of line C3 can be considered to be of lower quality. This is attributable to several factors, especially background plant noise. In general, plant noise registers at a variety of frequencies and in order to filter it out completely, desirable reflections would have to be deleted. Another factor involves the quality of coupling attained along line C3. Line C3 was shot entirely along an unpaved surface, so data quality was not as good along line C3 as along lines B or D.

Faint reflections are discernible along line C3. The RGA refractor and limestone bedrock reflector again appear at around 100 ms and 500 ms, respectively. The most noticeable

displacements within the reflector representing the top of the RGA occur near shotpoints 30 and 50. Here, the bedrock is downdropped. However, because of the weak bedrock reflector, these distinct displacements cannot be traced with certainty into the 500 ms reflector. The optimum offset method was used with data from line C3; this technique delivered clearer data than CDP data for line C3 and helped in correlating features among lines.

4.3.10 Line C3'

Line C3' runs south-to-north along a road northwest of the plant. An extension of the line runs east-to-west along a road roughly perpendicular to line C3' (Fig. 6). On this line, the top of the RGA and the limestone bedrock can be distinguished with varying degrees of certainty. The quality of data here could also be affected by plant noise, since PGDP facilities are nearby.

The top of the RGA and the bedrock are identified at 100 and 500 ms, respectively.

Although the bedrock reflector is not as strong as it is on other lines, the quality of data obtained along line C3' is still somewhat better than that acquired along line C3. An irregular bedrock surface is apparent; breaks in the bedrock reflector and RGA refractor occur near shotpoint 100. Other parts of this section display irregularity of both surfaces; it is not possible to say with certainty that these irregularities are fault-related.

Data quality for the east-west extension of line C3' is fair. The bedrock reflector is somewhat distinguishable at around 500 ms, and the top of the RGA is discernible at about 100 ms. Two distinct breaks can be observed in the RGA reflector near shotpoints 25 and 30. These displacements can tentatively be traced down into the bedrock, as indicated on the interpreted version of the extension of line C3'.

4.3.11 Line D

Line D runs west-to-east along McCaw Road, beginning at the intersection of McCaw Road and Dyke Road and extending for a length of 480 meters (Fig. 7). The tops of the RGA and the bedrock are identified at roughly 100 and 500 ms, respectively. The top of the Clayton-McNairy cannot be detected on the line D section.

Data quality along line D is very good, with a virtually continuous refraction from the top of the RGA. Although not as well defined, the surface of the bedrock still yields sufficient information from which to make interpretations. Breaks in the RGA refractor are apparent near shotpoints 12, 36, 60, and 84. The two breaks near 12 and 60 define a downdropped area visible within the RGA as well as the bedrock, indicating that fault-related movement has occurred. This downdropped area occurs near the bottom edge of the northeast-trending contaminant plume, suggesting that this zone of displacement may also be affecting the migration of the plume.

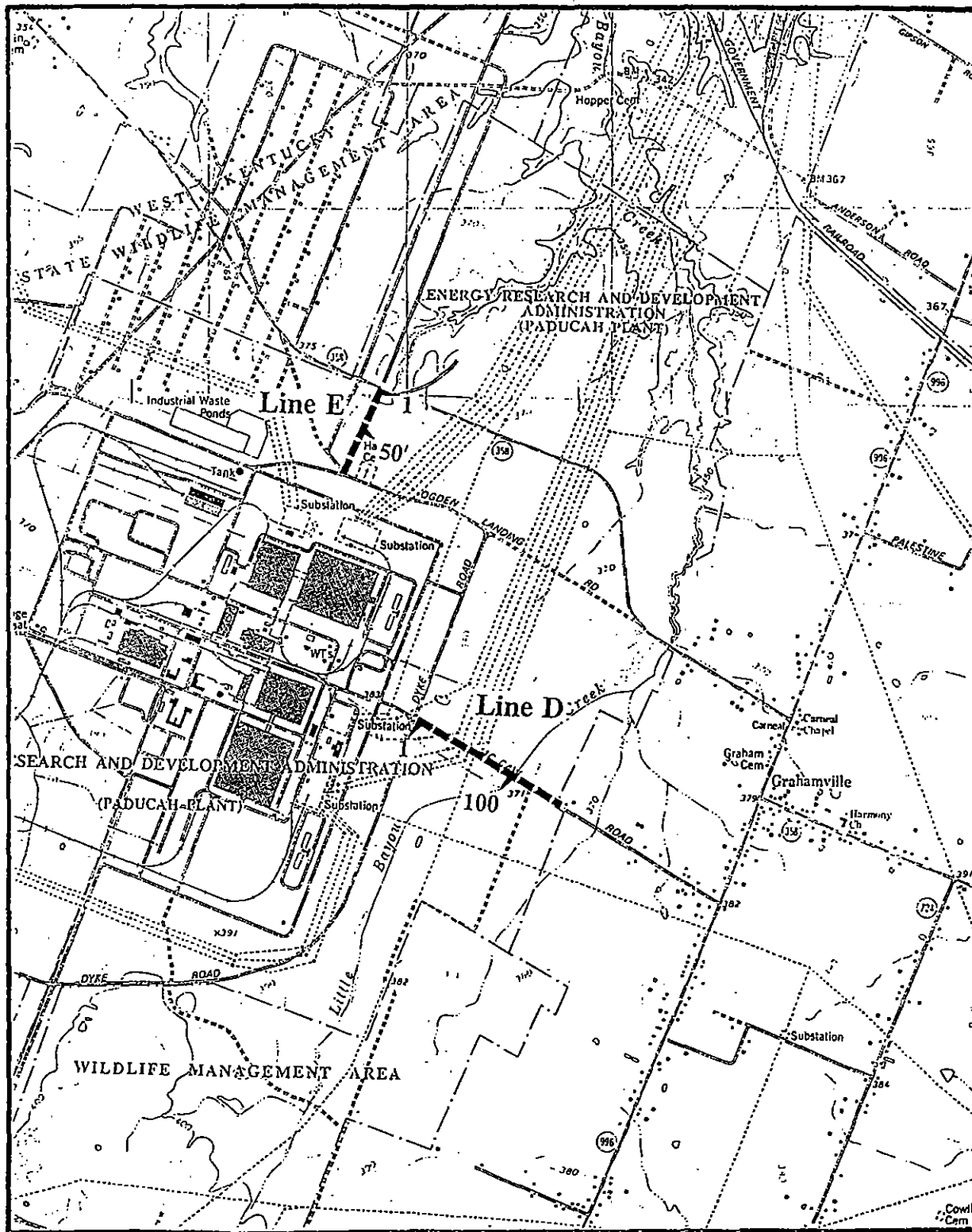


Figure 7. Shotpoint map, lines D, E.

4.3.12 Line E

Line E is located along New Harmony Road, running north-to-south from the intersection of Ogden Landing Road to the intersection of New Harmony Road with Old Ogden Landing Road (Fig. 7). Along this line, the bedrock has been identified at about 500 ms. However, the top of the RGA cannot be located with certainty. The only monitoring well near line E, well P4-F08, indicates the top of the RGA is at 44 feet and the bottom is at 92 feet; the velocity pick used along line E indicated a depth of approximately 71 feet at a time of 180 ms on the time section. No other significant reflections were visible at times between 0 and 180 ms or in the interval shortly after 180 ms. This reflector may be the top of the Clayton-McNairy, and the reflector representing the top of the RGA may simply have not been visible during processing. In any case, all prominent shallow reflectors in the CDP sections in Appendix A show displacement in areas that would allow features to be correlated through the reflectors (see interpreted section, line E).

Sharp displacements are evident in the 100, 180, and 500 ms reflectors on line E. These occur near shotpoints 24, 48, 60, and 72. The break near shotpoint 60 displaces the reflectors present at 100 and 180 ms in a down-to-the-north sense, suggesting that this break represents a fault. A similar drop is present in the bedrock, although it is not as pronounced. The displacement present near shotpoint 48 is also indicative of faulting. This zone of faulting could also be important in determining whether structure present in

the subsurface has any control on contaminant migration. The optimum offset method was used on line E, with favorable results.

4.3.13 Line G

Line G is a northeast–southwest profile along an access road that begins south of the Shawnee Steam Plant (Fig. 8). It is over 3800 meters long and ends near the northwest corner of PGDP. On this line, only the refractor representing the top of the RGA and the limestone bedrock reflector can be distinguished with certainty. They occur at about 100 and 500 ms, respectively, which is typical of other lines shot for this study.

From the beginning of line G in the northeast until roughly shotpoint 250, the graben that has been identified on lines A3 and B is observable within the bedrock reflector. Near shotpoint 125, the RGA refractor begins to show obvious displacement and ultimately dips down to the north to about 200 ms on the time section. Throughout the record until shotpoint 250, the bedrock surface within the graben is uneven and discontinuous. Near shotpoint 125, the RGA refractor is clearly broken, indicating that faulting likely related to graben formation or reactivation has penetrated the RGA. Just past the intersection of lines G and B, from shotpoints 673 to 697, the bedrock surface is lower than it was before the road crossing. There are slight undulations in the RGA reflector, but no obvious indicator of faulting. This lowered reflector could simply represent a weathered part of the bedrock surface. From this point on, the bedrock reflector is significantly weaker; the

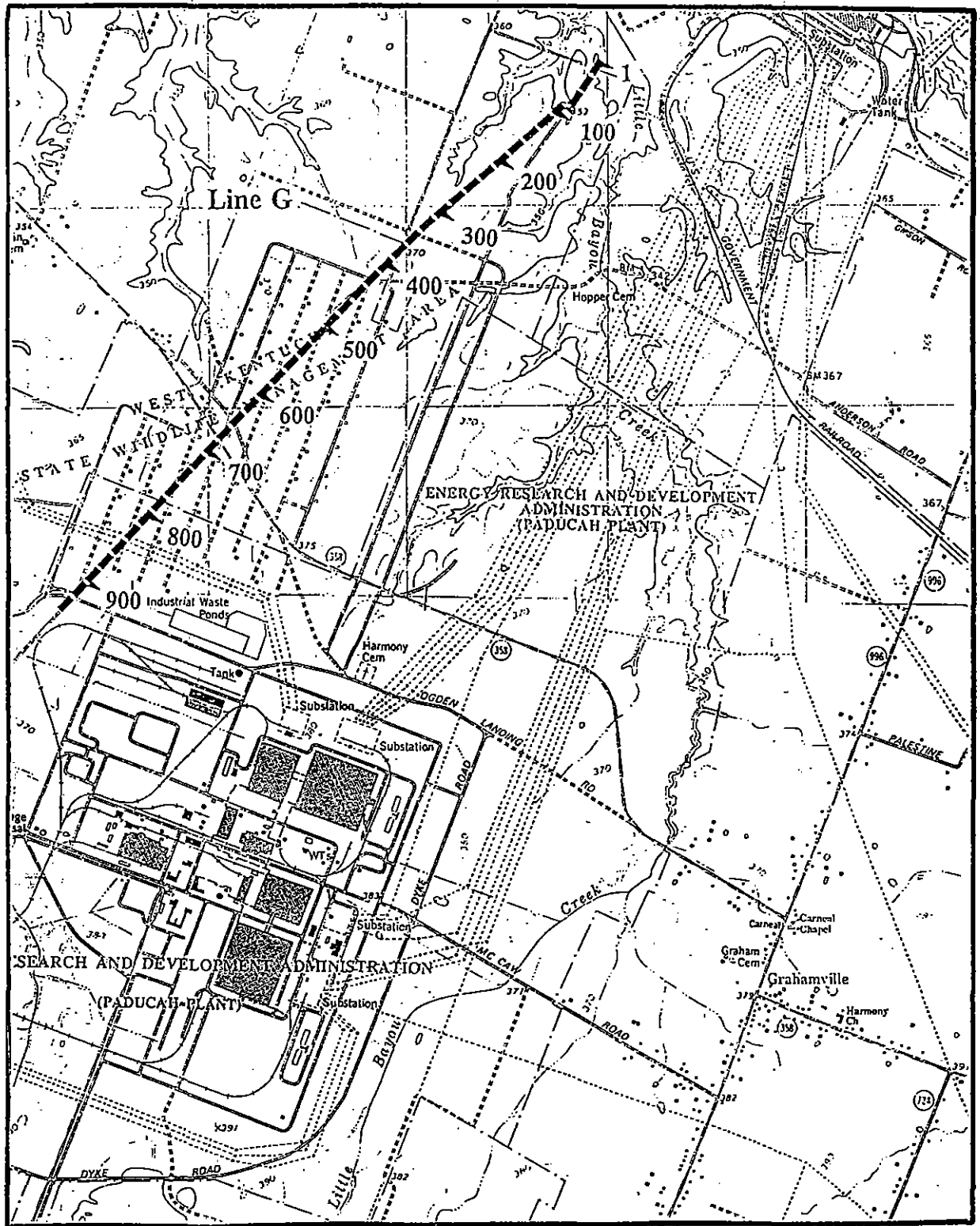


Figure 8. Shotpoint map, line G.

reason for this is unclear. No apparent breaks in either reflector occur until about shotpoint 877, when both reflectors drop down to the southwest.

4.4 CORRELATION OF OBSERVED FEATURES

Figure 9 is an area map of PGDP that presents the locations of the seismic profiles in the study as well as numbered faults that could be significant to the direction of contaminant plume migration. The map also shows the location of the two contaminant plumes in relation to these faults.

Based on the similarity of features from line to line, as well as the approximate locations of the two contaminant plumes, it is reasonable to conclude that the contaminant plumes are being structurally controlled to some extent. Perhaps the strongest evidence for this comes from faults observed across lines C1 and D. This fault zone is labeled '1' on both Figure 9 and on the interpreted seismic sections of both lines in Appendix A. As indicated in Figure 9, the fault zone is coincident with the lower boundary of the northeast plume and has the same strike as the edge of the plume. Additionally, the southern end of BNS could be part of this trend; however, data quality prohibits a definitive correlation of features at this point.

Other evidence for structural control of the northeast plume comes from data obtained using the optimum offset method. This technique was applied to lines C3, E, and a section

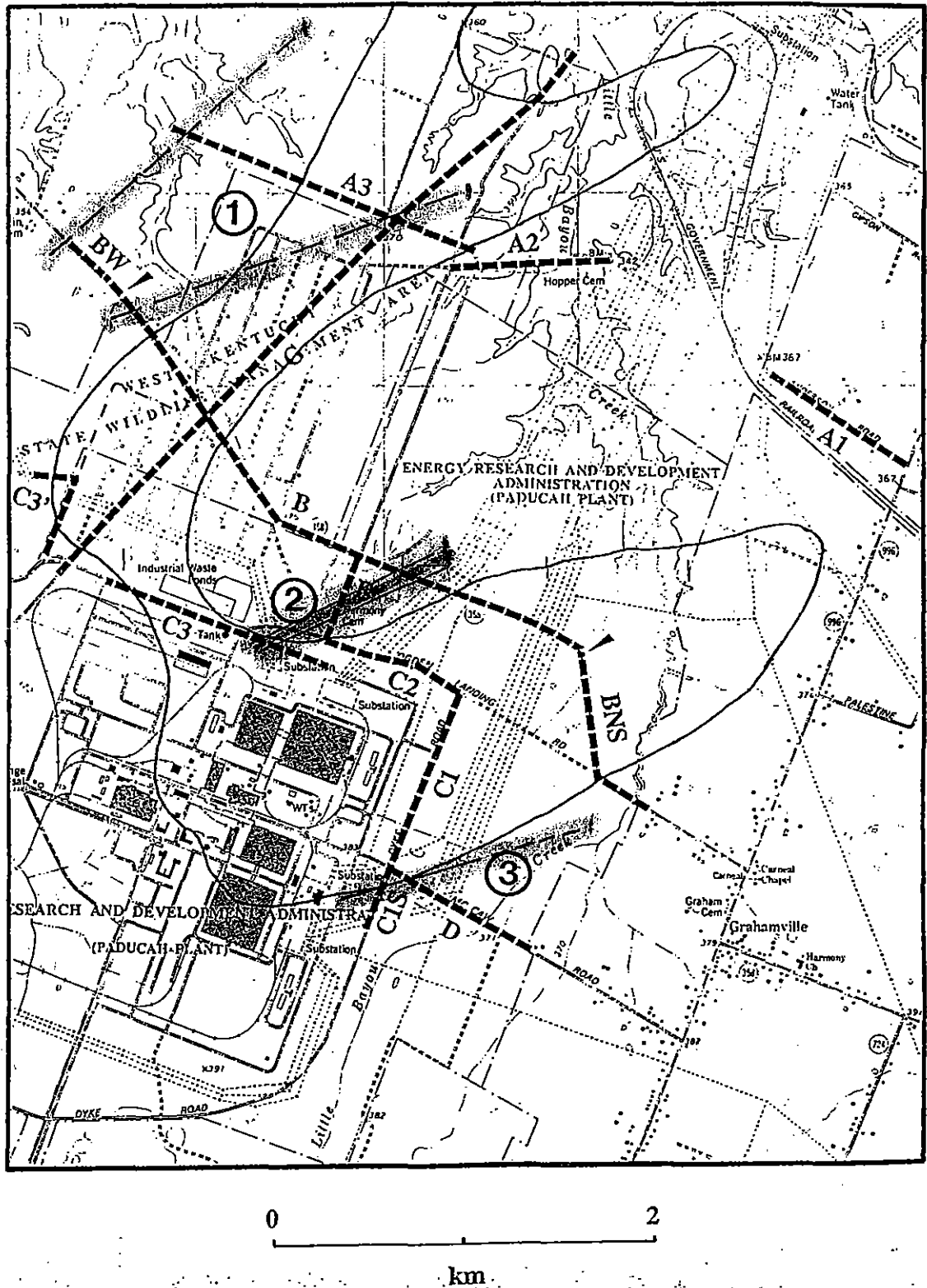


Figure 9. Map showing locations of fault zones in relation to locations of seismic lines and contaminant plumes.

of line B (corresponding to an area between shotpoints 505 and 672). The results are shown in Appendix D. Here, continuous subsurface coverage is obtained by taking data from single but successive traces within a desired area (Burger, 1992). When data from each line is oriented according to the actual positions of each line, a northeast-trending zone of displacement is apparent; the intersection of E and B is marked by a low point in the reflector at 200 ms; line C3 also exhibits a low point in the reflector past shotpoint 52. This zone of faulting coincides with the upper boundary of the northeast-trending contaminant plume. This area is indicated in Figure 9 as zone '2'; it is also indicated on the interpreted seismic sections in Appendix A.

4.5 OTHER FEATURES

As mentioned in the discussion of lines A3, G, and B, a large graben was found in the northwest corner of the study area. The graben is illustrated in Figure 9 as fault zone '3'. The strike of the graben is roughly N50°E to N60°E, which agrees with the general strikes of faults belonging to the Fluorspar Area Fault Complex that have been recently mapped in southern Illinois by Nelson et al. (1997). Nelson et al (1997) present evidence of movement along the Lusk Creek Fault Zone, Hobbs Creek Fault Zone, and Barnes Creek Fault Zone, indicating that faults have displaced Quaternary strata.

The existence of this graben is an indication that significant faulting and zones of faulting might also be present in the western Kentucky area, but have not been identified because

of the thick sedimentary cover of Cretaceous and younger sediments. Further work needs to be done in order to ascertain the extent of faulting of all ages in the area.

5.0 SUMMARY

Seventeen km of SH-wave seismic reflection and refraction data were collected in the vicinity of the Paducah Gaseous Diffusion Plant to test the hypothesis that faulting in Paleozoic bedrock and post-Paleozoic sediments could be controlling the migration of the contaminant plumes emanating from the PGDP facility.

Faulting in the bedrock and overlying sediments was found on all of the seismic lines shot for this study. Two major zones of faulting have been identified in the northeastern part of the DOE reservation and are coincidental with the direction of migration and edges of the northeast contaminant plume. In the northwestern quadrant of the study area, a large northeast-trending graben was imaged. The graben and faulting imaged by seismic data in this study are probably related to similar features being investigated by Nelson et al. (1997) in southernmost Illinois. The trend of the faults, and the fact that many of these faults appear to propagate from the bedrock into the RGA, strongly suggests that faulting is controlling the migration of the contaminant plumes associated with the PGDP.

References

Burger, H. R., 1992, Exploration Geophysics of the Shallow Subsurface: Prentice-Hall, Inc., Englewood Cliffs, New Jersey, 489 p.

Clausen, J. L., Douthitt, J. W., Davis, K. R., and Phillips, B. E., 1992, Report of the Paducah Gaseous Diffusion Plant Groundwater Investigation Phase III: KY/E-150, Martin Marietta Energy Systems, Inc., Paducah Gaseous Diffusion Plant.

Dobrin, M. B., and Savit, C. H., 1988, Introduction to Geophysical Prospecting: McGraw-Hill, Inc., 867 p.

Hansen, A. J., Jr., 1966, Availability of Ground Water in the Kentucky Parts of the Joppa and Metropolis Quadrangles, Jackson Purchase Region, Kentucky: Hydrologic Investigations Atlas HA-171, U. S. Department of the Interior, U. S. Geological Survey.

Harris, J. B., 1992, Site Amplification of Seismic Ground Motions in the Paducah, Kentucky Area: Ph.D. Dissertation, University of Kentucky, Lexington, Kentucky.

Heigold, P. C., and Kolata, D. R., 1993, Proterozoic Crustal Boundary in the Southern Part of the Illinois Basin: *Tectonophysics*, 217, p. 307-319.

Hildenbrand, T. G., and Hendricks, J. D., 1995, Geophysical Setting of the Reelfoot Rift and Relations Between Rift Structures and the New Madrid Seismic Zone: U. S. Geological Survey, Professional Paper 1538-E, 30 p.

Hunter, J. A., Pullan, S. E., Burns, R. A., Gagne, R. M., and Good, R. L., 1984, Shallow Seismic Reflection Mapping of the Overburden-Bedrock Interface with the Engineering Seismograph--Some Simple Techniques: *Geophysics*, v. 49, p. 1381-1385.

Nelson, W. J., Denny, F. B., Devera, J. A., Follmer, L. R., and Masters, J. M., 1997, Tertiary and Quaternary Tectonic Faulting in Southernmost Illinois: *Engineering Geology*, v. 46, p. 235-258.

Northeast Plume Preliminary Characterization Summary Report, Department of Energy, 1995.

Olive, W. W., 1966, Lake Paducah, of Late Pleistocene Age, in Western Kentucky and Southern Illinois: U. S., Geological Survey Professional Paper 550-D, p. D87-D88.

Olive, W. W., 1972, Geology of the Jackson Purchase Region, Kentucky: Geological Society of Kentucky Spring Field Conference, 11 p.

Olive, W. W., 1980, Geologic Maps of the Jackson Purchase Region, Kentucky: U. S. Geological Survey, Map I-1217.

Pryor, W. A., 1960, Cretaceous Sedimentation in Upper Mississippi Embayment: American Association of Petroleum Geologists Bulletin, v. 44, no. 9, p. 1473-1504.

Results of Site Investigation Phase II at the Paducah Gaseous Diffusion Plant, Paducah, Kentucky, Department of Energy, 1992.

Schwalb, H. R., 1969, Paleozoic Geology of the Jackson Purchase Region, Kentucky, with Reference to Petroleum Possibilities: Kentucky Geological Survey, Ser. 10, Rept. Inv. 10, 40 p.

Seismic Image Software, Ltd., 1995, Vista 7.1 Notes, 261 p.

Sheriff, R. E., 1973, Encyclopedic Dictionary of Exploration Geophysics: Tulsa, Society of Exploration Geophysicists.

Sheriff, R. E., and Geldart, L. P., 1982, Exploration Seismology; Volume 1: History, Theory, and Data Acquisition: Cambridge, Cambridge University Press, 253 p.

Sykora, D. W., and Davis, J. J., 1993, Site-Specific Earthquake Response Analysis for Paducah Gaseous Diffusion Plant, Paducah, Kentucky: U. S. Army Corps of Engineers Miscellaneous Paper GL-93-14, 118 p.

Williams, R. A., Odum, J. K., Pratt, T. L., Shedlock, K. M., and Stephenson, W. J., 1995, Seismic Surveys Assess Earthquake Hazard in the New Madrid Area: The Leading Edge, v. 14, no. 1, p. 30-34.

Appendix A

UNINTERPRETED AND INTERPRETED SEISMIC SECTIONS

Appendix B

PROCESSING PROCEDURES, LINES A1-G

Line A1

files 1-120:

1. Preprocessing
 - band-pass filtering (25 35 50 55)Hz
 - 200 AGC scaling
 - reformatting of data to SEG-Y format
2. Configuration of field geometry into headers
3. Application of headers to SEG-Y files
4. Velocity Analysis
5. Normal-Moveout Correction
6. CDP Sort
7. CDP Stack
8. 250 AGC post-stack scaling
9. post-stack 3-trace mixing (25 50 25 weights)

files 97-240:

1. Preprocessing
 - band-pass filtering (25 35 50 55)Hz
 - 200 AGC scaling
 - reformatting of data to SEG-Y format
2. Configuration of field geometry into headers
3. Application of headers to SEG-Y files
4. Velocity Analysis
5. Normal-Moveout Correction
6. CDP Sort
7. CDP Stack

Line A2

1. Preprocessing
 - band-pass filtering (25 35 50 55)Hz
 - 200 AGC scaling
 - reformatting of data to SEG-Y format
2. Configuration of field geometry into headers
 - elevation static corrections
3. Application of headers to SEG-Y files
4. Velocity Analysis
5. Normal-Moveout Correction
6. CDP Sort
7. CDP Stack
8. post-stack F-K filtering
9. 250 AGC post-stack scaling
10. post-stack 3 trace mixing (25 50 25 weights)

Line A3

1. Preprocessing
 - band-pass filtering (15 25 50 60)Hz
 - 200 AGC scaling
 - reformatting of data to SEG-Y format
2. Configuration of field geometry into headers
 - elevation static corrections
3. Application of headers to SEG-Y files
4. Velocity Analysis
5. Normal-Moveout Correction
6. CDP Sort
7. CDP Stack
8. 250 AGC post-stack scaling
9. post-stack 3 trace mixing (25 50 25 weights)

Line B

BW:

1. Preprocessing
 - band-pass filtering (25 35 50 60)Hz
 - 200 AGC scaling
 - reformatting of data to SEG-Y format
2. Configuration of field geometry into headers
3. Application of headers to SEG-Y files
4. Velocity Analysis
5. Normal-Moveout Correction
6. CDP Sort
7. CDP Stack
8. post-stack F-K filtering
9. 250 AGC post-stack scaling
10. post-stack 3-trace mixing (25 50 25 weights)

files 1-216:

1. Preprocessing
 - band-pass filtering (25 35 50 60)Hz
 - 200 AGC scaling
 - reformatting of data to SEG-Y format
2. Configuration of field geometry into headers
3. Application of headers to SEG-Y files
4. Velocity Analysis
5. Normal-Moveout Correction
6. CDP Sort
7. CDP Stack
8. 250 AGC post-stack scaling
9. post-stack 3 trace mixing (25 50 25 weights)

files 193-384:

1. Preprocessing
 - band-pass filtering (25 35 50 60)Hz
 - 200 AGC scaling
 - reformatting of data to SEG-Y format
2. Configuration of field geometry into headers
3. Application of headers to SEG-Y files
4. Velocity Analysis
5. Normal-Moveout Correction
6. CDP Sort
7. CDP Stack
8. 250 AGC post-stack scaling
9. post-stack 3 trace mixing (25 50 25 weights)

files 361-720:

1. Preprocessing
 - band-pass filtering (25 35 50 60)Hz
 - 200 AGC scaling
 - reformatting of data to SEG-Y format
2. Configuration of field geometry into headers
3. Application of headers to SEG-Y files
4. Velocity Analysis
5. Normal-Moveout Correction
6. CDP Sort
7. CDP Stack
8. 250 AGC post-stack scaling
9. post-stack 3 trace mixing (25 50 25 weights)

files 697-816:

1. Preprocessing
 - band-pass filtering (25 35 50 60)Hz
 - 200 AGC scaling
 - reformatting of data to SEG-Y format
2. Configuration of field geometry into headers
3. Application of headers to SEG-Y files
4. Velocity Analysis
5. Normal-Moveout Correction
6. CDP Sort
7. CDP Stack
8. post-stack F-K filtering
9. 250 AGC post-stack scaling
10. post-stack 3 trace mixing (25 50 25 weights)

files 793-1008:

1. Preprocessing
 - band-pass filtering (25 35 50 60)Hz
 - 200 AGC scaling
 - reformatting of data to SEG-Y format
2. Configuration of field geometry into headers
3. Application of headers to SEG-Y files
4. Velocity Analysis
5. Normal-Moveout Correction
6. CDP Sort
7. CDP Stack
8. post-stack F-K filtering
9. 250 AGC post-stack scaling
10. post-stack 3 trace mixing (25 50 25 weights)

files 985-1090:

1. Preprocessing
 - band-pass filtering (25 35 50 60)Hz
 - 200 AGC scaling
 - reformatting of data to SEG-Y format
2. Configuration of field geometry into headers
3. Application of headers to SEG-Y files
4. Velocity Analysis
5. Normal-Moveout Correction
6. CDP Sort
7. CDP Stack
8. post-stack F-K filtering
9. 250 AGC post-stack scaling
10. post-stack 3 trace mixing (25 50 25 weights)

Line C1

1. Preprocessing
 - band-pass filtering (25 35 55 60)Hz
 - 200 AGC scaling
 - reformatting of data to SEG-Y format
2. Configuration of field geometry into headers
3. Application of headers to SEG-Y files
4. Velocity Analysis
5. Normal-Moveout Correction
6. CDP Sort
7. CDP Stack
8. 500 AGC post-stack scaling
9. post-stack F-K filtering
10. post-stack 3 trace mixing (25 50 25 weights)

Line C1S

1. Preprocessing
 - band-pass filtering (25 35 55 60)Hz
 - 200 AGC scaling
 - reformatting of data to SEG-Y format
2. Configuration of field geometry into headers
3. Application of headers to SEG-Y files
4. Velocity Analysis
5. Normal-Moveout Correction
6. CDP Sort
7. CDP Stack
8. post-stack F-K filtering
9. 500 AGC post-stack scaling
10. post-stack 3 trace mixing (25 50 25 weights)

Line C2

1. Preprocessing
 - band-pass filtering (25 35 55 60)Hz
 - 200 AGC scaling
 - reformatting of data to SEG-Y format
2. Configuration of field geometry into headers
3. Application of headers to SEG-Y files
4. Velocity Analysis
5. Normal-Moveout Correction
6. CDP Sort
7. CDP Stack
8. post-stack 3 trace mix (25 50 25 weights)

Line C3

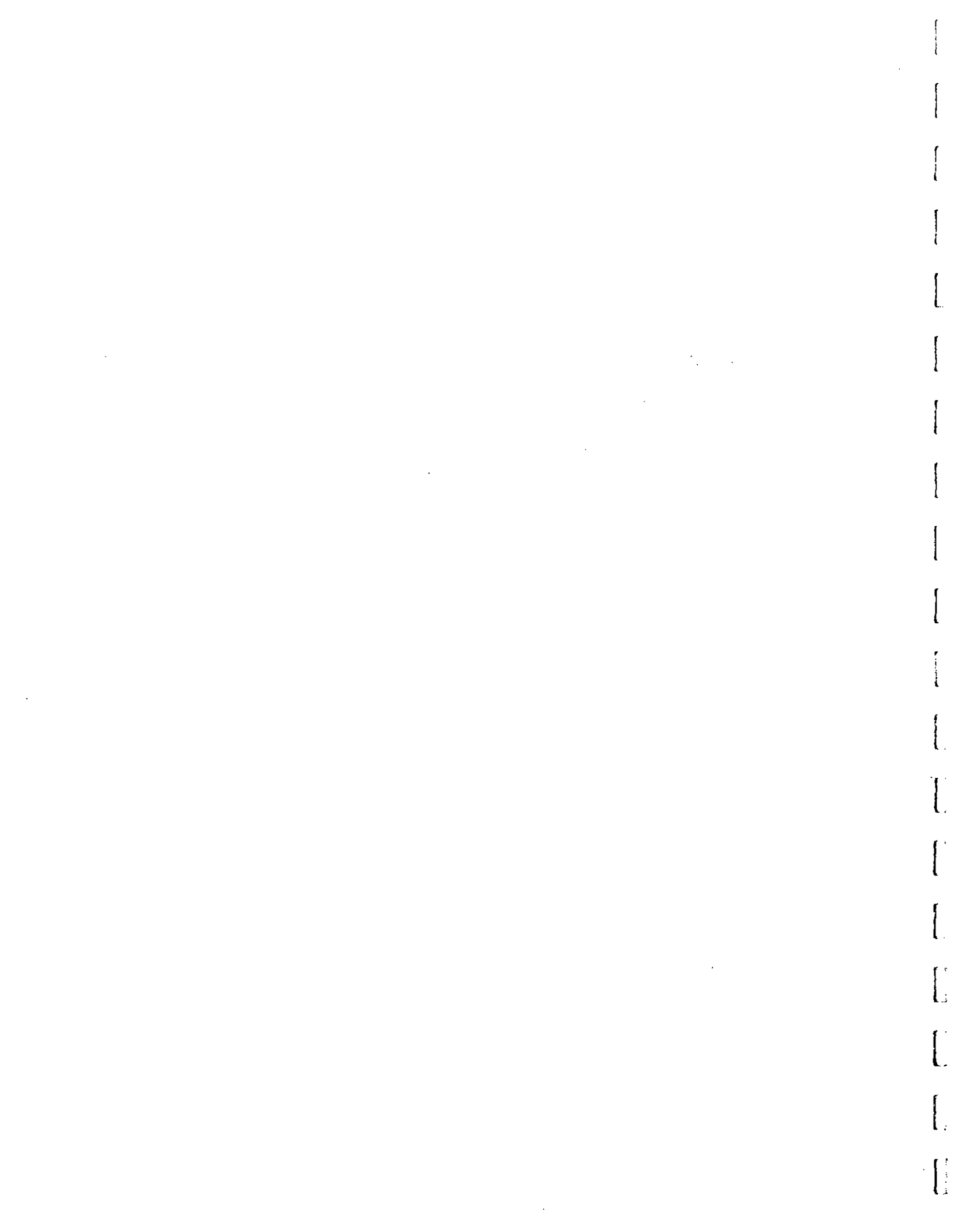
1. Preprocessing
 - band-pass filtering (25 35 55 60)Hz
 - 300 AGC scaling
 - reformatting of data to SEG-Y format
2. Configuration of field geometry into headers
3. Application of headers to SEG-Y files
4. Velocity Analysis
5. Normal-Moveout Correction
6. CDP Sort
7. CDP Stack
8. 250 AGC post-stack scaling
9. post-stack 3 trace mixing (25 50 25 weights)

Line C3'

1. Preprocessing
 - band-pass filtering (25 35 55 60)Hz
 - 200 AGC scaling
 - reformatting of data to SEG-Y format
2. Configuration of field geometry into headers
3. Application of headers to SEG-Y files
4. Velocity Analysis
5. Normal-Moveout Correction
6. CDP Sort
7. CDP Stack

Line C3' extended

1. Preprocessing
 - band-pass filtering (25 35 55 60)Hz
 - 200 AGC scaling
 - reformatting of data to SEG-Y format
2. Configuration of field geometry into headers
3. Application of headers to SEG-Y files
4. Velocity Analysis
5. Normal-Moveout Correction
6. CDP Sort
7. CDP Stack
8. 250 AGC post-stack scaling
9. post-stack 3 trace mixing (25 50 25 weights)



Line D

1. Preprocessing
 - band-pass filtering (5 10 45 50)Hz
 - 500 AGC scaling
 - reformatting of data to SEG-Y format
2. Configuration of field geometry into headers
3. Application of headers to SEG-Y files
4. Velocity Analysis
5. Normal-Moveout Correction
6. CDP Sort
7. CDP Stack
8. post-stack F-K filtering
9. 500 AGC post-stack scaling
10. post-stack 3 trace mixing (25 50 25 weights)

Line E

1. Preprocessing
 - band-pass filtering (15 25 50 60)Hz
 - 200 AGC scaling
 - reformatting of data to SEG-Y format
2. Configuration of field geometry into headers
3. Application of headers to SEG-Y files
4. Velocity Analysis
5. Normal-Moveout Correction
6. CDP Sort
7. CDP Stack
8. 200 AGC post-stack scaling
9. post-stack 3 trace mixing (25 50 25 weights)

Line G

files 1-216:

1. Preprocessing
 - band-pass filtering (25 35 50 60)Hz
 - 200 AGC scaling
 - reformatting of data to SEG-Y format
2. Configuration of field geometry into headers
 - elevation static corrections
3. Application of headers to SEG-Y files
4. Velocity Analysis
5. Normal-Moveout Correction
6. CDP Sort
7. CDP Stack
8. 250 AGC post-stack scaling
9. post-stack 3 trace mixing (25 50 25 weights)

files 193-408:

1. Preprocessing
 - band-pass filtering (25 35 50 60) Hz
 - 200 AGC scaling
 - reformatting of data to SEG-Y format
2. Configuration of field geometry into headers
3. Application of headers to SEG-Y files
4. Velocity Analysis
5. Normal-Moveout Correction
6. CDP Sort
7. CDP Stack
8. 250 AGC post-stack scaling
9. post-stack 3 trace mixing (25 50 25 weights)

files 385-552:

1. Preprocessing
 - band-pass filtering (25 35 50 60)Hz
 - 200 AGC scaling
 - reformatting of data to SEG-Y format
2. Configuration of field geometry into headers
3. Application of headers to SEG-Y files
4. Velocity Analysis
5. Normal-Moveout Correction
6. CDP Sort
7. CDP Stack
8. 250 AGC post-stack scaling
9. post-stack 3 trace mixing (25 50 25 weights)

files 529-696:

1. Preprocessing
 - band-pass filtering (25 35 50 60)Hz
 - 200 AGC scaling
 - reformatting of data to SEG-Y format
2. Configuration of field geometry into headers
3. Application of headers to SEG-Y files
4. Velocity Analysis
5. Normal-Moveout Correction
6. CDP Sort
7. CDP Stack
8. 250 AGC post-stack scaling
9. post-stack 3 trace mixing (25 50 25 weights)

files 673-768:

1. Preprocessing
 - band-pass filtering (25 35 50 60)Hz
 - 200 AGC scaling
 - reformatting of data to SEG-Y format
2. Configuration of field geometry into headers
3. Application of headers to SEG-Y files
4. Velocity Analysis
5. Normal-Moveout Correction
6. CDP Sort
7. CDP Stack
8. 250 AGC post-stack scaling
9. post-stack 3 trace mixing (25 50 25 weights)

files 745-864:

1. Preprocessing
 - band-pass filtering (25 35 50 60)
 - 200 AGC scaling
 - reformatting of data to SEG-Y format
2. Configuration of field geometry into headers
3. Application of headers to SEG-Y files
4. Velocity Analysis
5. Normal-Moveout Correction
6. CDP Sort
7. CDP Stack
8. 250 AGC post-stack scaling
9. post-stack 3 trace mixing (25 50 25 weights)

files 841-960:

1. Preprocessing
 - band-pass filtering (25 35 50 60)Hz
 - 200 AGC scaling
 - reformatting of data to SEG-Y format
2. Configuration of field geometry into headers
3. Application of headers to SEG-Y files
4. Velocity Analysis
5. Normal-Moveout Correction
6. CDP Sort
7. CDP Stack
8. 250 AGC post-stack scaling
9. post-stack 3 trace mixing (25 50 25 weights)

Appendix C

VELOCITY PICKS, LINES A1-G

Line A1

Velocity Analysis

<u>time (ms)</u>	<u>velocity (m/s)</u>	<u>depth (m)</u>
175	210	18.4
325	225	36.6
555	370	102.7
675	490	165.4
820	570	233.7

Existing well data for Line A1:

MW-133

RGA top: 20.2 m

P4-A2

RGA top: 14 m

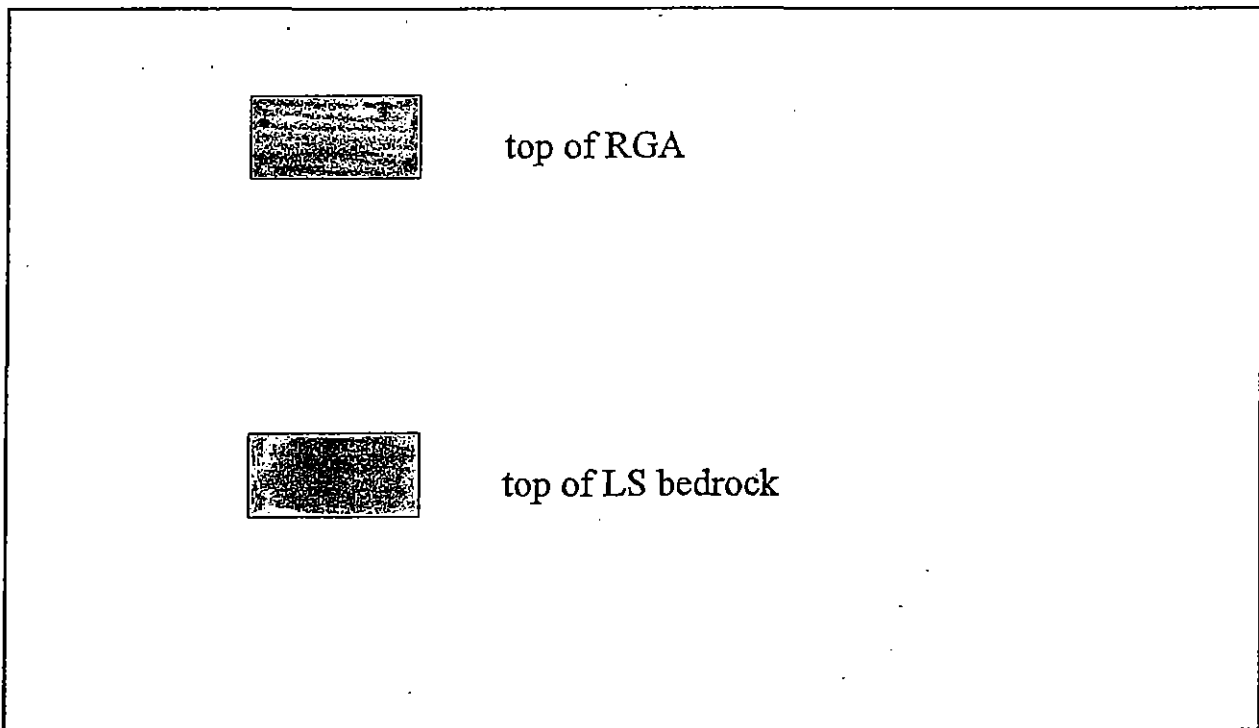
TKcm top: 29.6 m

P4-A3

RGA top: 14 m

TKcm top: 31.8 m

* TKcm denotes Clayton-McNairy interval



Line A2

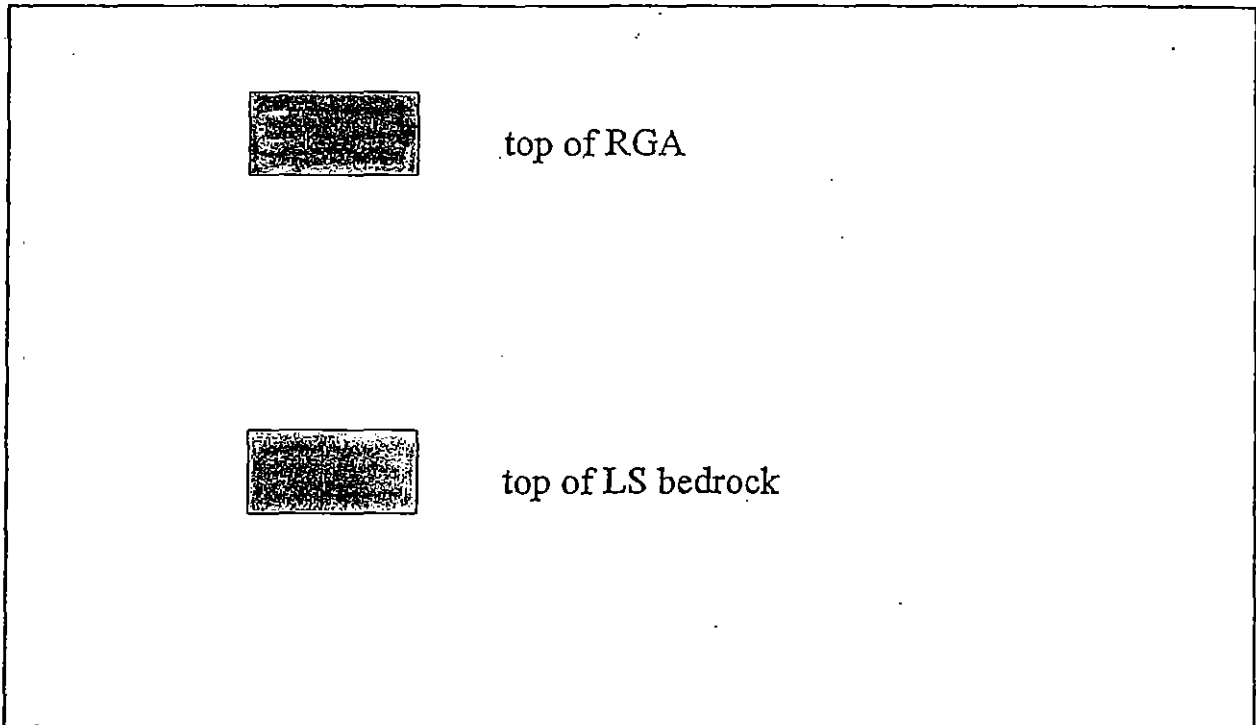
Velocity Analysis

<u>time (ms)</u>	<u>velocity (m/s)</u>	<u>depth (m)</u>
145	205	14.9
250	245	30.6
500	420	105
700	500	175
800	575	230

Existing well data for Line A2:

MW-133

RGA top: 20.2 m (approx.)



Line A3

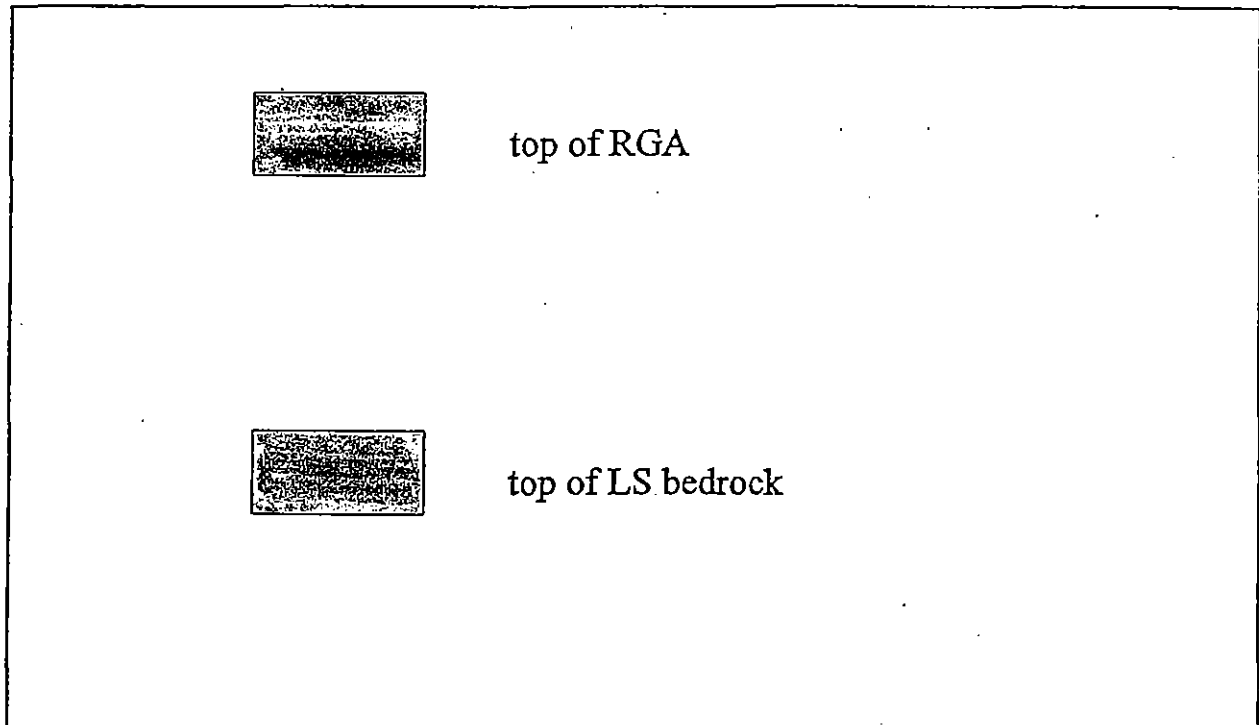
Velocity Analysis

<u>time (ms)</u>	<u>velocity (m/s)</u>	<u>depth (m)</u>
100	285	14.3
160	290	23.2
275	305	41.9
565	350	98.9
835	455	189
960	570	273.6

Existing well data for Line A3:

MW-202

RGA top: 21.9 m (approx.)



Line B (BW, B, BNS)

Velocity Analysis

<u>time (ms)</u>	<u>velocity (m/s)</u>	<u>depth (m)</u>
80	295	11.8
230	345	39.7
380	385	73.2
505	440	111.1
560	460	128.8
610	490	149.4

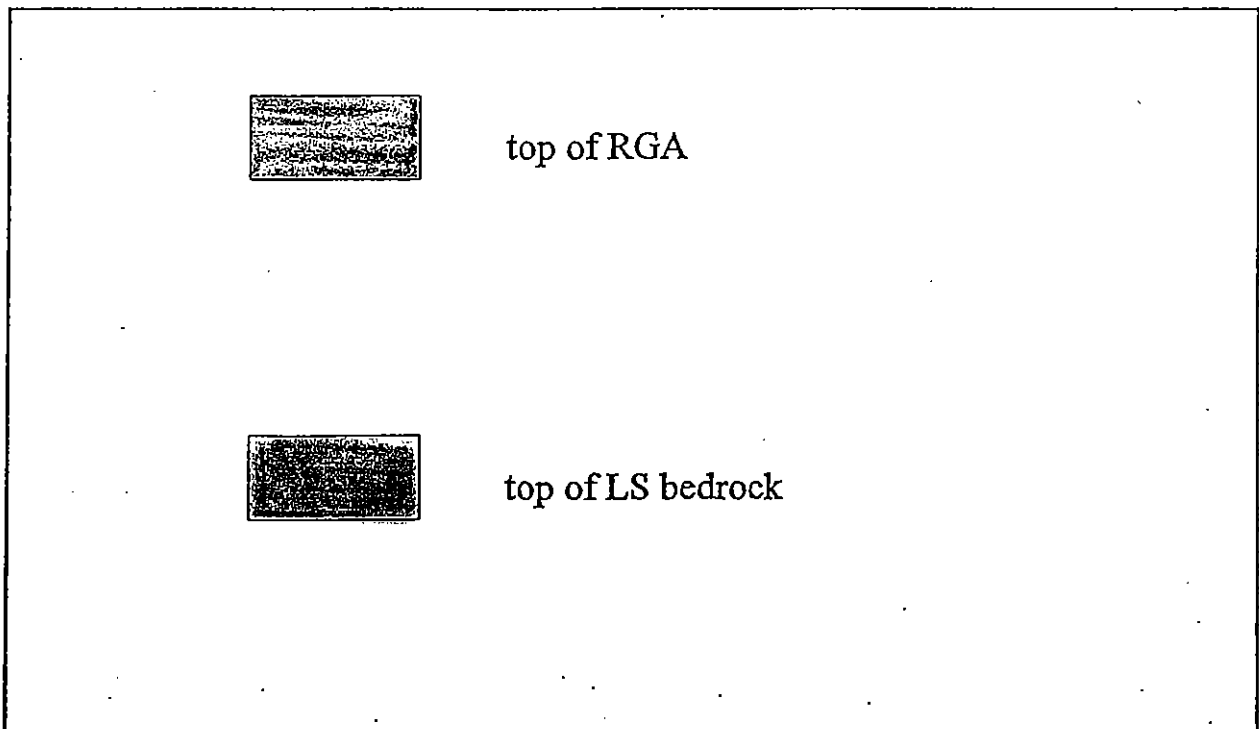
Existing well data for line B:

<u>P4-C2</u> RGA top: 16.8 m TKcm top: 27.1 m	<u>P4-C4</u> RGA top: 17.1 m TKcm top: 30.8 m	<u>P4-C5</u> RGA top: 16.2 m TKcm top: 32.9 m	<u>P4-C7</u> RGA top: 18.3 m TKcm top: 32.6 m
---	---	---	---

<u>P4-C9</u> RGA top: 17.2 m TKcm top: 34.4 m	<u>P4-C10</u> RGA top: 18.6 m TKcm top: 36 m	<u>MW-181</u> RGA top: 17.4 m	<u>MW-193</u> RGA top: 20.7 m
---	--	----------------------------------	----------------------------------

<u>MW-122</u> RGA top: 18.9 m	<u>MW-140</u> RGA top: 17.7 m
----------------------------------	----------------------------------

* TKcm denotes Clayton-McNairy interval



Line C1, C1S

Velocity Analysis

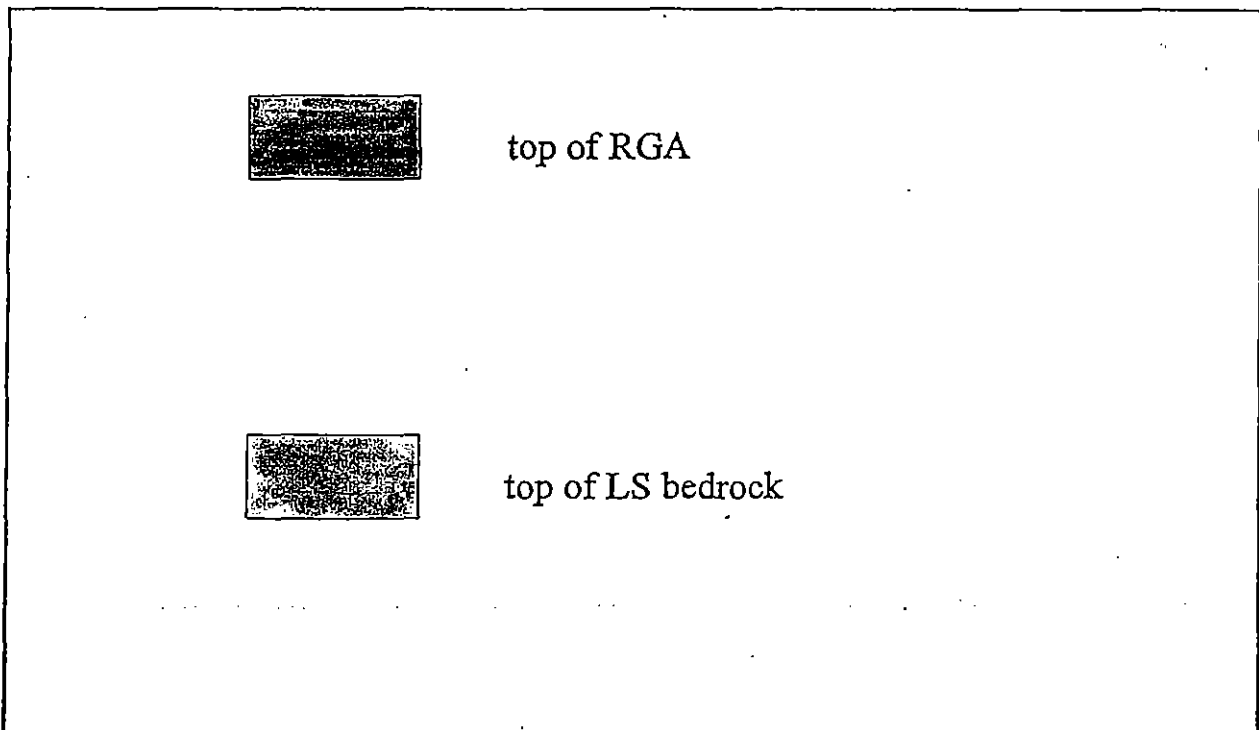
<u>time (ms)</u>	<u>velocity (m/s)</u>	<u>depth (m)</u>
110	345	19
540	370	99.9

Existing well data for Line C1, C1S:

<u>MW-144</u> RGA top: 21.6 m	<u>P4-D6</u> RGA top: 15.9 m TKcm top: 104.6 m	<u>P4-D7</u> RGA top: 18.3 m TKcm top: 50.6 m	<u>P4-D8</u> RGA top: 17.3 m TKcm top: 31.4 m
<u>P4-D9</u> RGA top: 19.5 m TKcm top: 32 m	<u>P4-D10</u> RGA top: 18.6 m TKcm top: 32.4 m	<u>P4-D12</u> RGA top: 18.8 m TKcm top: 33.2 m	<u>P4-D12A</u> RGA top: 19.1 m TKcm top: 32.2 m

P4-D11
RGA top: 18.3 m
TKcm top: 34.3 m

* TKcm denotes Clayton-McNairy interval



Line C2

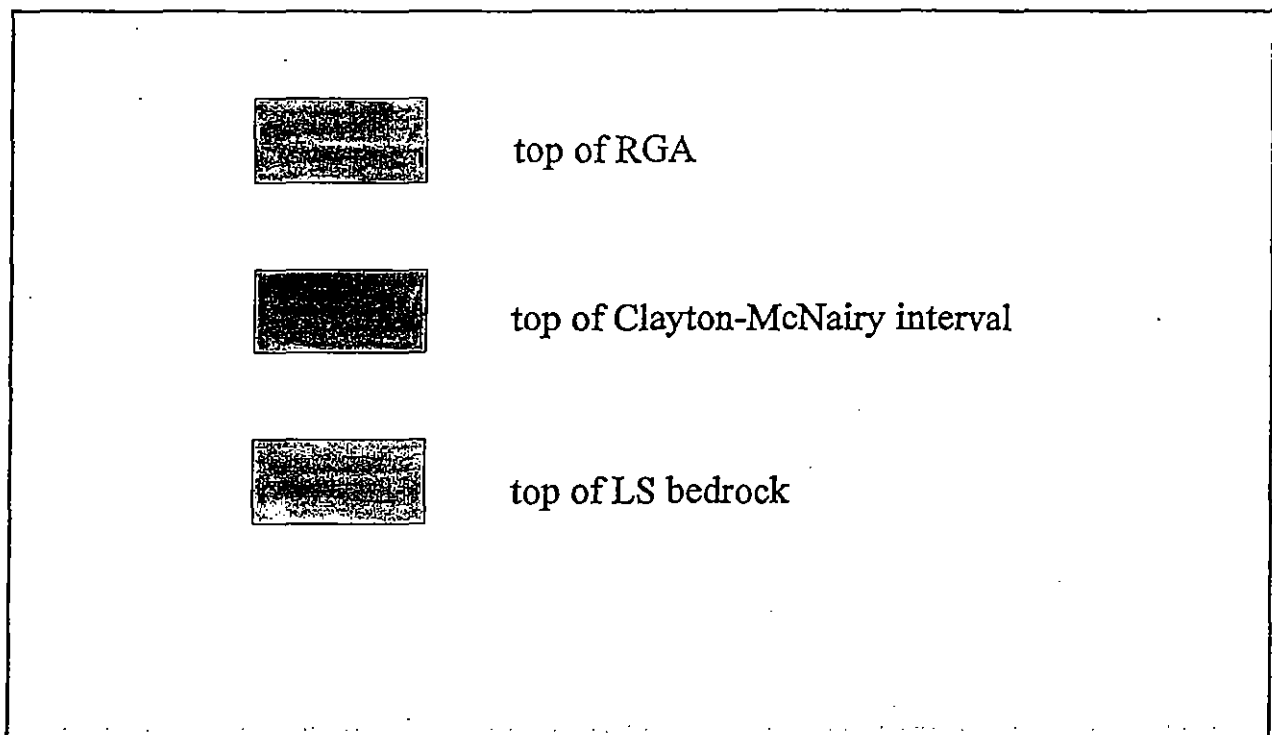
Velocity Analysis

<u>time (ms)</u>	<u>velocity (m/s)</u>	<u>depth (m)</u>
110	235	12.9
235	240	28.2
340	265	45.1
530	385	102

Existing well data for Line C2:

<u>P4-D4</u>	<u>P4-D5</u>
RGA top: 16.4 m	RGA top: 16.3 m
TKcm top: 31.1 m	TKcm top: 31.2 m

* TKcm denotes Clayton-McNairy interval



Line C3

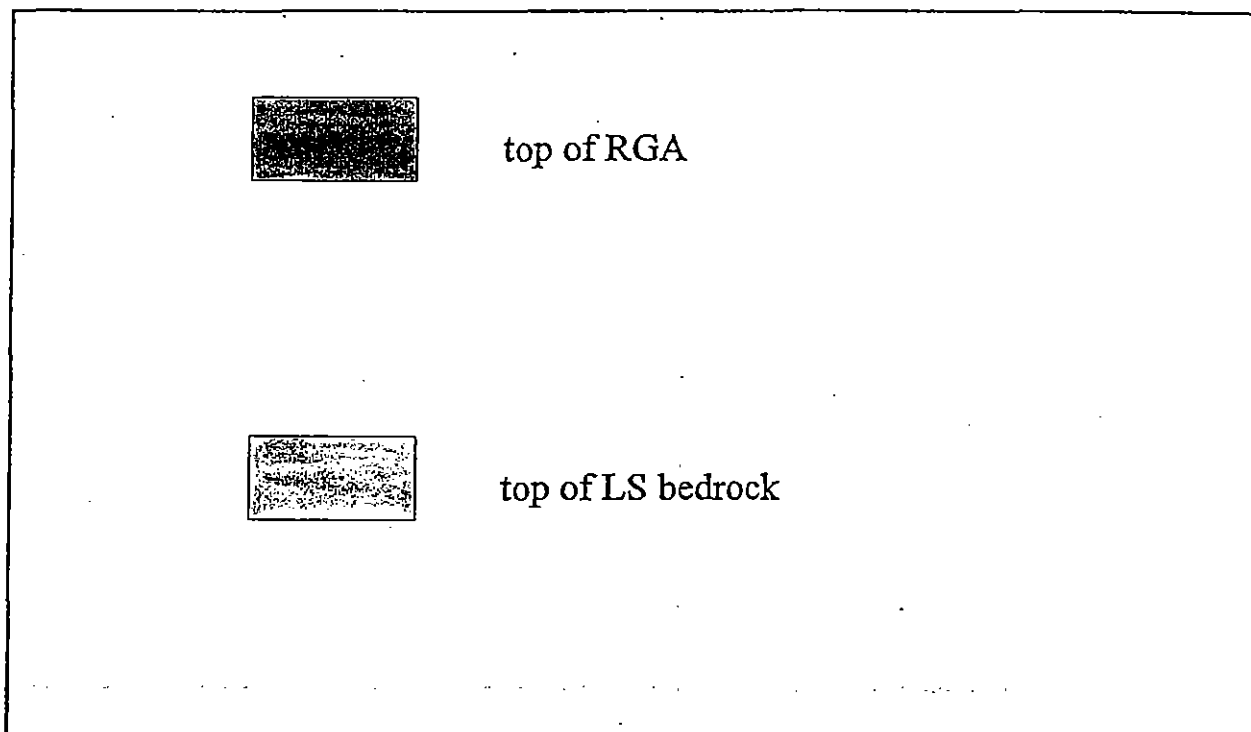
Velocity Analysis

<u>time (ms)</u>	<u>velocity (m/s)</u>	<u>depth (m)</u>
120	210	12.6
335	225	37.7
550	380	104.5
625	415	129.7
860	545	234.4
960	575	276

Existing well data for Line C3:

<u>P4-F8</u>	<u>MW-66</u>
RGA top: 13.4 m	RGA top: 17.1 m
TKcm top: 27.5 m	
LS top: 105.2 m	

*TKcm denotes Clayton-McNairy interval
LS denotes Mississippian bedrock



Line C3', C3' extended

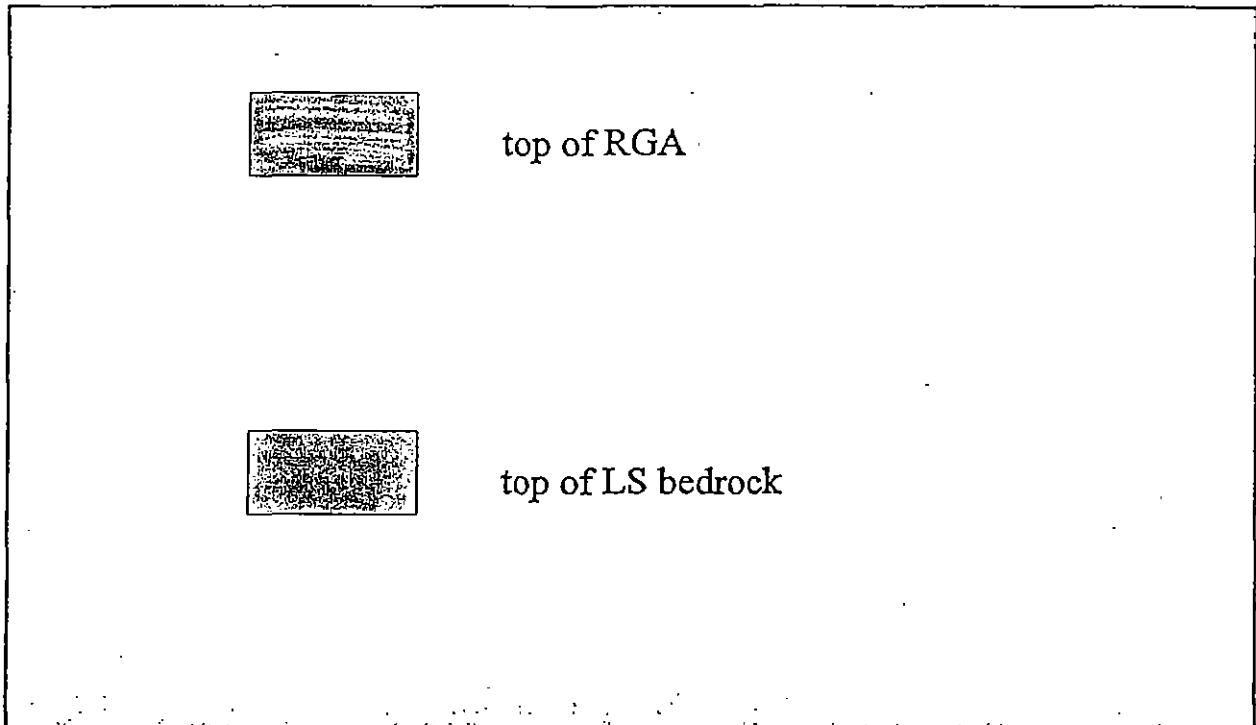
Velocity Analysis

<u>C3'</u>			<u>C3' extended</u>		
<u>time (ms)</u>	<u>velocity (m/s)</u>	<u>depth (m)</u>	<u>time (ms)</u>	<u>velocity (m/s)</u>	<u>depth (m)</u>
95	270	12.8	95	240	11.4
290	280	40.6	300	250	37.5
360	285	51.3	475	445	105.7
485	435	105	580	560	162.4
515	435	112			

Existing well data for C3', C3' extended:

MW-106
RGA top: 16.6 m

MW-194
RGA top: 19.3 m



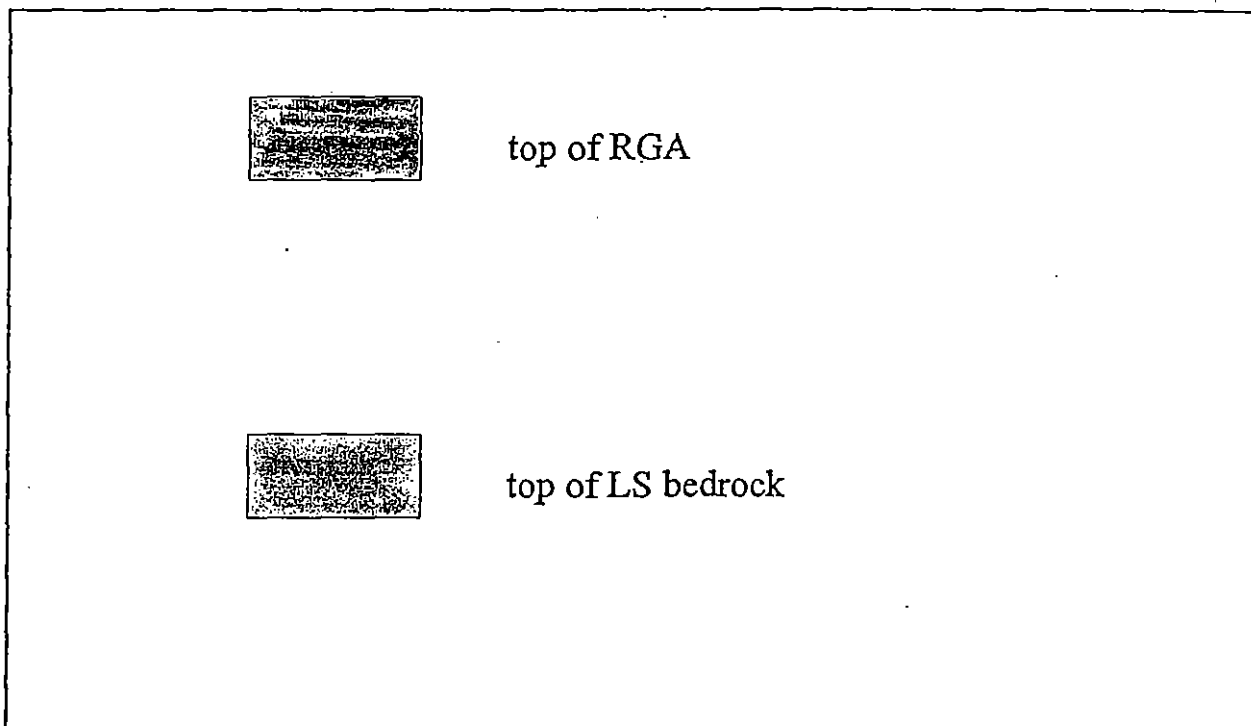
Line D

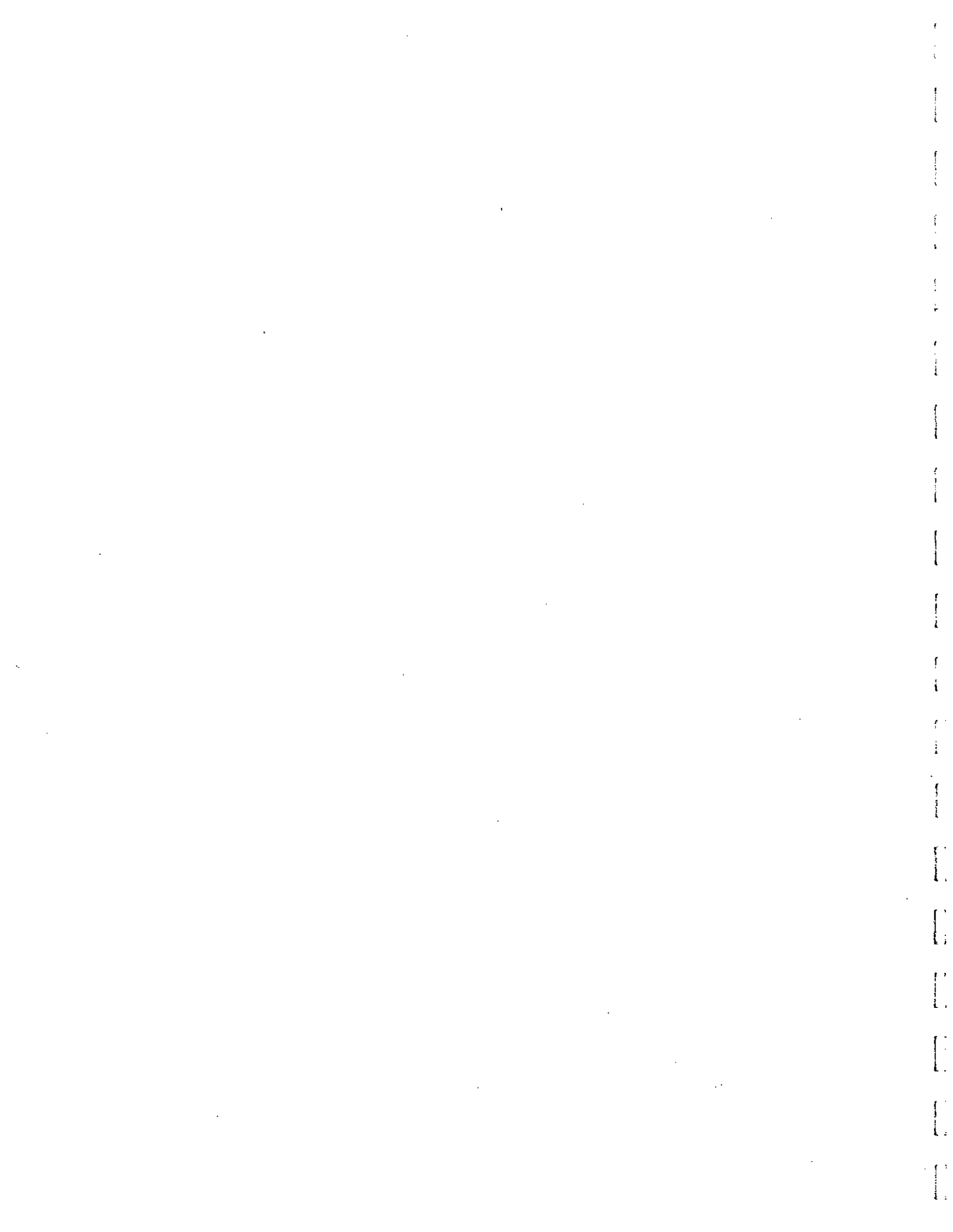
Velocity Analysis

<u>time (ms)</u>	<u>velocity (m/s)</u>	<u>depth (m)</u>
110	345	18.9
540	370	99.9

Existing well data for Line D:

<u>P4-D11</u>	<u>P4-D12</u>	<u>P4-D12A</u>	<u>P4-D10</u>
RGA top: 18.3 m	RGA top: 18.9 m	RGA top: 18.6 m	RGA top: 18.8 m





Line E

Velocity Analysis

<u>time (ms)</u>	<u>velocity (m/s)</u>	<u>depth (m)</u>
190	255	24
265	255	33.8
540	375	101.3

Existing well data for Line E:

P4-F8

RGA top: 13.4 m

TKcm top: 27.5 m

LS top: 105.2 m

P4-D4

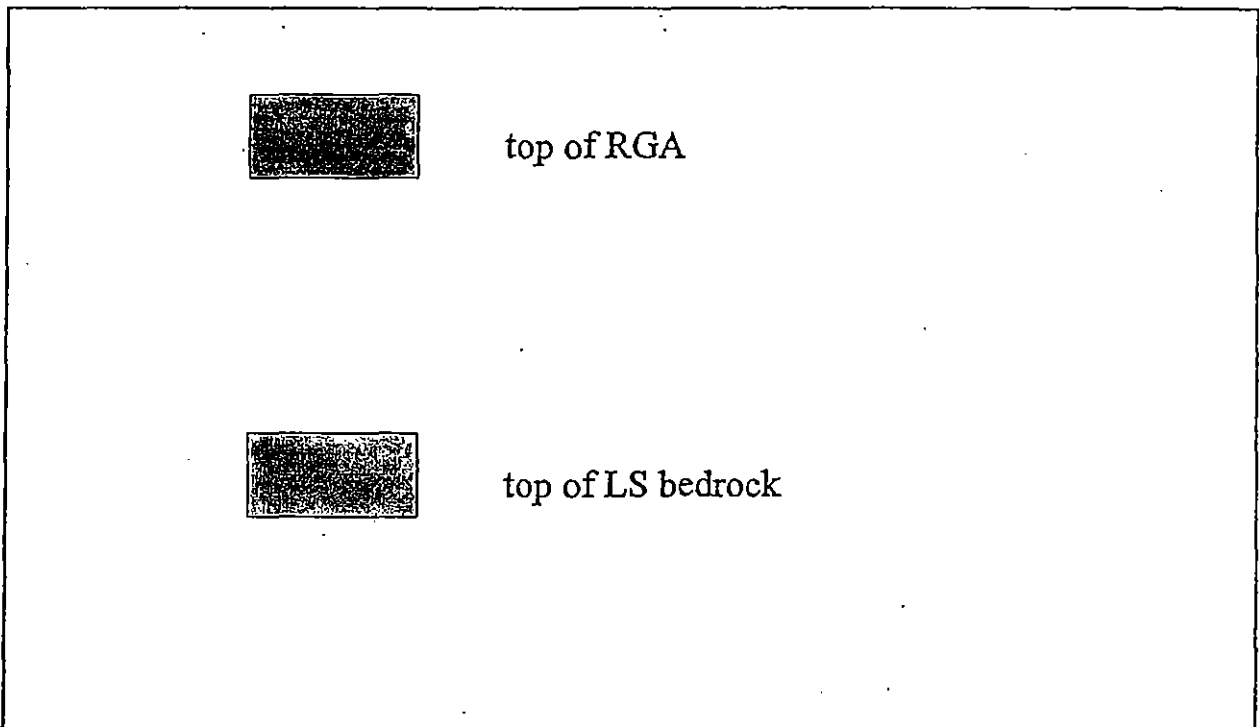
RGA top: 16.5 m

TKcm top: 31.1 m

MW-181

RGA top: 16.8 m

* TKcm denotes Clayton-McNairy interval
LS denotes Mississippian bedrock



Line G

Velocity Analysis

<u>time (ms)</u>	<u>velocity (m/s)</u>	<u>depth (m)</u>
100	250	12.5
250	290	50.8
555	370	102.7

Existing well data for Line G:

MW-Z12

RGA top: 28.6 m

TKcm top: 39.3 m

LS top: 111.8 m

MW-202

RGA top: 22 m

MW-121

RGA top: 15.1 m

TKcm top: 26.1 m

MW-106

RGA top: 16.3 m

MW-Z16

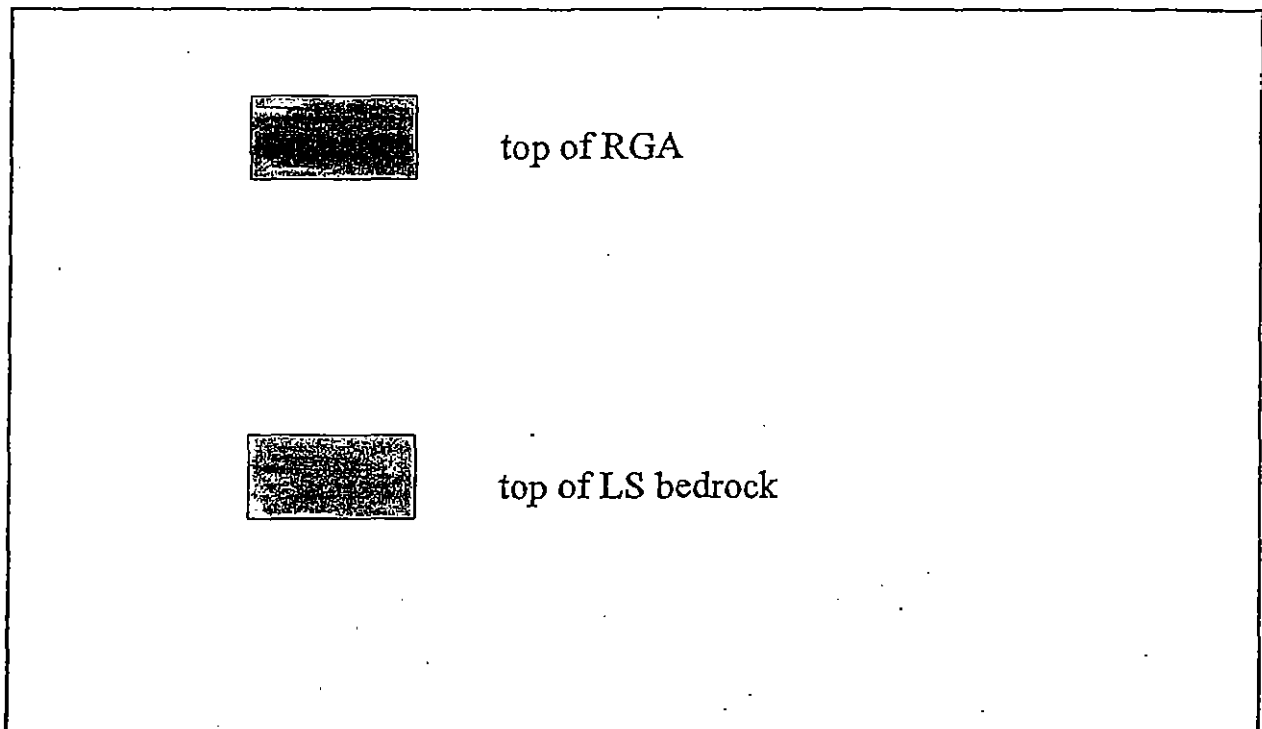
RGA top: 18.6 m

TKcm top: 30.5 m

LS top: 108.4 m

* TKcm denotes Clayton-McNairy interval

LS denotes Mississippian bedrock

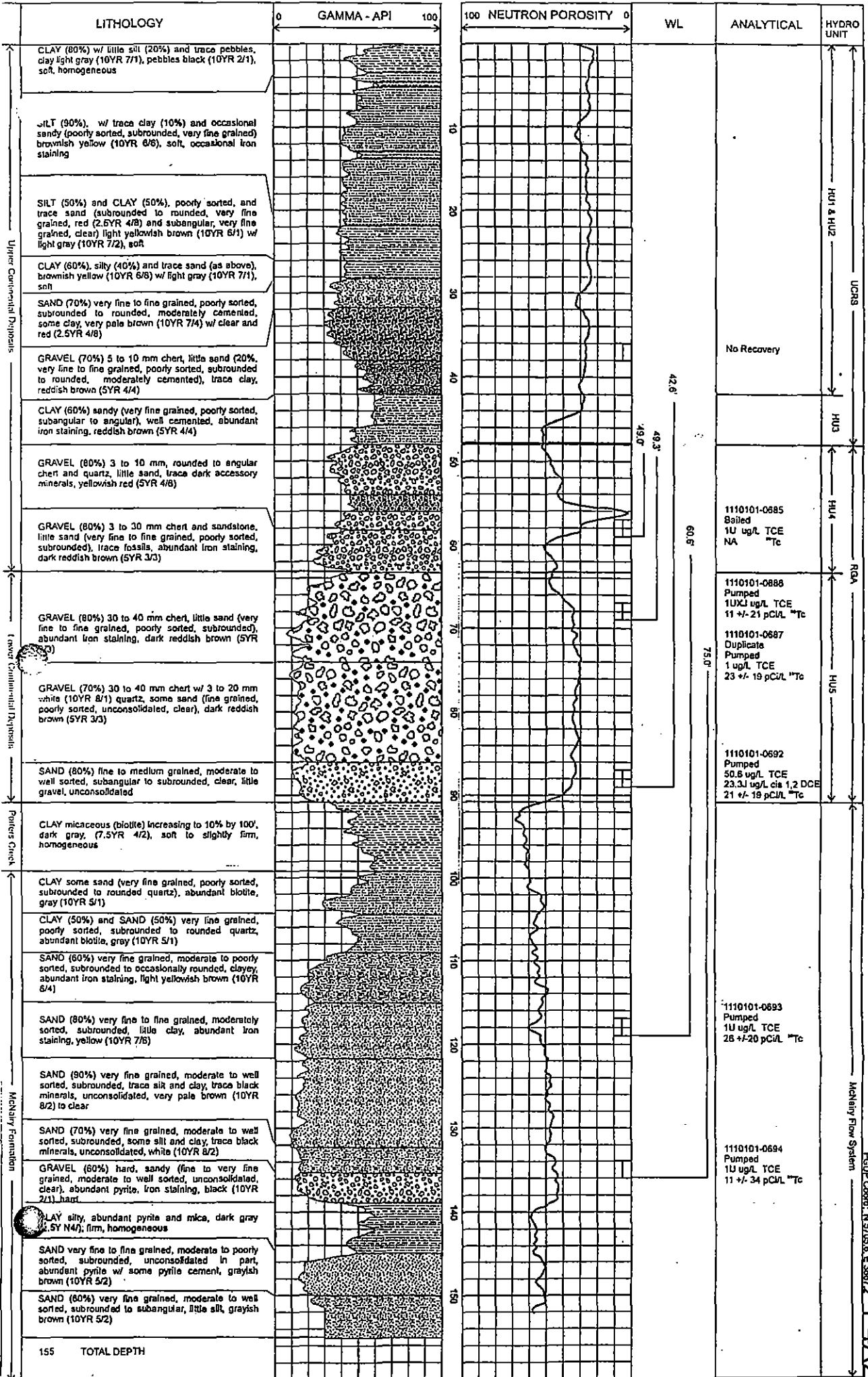


Appendix D

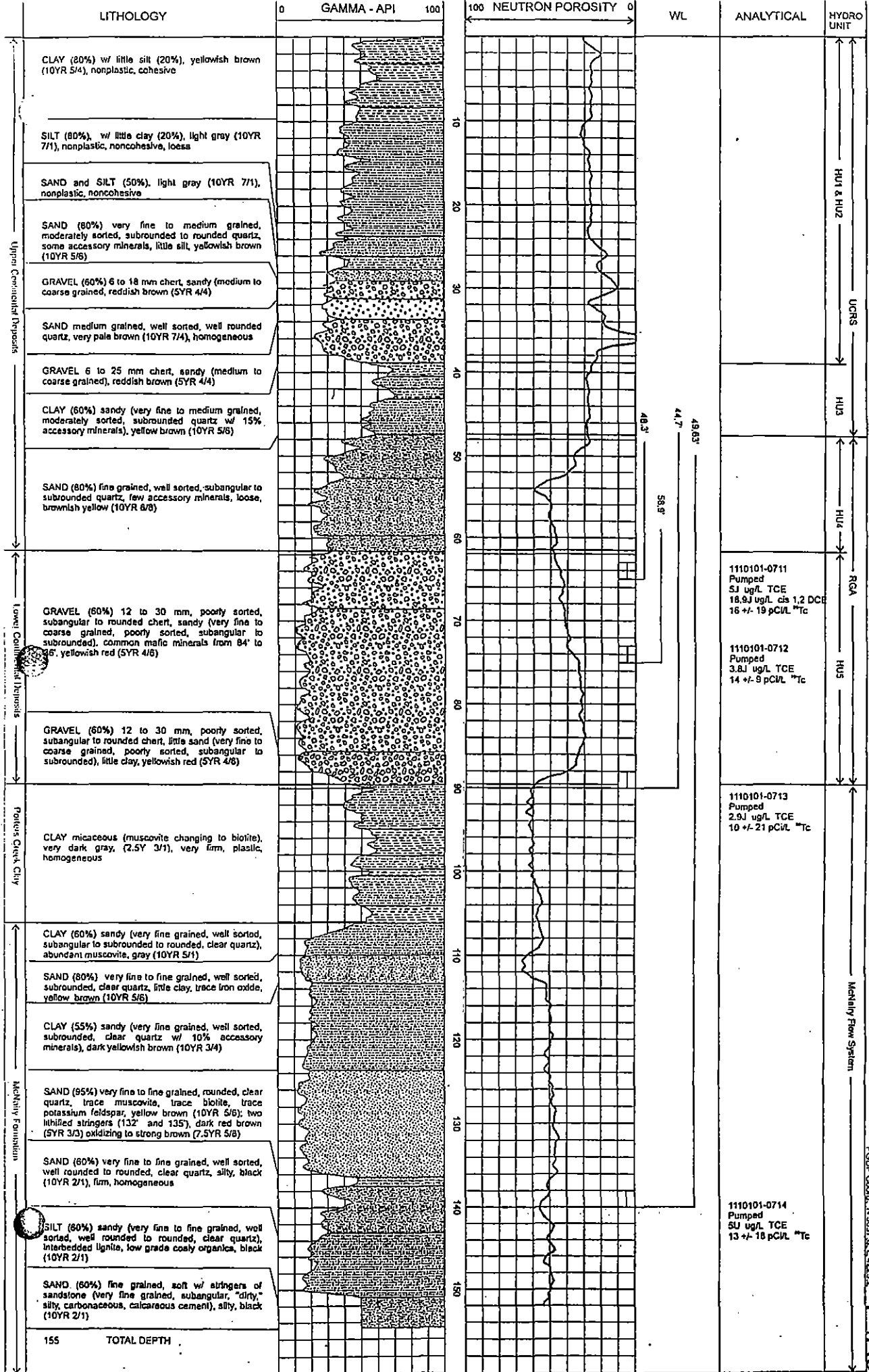
OPTIMUM OFFSET LINES

Appendix E

SOIL BORING LOGS



Elevation: 371.88
 RDP# 00001, N 3705, S 5387.2
 PAA2



Revision: 3/1/57
 RSDP Cont. N.5697.A.E.429.2

P4A3

LITHOLOGY

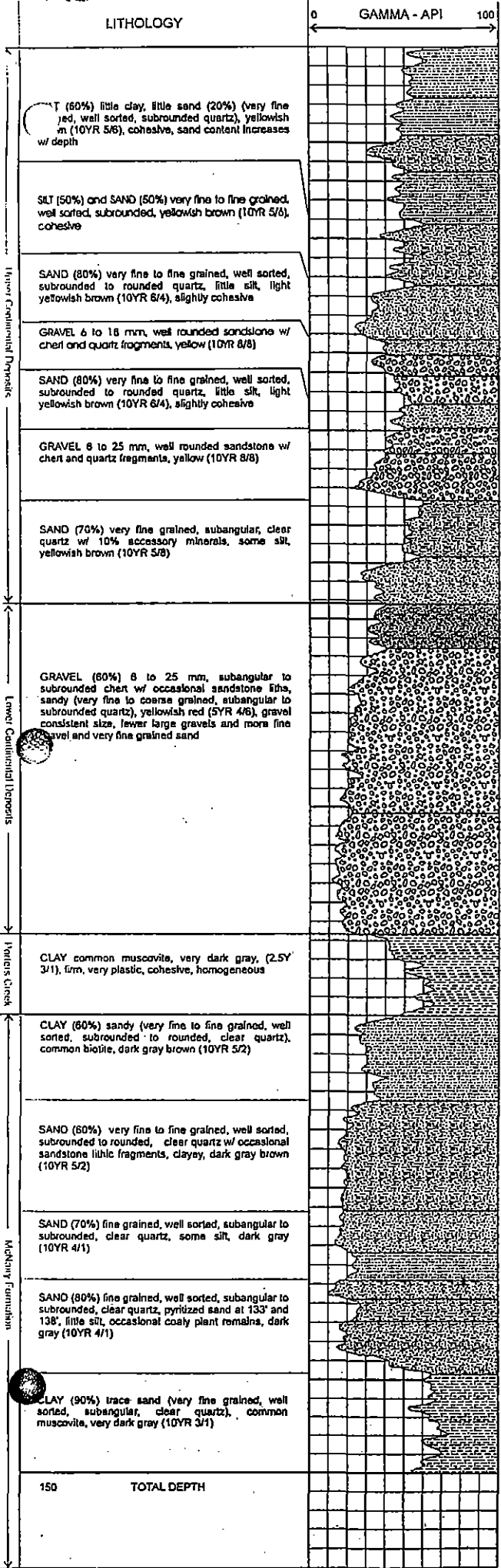
GAMMA - API

NEUTRON POROSITY

WL

ANALYTICAL

HYDRO UNIT



1110101-0715	Pumped	40.8 ug/L TCE	4 +/- 6 pCi/L ¹³⁷ Cs
1110101-0716	(Duplicate) Pumped	60.8 ug/L TCE	2 +/- 3 pCi/L ¹³⁷ Cs
1110101-0717	Bailed	183.9 ug/L TCE	NA ¹³⁷ Cs
1110101-0718	Bailed	1.1J ug/L TCE	27.4J ug/L ds DCE
1110101-0718	Bailed	1.1J ug/L TCE	27.4J ug/L ds DCE
1110101-0719	Pumped	180.1 ug/L TCE	9 +/- 17 pCi/L ¹³⁷ Cs
1110101-0720	(Duplicate) Pumped	172.3 ug/L TCE	16 +/- 17 pCi/L ¹³⁷ Cs
1110101-0721	Pumped	1.1J ug/L TCE	7 +/- 43 pCi/L ¹³⁷ Cs
1110101-0722	(Duplicate) Pumped	1.1J ug/L TCE	14 +/- 19 pCi/L ¹³⁷ Cs
1110101-0723	Pumped	5U ug/L TCE	12 +/- 17 pCi/L ¹³⁷ Cs
1110101-0724	(Duplicate) Pumped	5U ug/L TCE	11 +/- 20 pCi/L ¹³⁷ Cs

Elevation: 367.37
 PGDP Coord: N 3751.9, E 3008.9
 P4B3

Mandatory Flow System

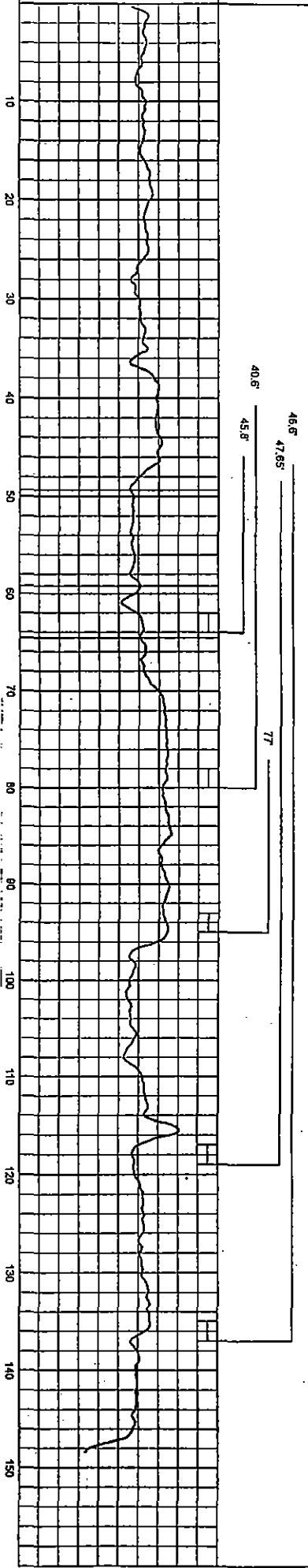
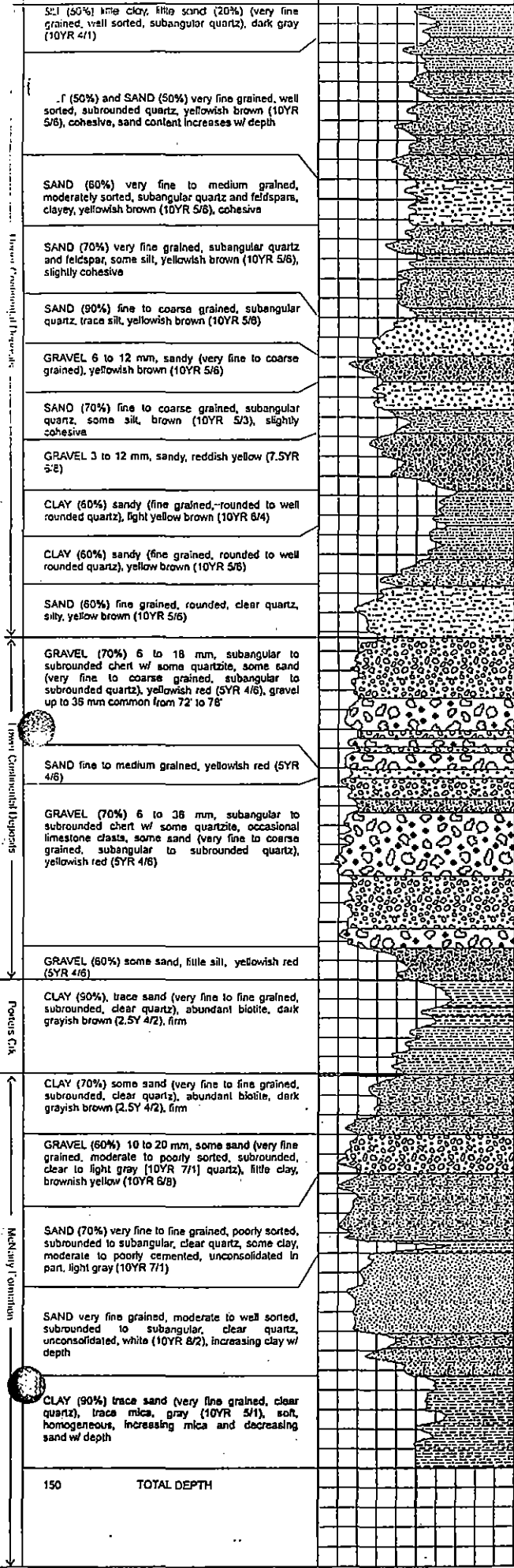
LITHOLOGY

GRAVEL - ART

WL

ANALYTICAL

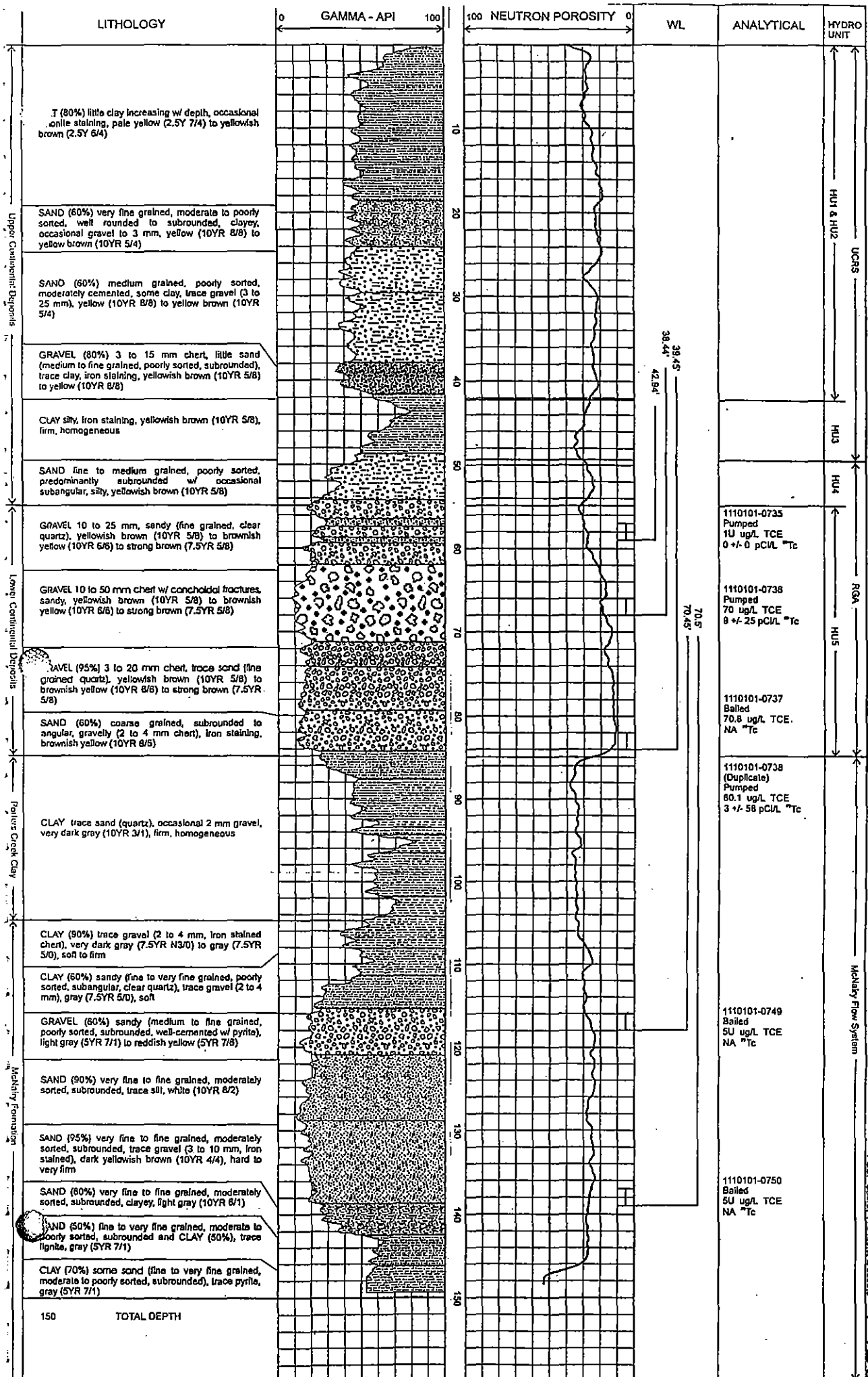
HYDRO UNIT



HYDRO UNIT	ANALYTICAL
HU1 & HU2	
UCRS	
HU3	
HU4	
RQA	<p>1110101-0729 Pumped 240 ug/L TCE 0.7J ug/L 1,1 DCE 4 +/- 9 pCi/L ²²⁶Rn</p> <p>1110101-0730 Pumped 370 ug/L TCE 3.7J ug/L 1,1 DCE 20.4J ug/L cis DCE 14 +/- 21 pCi/L ²²⁶Rn</p> <p>1110101-0731 (Duplicate) Pumped 438.6 ug/L TCE 2.8J ug/L 1,1 DCE 27.8J ug/L cis DCE 10 +/- 21 pCi/L ²²⁶Rn</p> <p>1110101-0732 Pumped 301.5 ug/L TCE 2.6J ug/L 1,1 DCE 29.9J ug/L cis DCE 2.2J ug/L carbon tet 5 +/- 8 pCi/L ²²⁶Rn</p>
HU5	
Mechanical Flow System	<p>1110101-0733 Pumped 2 ug/L TCE 0 +/- 0 pCi/L ²²⁶Rn</p> <p>1110101-0734 Bailed 1U ug/L TCE NA ²²⁶Rn</p>

Revision: 368.59
PCDP Control: N36602, E 33412

P4B4



Elevation: 366.26
 PSEP Coord: N 3428 & E 3590.3

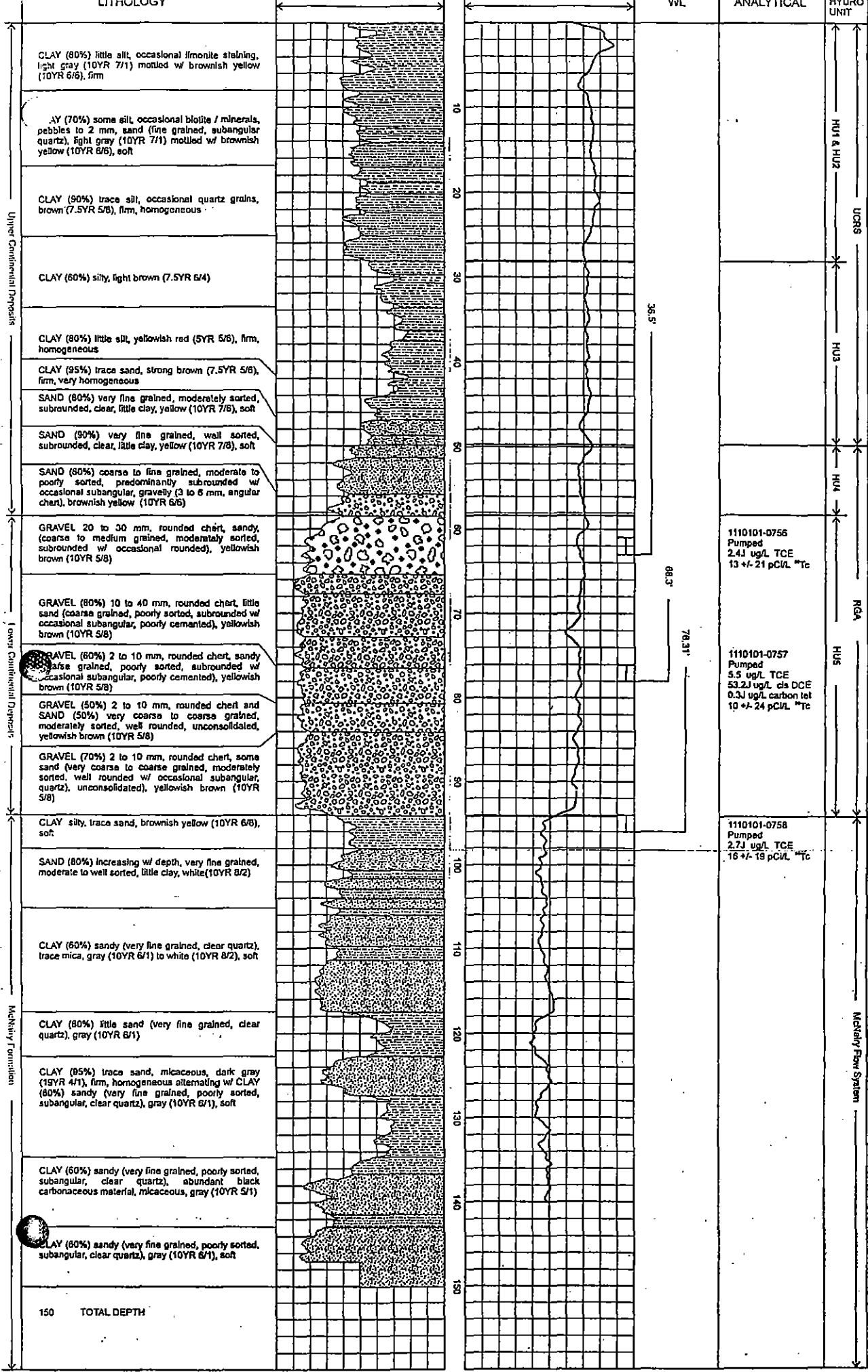
PAB5

LITHOLOGY

WL

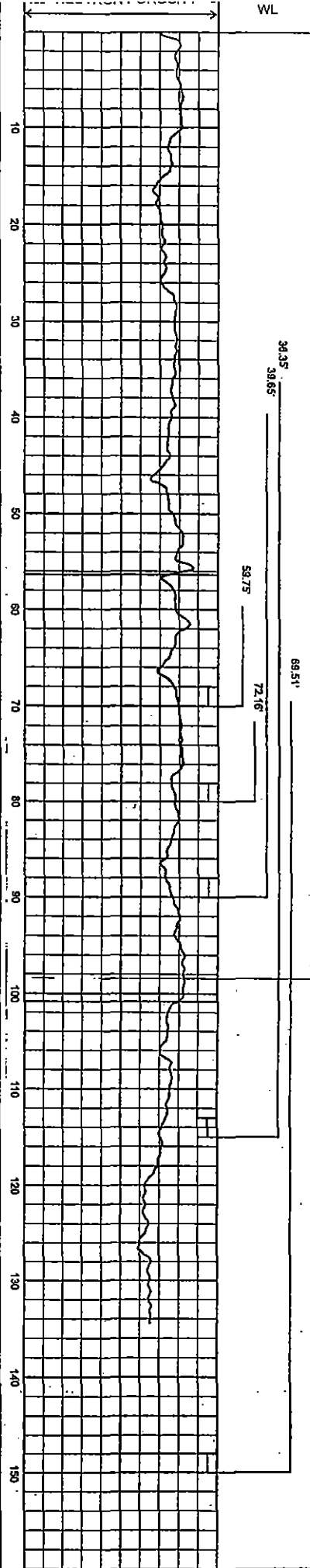
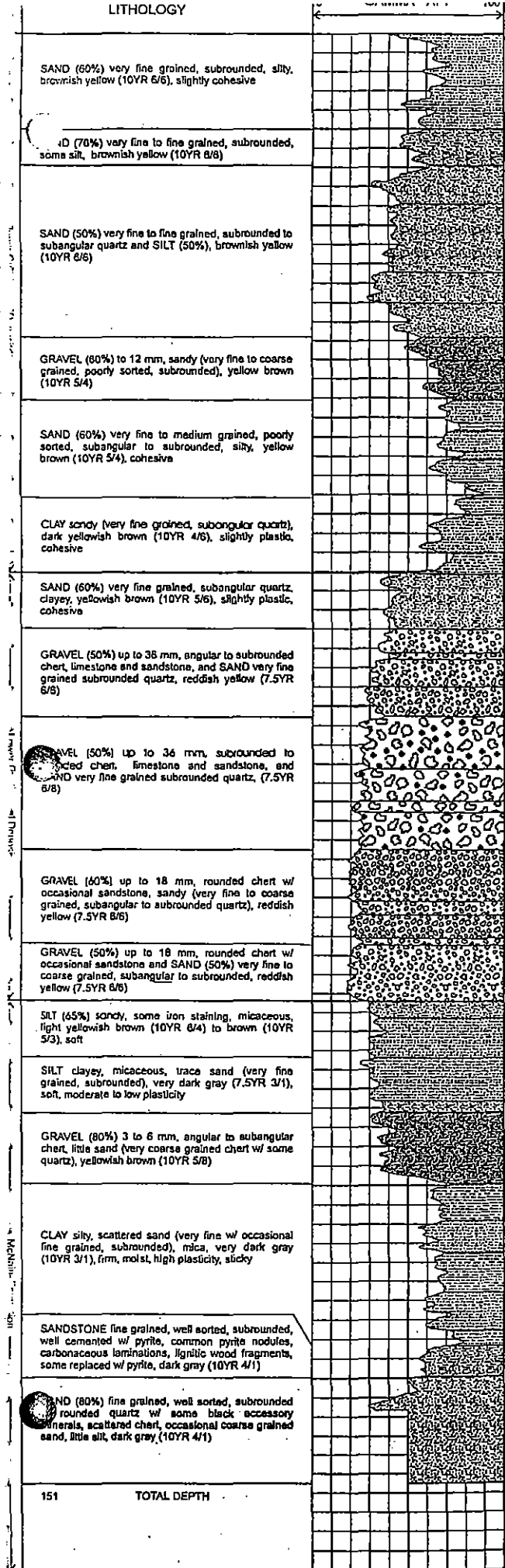
ANALYTICAL

HYDRO UNIT



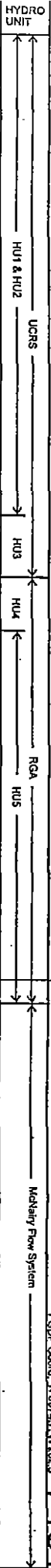
Elevation: 365.1
 PGDP Coord: N 3124.0 W 1090.1

P4C2



ANALYTICAL

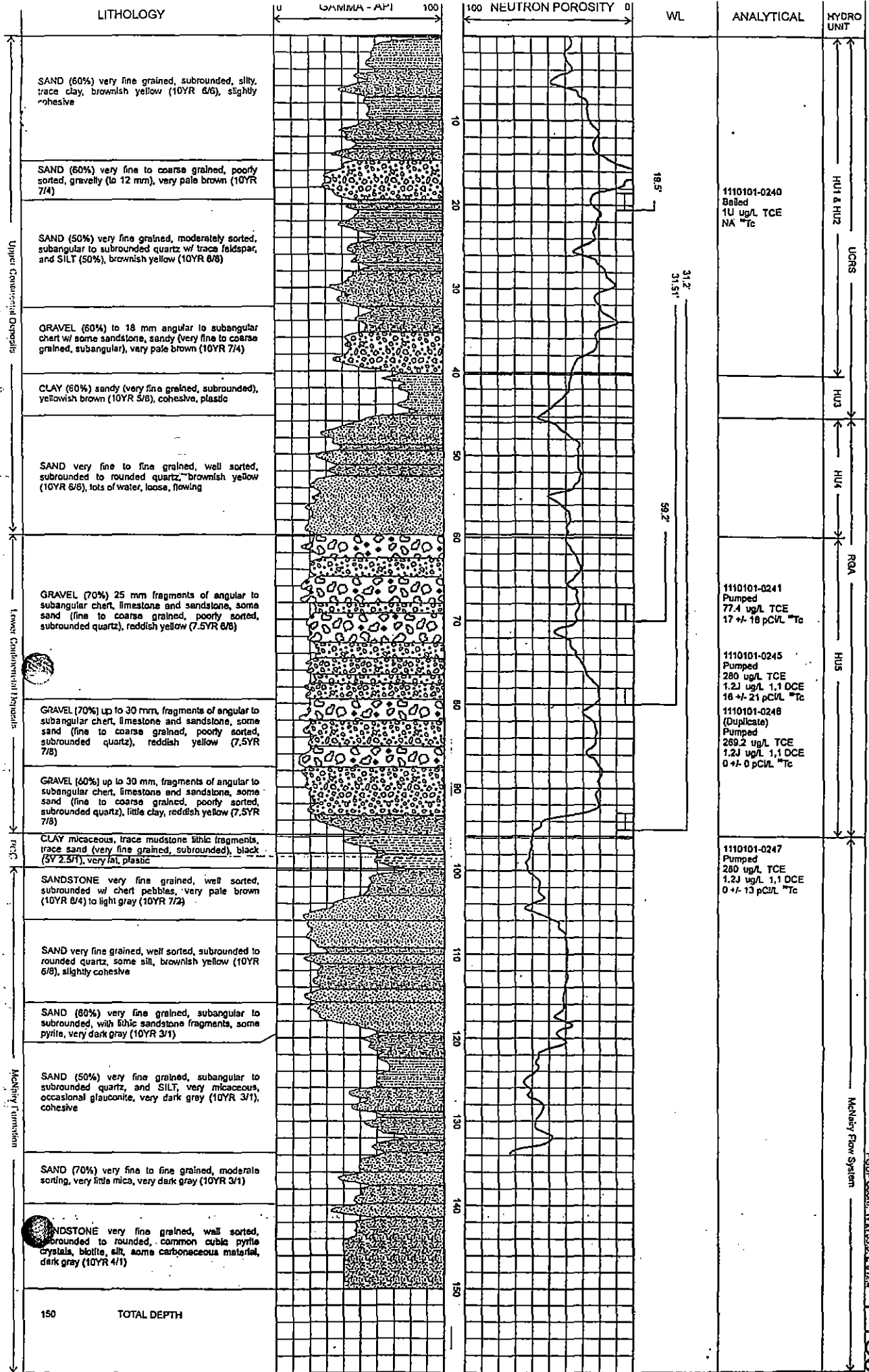
1110101-0266 Pumped 5U mg/L TCE 14 +/- 24 pCi/L ²²² Rn
1110101-0267 Pumped 5U mg/L TCE 0 +/- 0 pCi/L ²²² Rn
1110101-0268 Pumped 28.2 mg/L TCE 0 +/- 0 pCi/L ²²² Rn
1110101-0269 Pumped 7.7 ug/L TCE 0 +/- 0 pCi/L ²²² Rn
1110101-0270 Pumped 5U ug/L TCE NA ²²² Rn



Elevation: 370.83
 PSCP Coord: N 3074.2 W 282.5

P4C4

151 TOTAL DEPTH



Emulsion: 392.44
RSDP Count: N:2153, E:8124
P4C5

LITHOLOGY

GAMMA - API 100

100 NEUTRON POROSITY

WL

ANALYTICAL

HYDRO UNIT

Upper Continental Deposits

Lower Continental Deposits

Forties Creek Clay

McNairy Formation

SILT (60%) trace clay, trace gravel (1 to 2 mm, rounded to subrounded), dark yellow brown (10YR 4/4 to 4/6)

SILT (60%) clayey, some scattered gravel, increasing sand (very fine grained) w/ depth, dark yellow brown (10YR 4/4 to 4/6)

GRAVEL 1 to 4 mm w/ occasional 10 to 20 mm, angular, dark yellow brown (10YR 4/4 to 4/6)

CLAY silty, yellow brown (10YR 5/4)

CLAY (60%) silty at top becoming sandy (very fine grained) w/ depth, brownish yellow (10YR 6/6)

GRAVEL (80%) 1 to 2 mm w/ occasional 10 mm, angular limestone, chert, and sandstone, little silt, brownish yellow (10YR 6/6)

SILT clayey, brownish yellow (10YR 6/6)

SAND (90%) fine to coarse grained, trace silt, light yellow brown (10YR 5/6), fining upward sequence

GRAVEL (60%) 1 to 4 mm w/ occasional 10 to 30 mm, subangular, sandy, light yellow brown (10YR 5/6)

SAND (60%) very fine grained, little silt, little clay, yellow brown (10YR 5/6)

SILT (60%) sandy (very fine grained), pale yellow (2.5Y 8/4)

GRAVEL (70%) 2 to 5 mm w/ scattered 10 to 30 mm, angular, some sand (very coarse grained), very pale brown (10YR 8/3)

GRAVEL (80%) 30 to 50 mm, little sand becoming sandier w/ depth, abundant iron oxides, yellow brown (10YR 5/6)

GRAVEL dark gray brown (10YR 4/2)

GRAVEL brownish yellow (10YR 6/6)

CLAY (90%) trace silt becoming sandier w/ depth, very dark gray (2.5YR N3/1), dense, firm, homogeneous

SAND very fine grained, dark gray (2.5Y N/4)

SAND silty, dark gray (2.5Y N/4)

SAND (90%) very fine to fine grained, becoming coarser at depth, lithified at 117, trace silt, dark gray (2.5Y N/4)

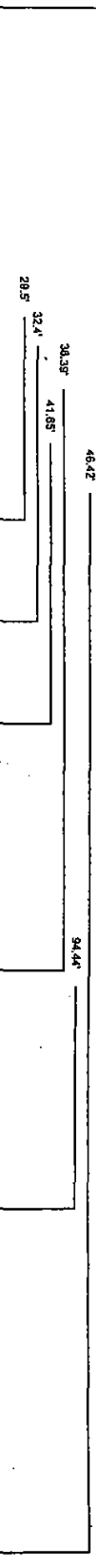
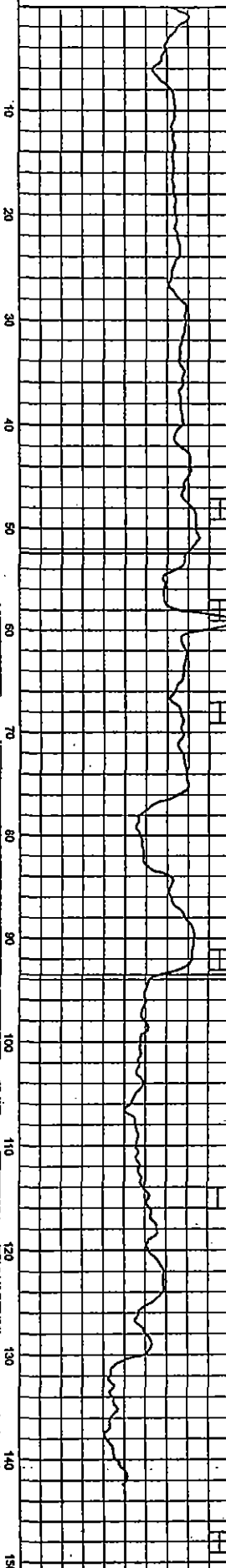
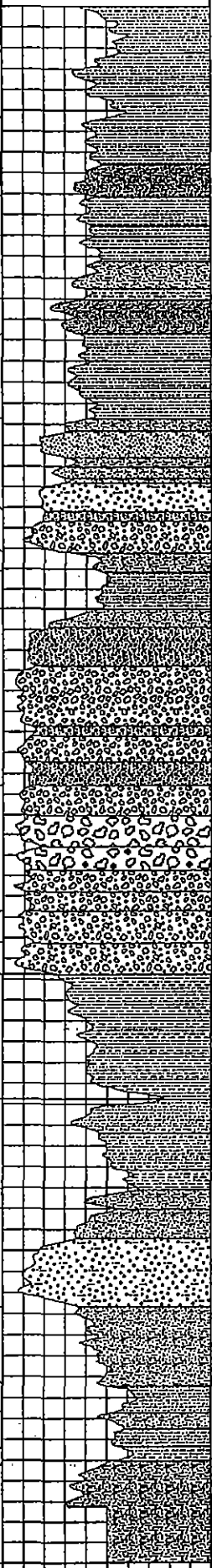
SAND (85%) very fine grained, micaceous, dark gray (10YR 4/1)

CLAY sandy (very fine grained, subangular, clear to translucent quartz), micaceous dark gray (10YR 4/1), damp, stiff

SAND medium grained, slightly lithified w/ pyrite, dark gray (10YR 4/1), grades to sandy clay w/ depth

CLAY (85%), little sand (very fine grained, subangular), dark gray (10YR 4/1)

SAND very fine grained, hard, abundant pyrite and pyritized sand, dark gray (10YR 4/1) w/ some light yellow brown sand throughout



20.5'

32.4'

30.35'

41.85'

46.42'

54.44'

HU1 & HU2

UCRS

HU3

HU4

HU5

RGA

McNairy Flow System

1110101-0854
Pumped
5U ug/L TCE
2 +/- 9 pCi/L ²²⁶Tc

1110101-0855
Pumped
2.3J ug/L TCE
4 +/- 29 pCi/L ²²⁶Tc

1110101-0856
Pumped
42 ug/L TCE
6 +/- 31 pCi/L ²²⁶Tc

1110101-0857
Pumped
429 ug/L TCE
16 +/- 20 pCi/L ²²⁶Tc

1110101-0858
(Duplicate)
Pumped
462 ug/L TCE
14 +/- 18 pCi/L ²²⁶Tc

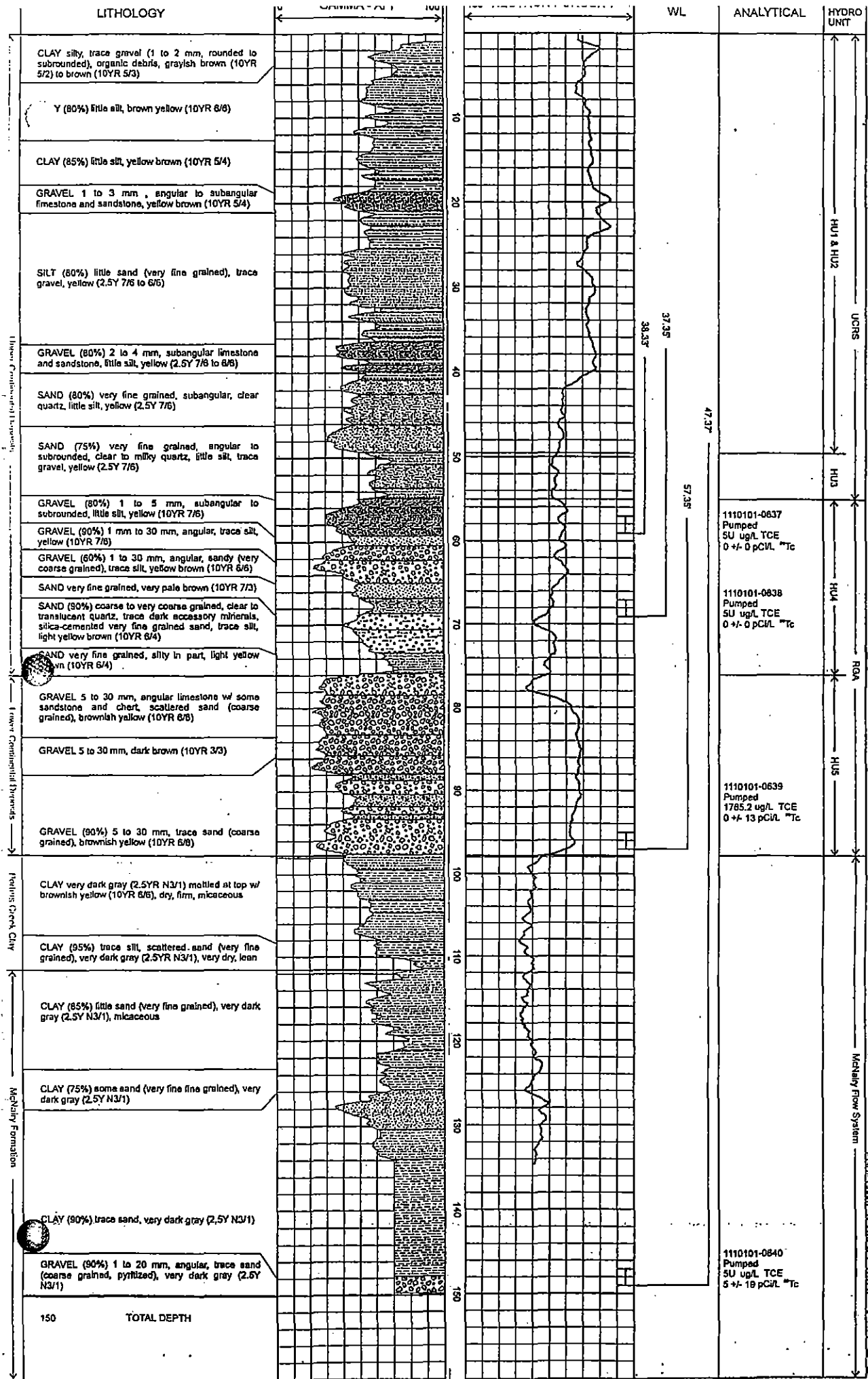
1110101-0859
Pumped
5U ug/L TCE
19 +/- 18 pCi/L ²²⁶Tc

1110101-0860
Pumped
1U ug/L TCE
17 +/- 20 ²²⁶Tc

Elevation: 368.78
PGSP Coord: N 2099 2.5 1357.6

PAC7

150 TOTAL DEPTH



CLAY silty, trace gravel (1 to 2 mm, rounded to subrounded), organic debris, grayish brown (10YR 5/2) to brown (10YR 5/3)

Y (80%) little silt, brown yellow (10YR 6/8)

CLAY (85%) little silt, yellow brown (10YR 5/4)

GRAVEL 1 to 3 mm, angular to subangular limestone and sandstone, yellow brown (10YR 5/4)

SILT (80%) little sand (very fine grained), trace gravel, yellow (2.5Y 7/6 to 6/6)

GRAVEL (80%) 2 to 4 mm, subangular limestone and sandstone, little silt, yellow (2.5Y 7/6 to 6/6)

SAND (80%) very fine grained, subangular, clear quartz, little silt, yellow (2.5Y 7/6)

SAND (75%) very fine grained, angular to subrounded, clear to milky quartz, little silt, trace gravel, yellow (2.5Y 7/6)

GRAVEL (80%) 1 to 5 mm, subangular to subrounded, little silt, yellow (10YR 7/6)

GRAVEL (90%) 1 mm to 30 mm, angular, trace silt, yellow (10YR 7/6)

GRAVEL (60%) 1 to 30 mm, angular, sandy (very coarse grained), trace silt, yellow brown (10YR 6/6)

SAND very fine grained, very pale brown (10YR 7/3)

SAND (80%) coarse to very coarse grained, clear to translucent quartz, trace dark accessory minerals, silica-cemented very fine grained sand, trace silt, light yellow brown (10YR 6/4)

SAND very fine grained, silty in part, light yellow brown (10YR 6/4)

GRAVEL 5 to 30 mm, angular limestone w/ some sandstone and chert, scattered sand (coarse grained), brownish yellow (10YR 6/6)

GRAVEL 5 to 30 mm, dark brown (10YR 3/3)

GRAVEL (90%) 5 to 30 mm, trace sand (coarse grained), brownish yellow (10YR 6/6)

CLAY very dark gray (2.5YR N3/1) mottled at top w/ brownish yellow (10YR 6/6), dry, firm, micaceous

CLAY (95%) trace silt, scattered sand (very fine grained), very dark gray (2.5YR N3/1), very dry, lean

CLAY (85%) little sand (very fine grained), very dark gray (2.5Y N3/1), micaceous

CLAY (75%) some sand (very fine fine grained), very dark gray (2.5Y N3/1)

CLAY (90%) trace sand, very dark gray (2.5Y N3/1)

GRAVEL (90%) 1 to 20 mm, angular, trace sand (coarse grained, pyritized), very dark gray (2.5Y N3/1)

150 TOTAL DEPTH

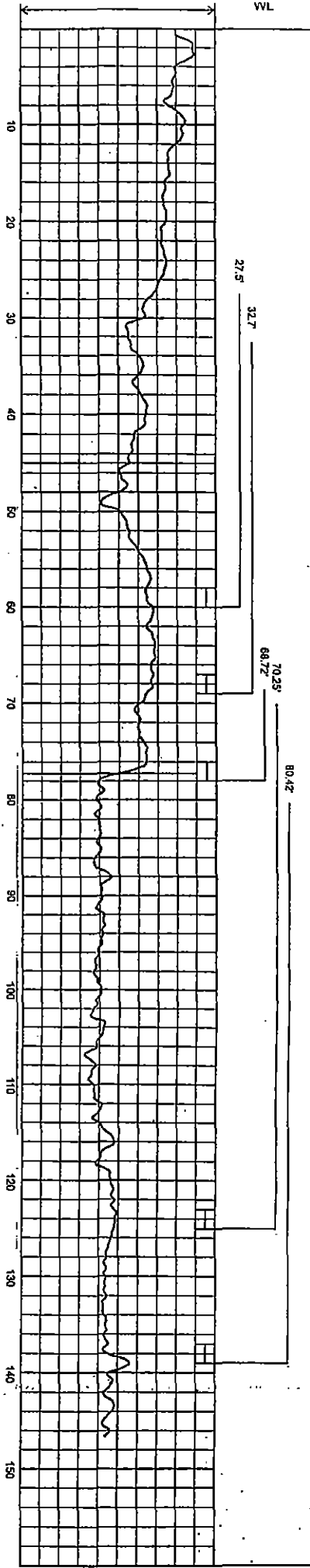
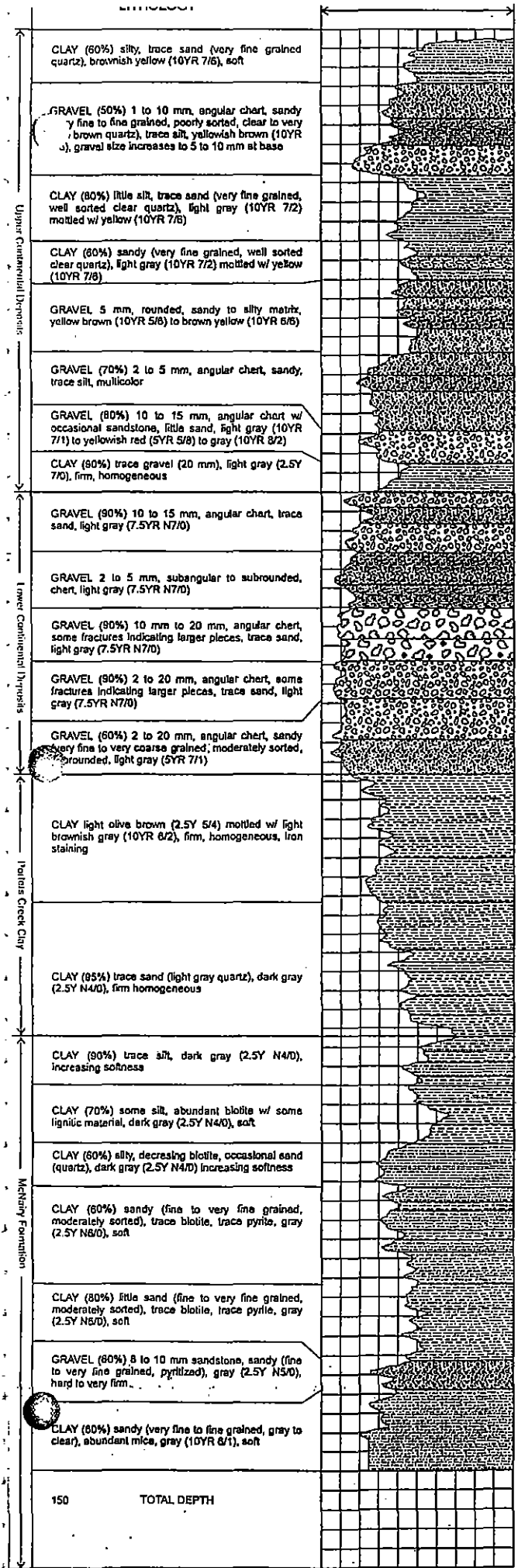
37.35
38.33
47.37
57.35

1110101-0637
Pumped
50 ug/L TCE
0 +/- 0 pCi/L Tc

1110101-0838
Pumped
51 ug/L TCE
0 +/- 0 pCi/L Tc

1110101-0639
Pumped
1785.2 ug/L TCE
0 +/- 13 pCi/L Tc

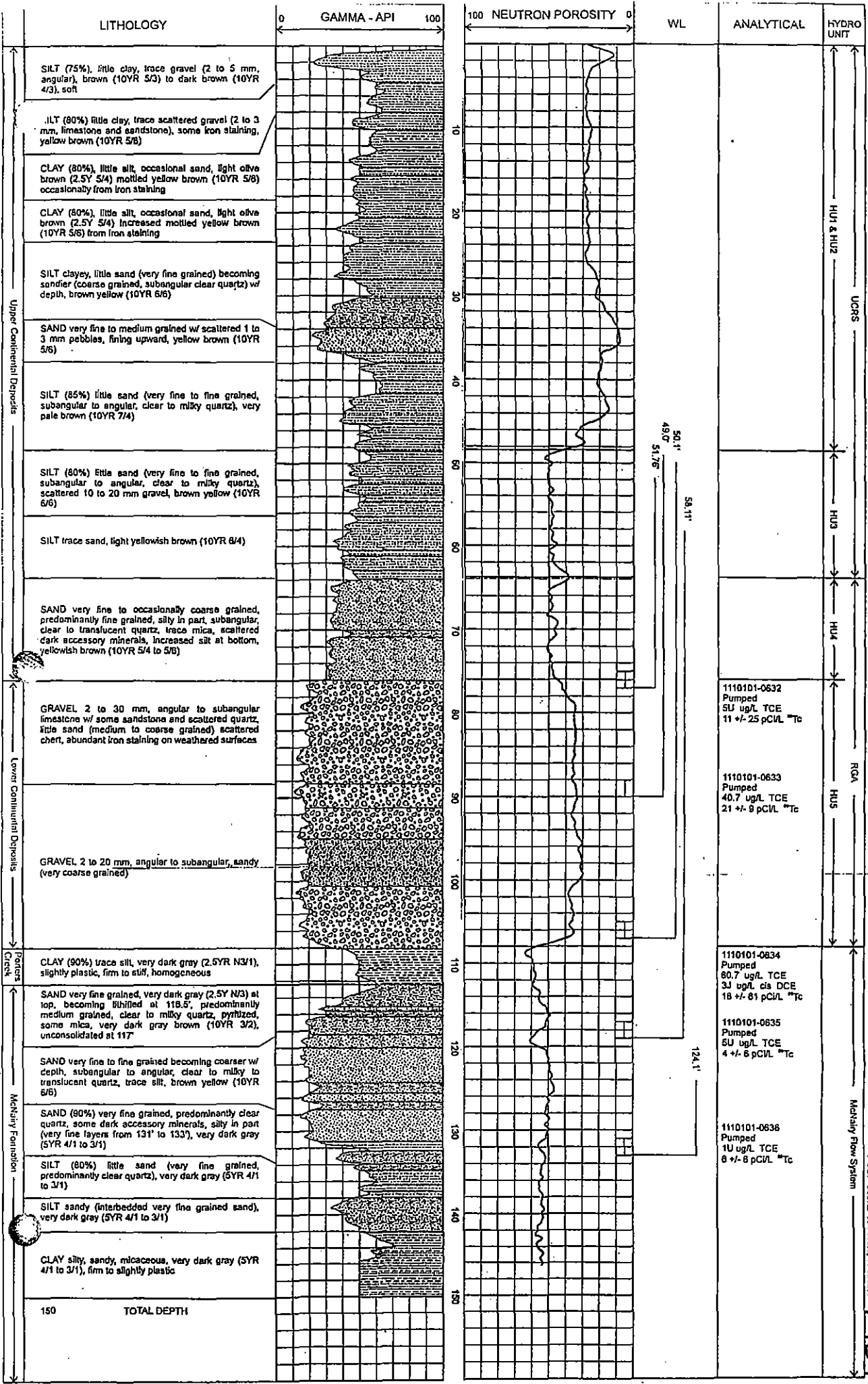
1110101-0840
Pumped
51 ug/L TCE
5 +/- 19 pCi/L Tc



ANALYTICAL	HYDRO UNIT
	UCRS
	HU1 & HU2
	HU3
	RCA
	HU5
	McKainy Flow System
1110101-0751 Pumped 5U ug/L TCE 4 +/- 3 pCVL TM Tc	
1110101-0753 Pumped 5U ug/L TCE 0 +/- 0 pCVL TM Tc	
1110101-0752 Pumped 5U ug/L TCE 0 +/- 0 pCVL TM Tc	
1110101-0754 Pumped 5U ug/L TCE 9 +/- 42 pCVL TM Tc	
1110101-0755 Pumped 5U ug/L TCE 3 +/- 70 pCVL TM Tc	

Elevation: 357.11
 P4C10
 P50P Coord: N 582.81 E 2820.1





Elevation: 380.14
 PGDP Coord: N 1413.0, W 1815.1
P4D4

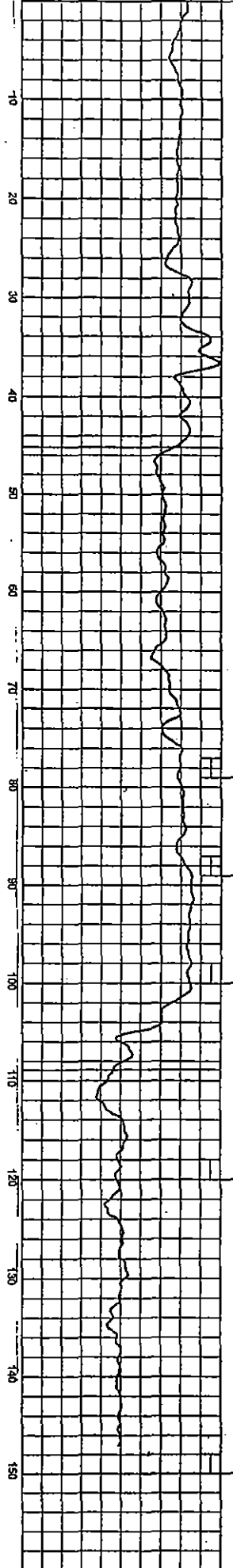
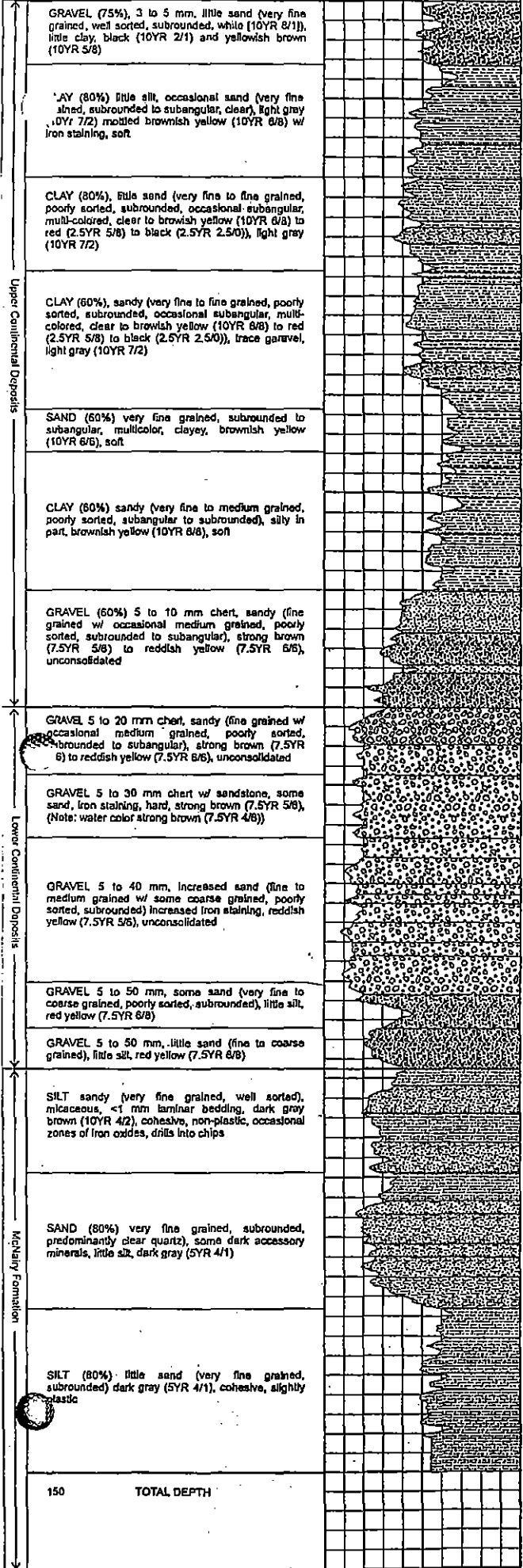
LITHOLOGY

WATER CONTENT

WL

ANALYTICAL

HYDRO UNIT

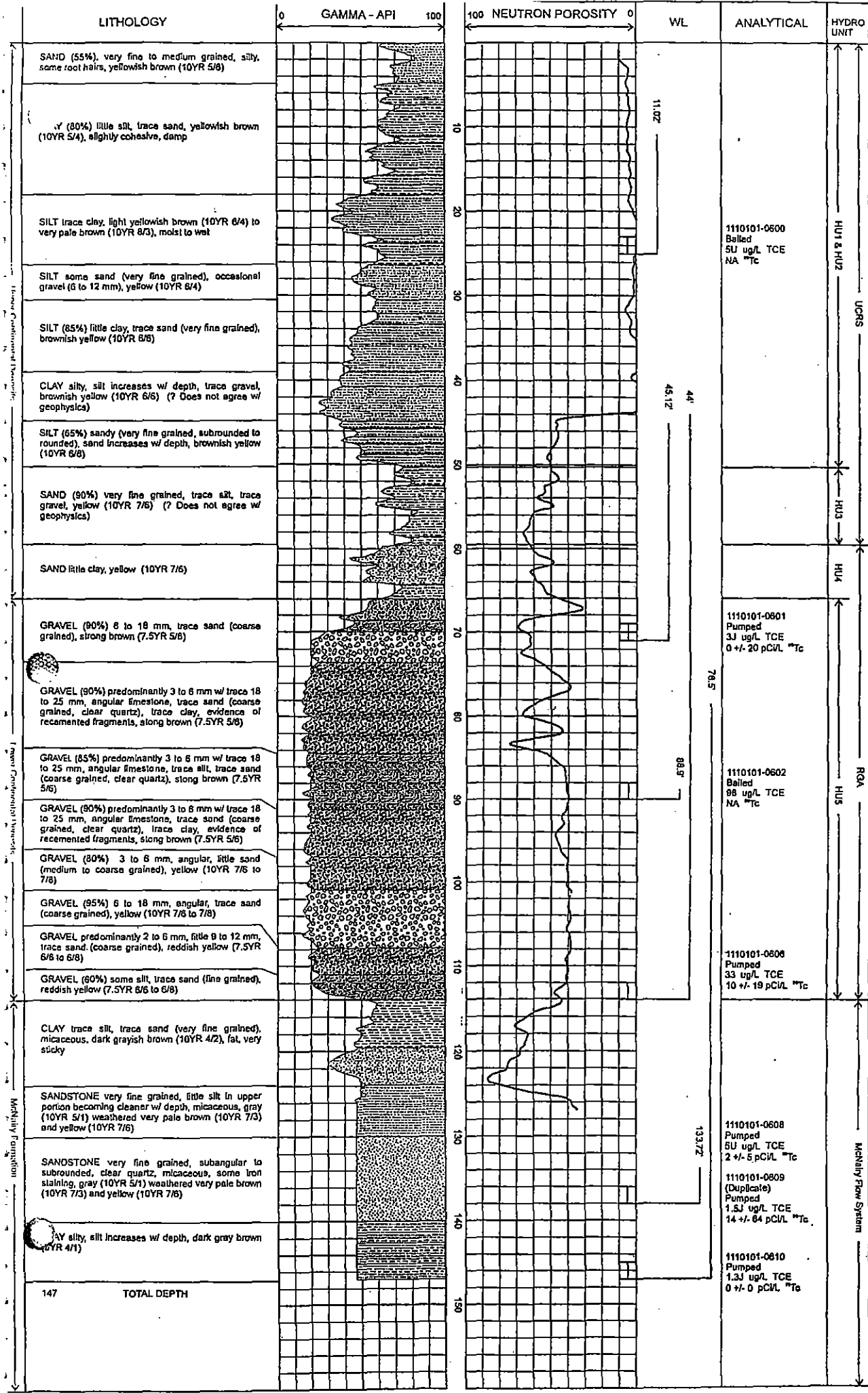


Depth (ft)	Sample ID	Sample Type	Concentration (ug/L)	Concentration (pCi/L)
47.22'	1110101-0695	Pumped	7.2 ug/L TCE	19 +/- 21 pCi/L Tc
50.41'	1110101-0696	Pumped	33.5 ug/L TCE	16J ug/L cis DCE
58.6'	1110101-0697	Pumped	61 ug/L TCE	28J ug/L cis DCE
60.05'	1110101-0698	Pumped	3.3J ug/L TCE	0 +/- 0 pCi/L Tc
101.35'	1110101-0689	Pumped	5U ug/L TCE	26 +/- 21 pCi/L Tc

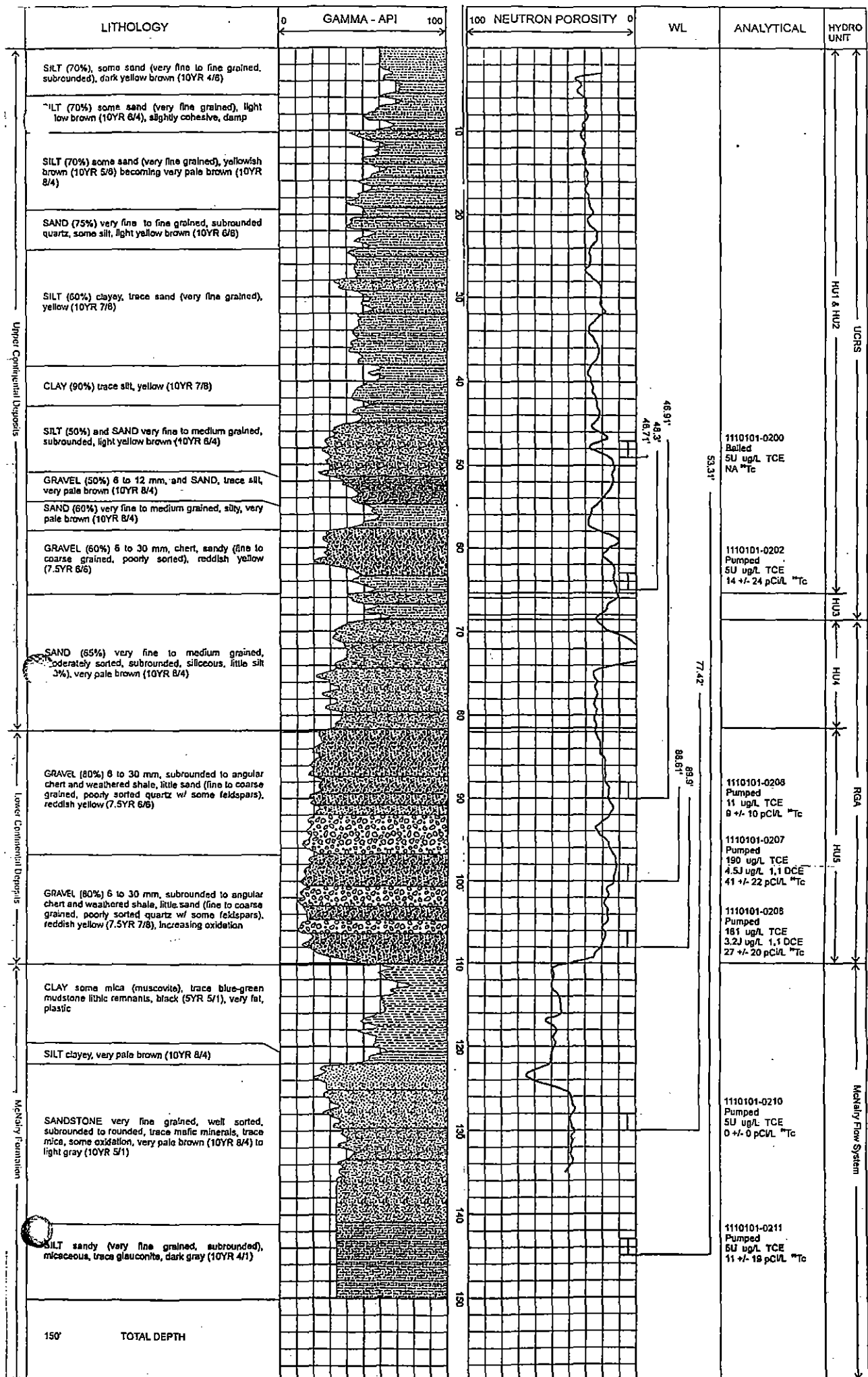
Hydro Unit: HU1 & HU2, UCRS, HU3, HU4, RGA, HUS

Mechery Flow System

Elevation: 378.57
 PDDP Coord: N 155.1, W 115.8
P4D5



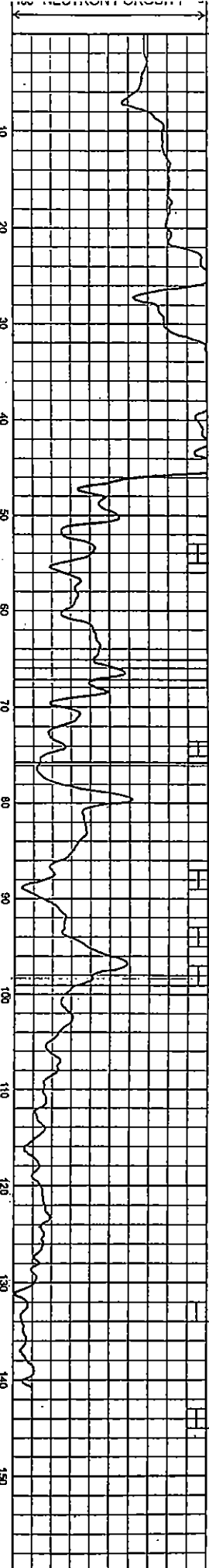
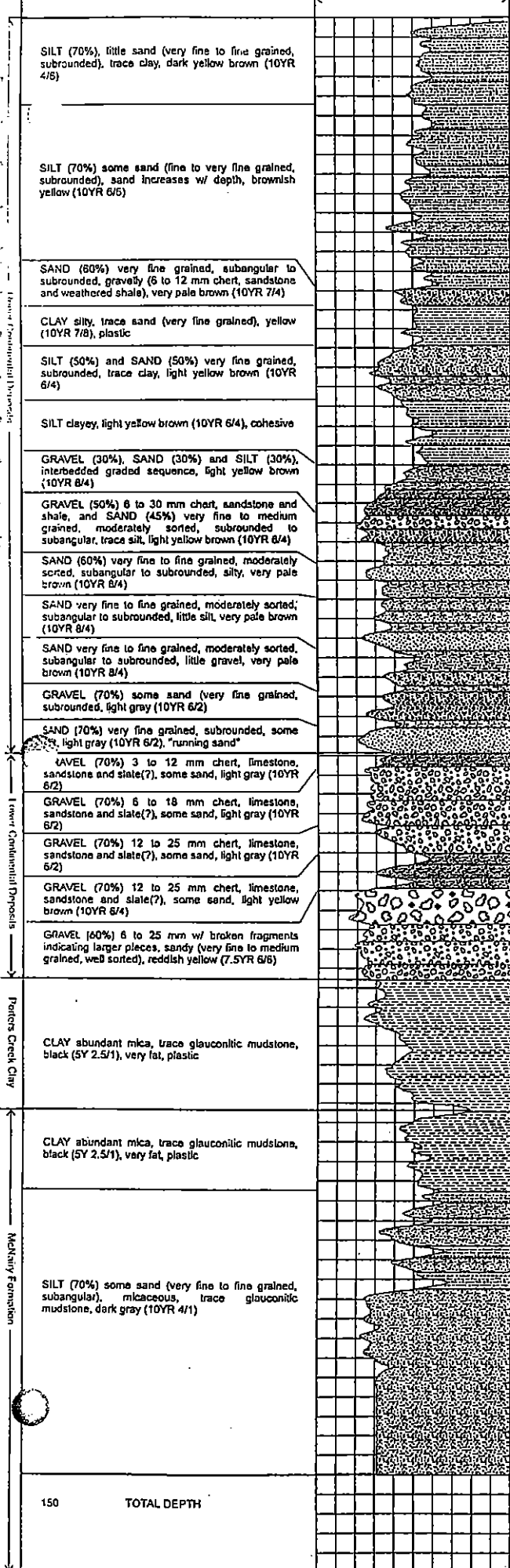
Elevation: 377.43
 PGP Coord: N 887 A W 725.3
P4D6



Elevation: 378.89
PGOP Coord: S 35.6 W 723.0

P4D7

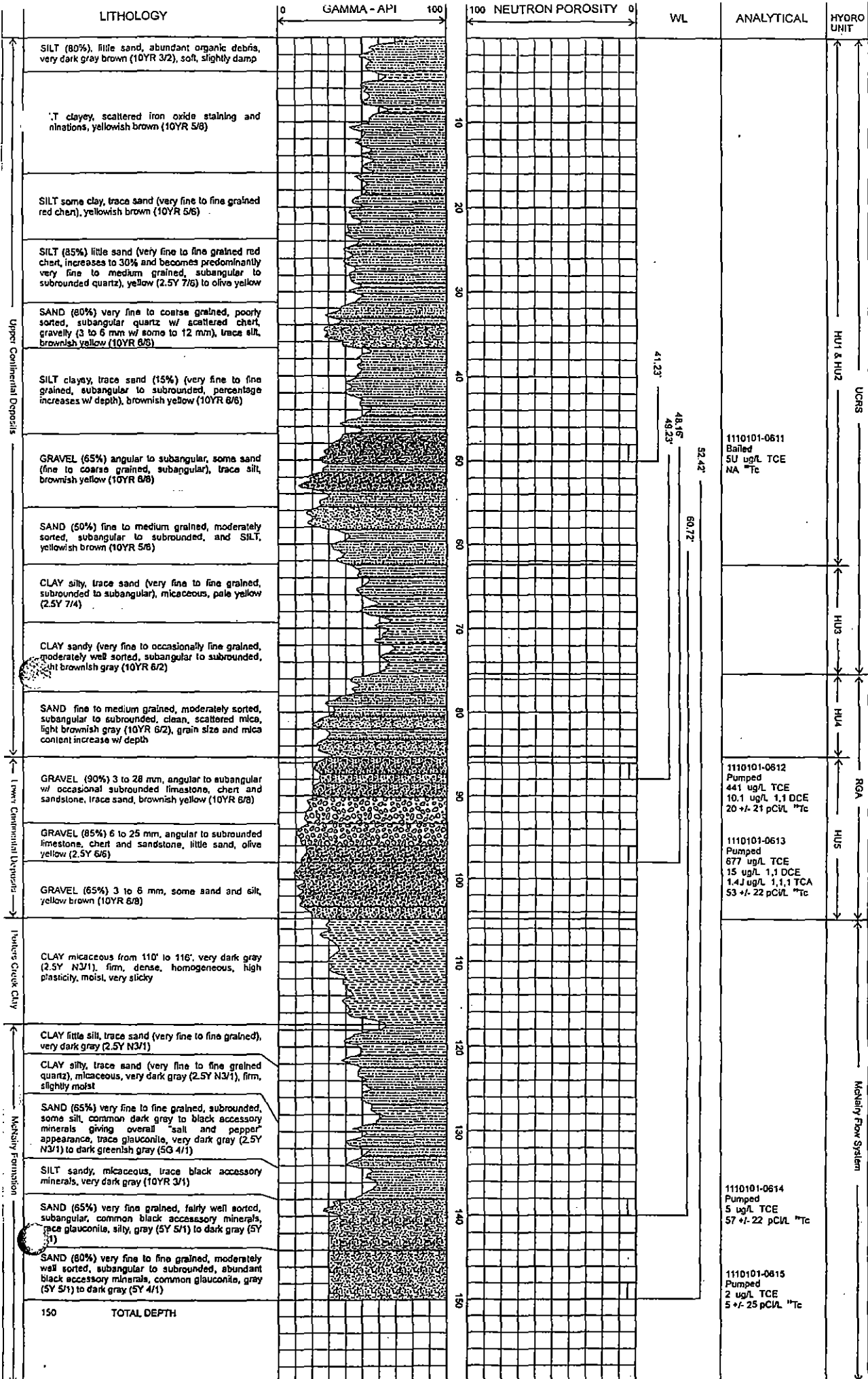
LITHOLOGY



ANALYTICAL	HYDRO UNIT
1110101-0212 Bailed 5U ug/L TCE NA ^m Tc	HU1 & HU2
1110101-0213 Pumped 5U ug/L TCE 10 +/- 25 pCi/L ^m Tc	HU3
1110101-0226 Pumped 2J ug/L TCE 8 +/- 17 pCi/L ^m Tc	HU4
1110101-0214 Pumped 139 ug/L TCE 7.7J ug/L 1,1 DCE 1J ug/L CCl 34 +/- 21 pCi/L ^m Tc	HU5
1110101-0223 Pumped 119 ug/L TCE 6J ug/L 1,1 DCE 33 +/- 21 pCi/L ^m Tc	RG1
1110101-0224 Pumped 5U ug/L TCE 0 +/- 0 pCi/L ^m Tc	McNairy Flow System
1110101-0225 Pumped 5U ug/L TCE 0 +/- 6 pCi/L ^m Tc	McNairy Flow System

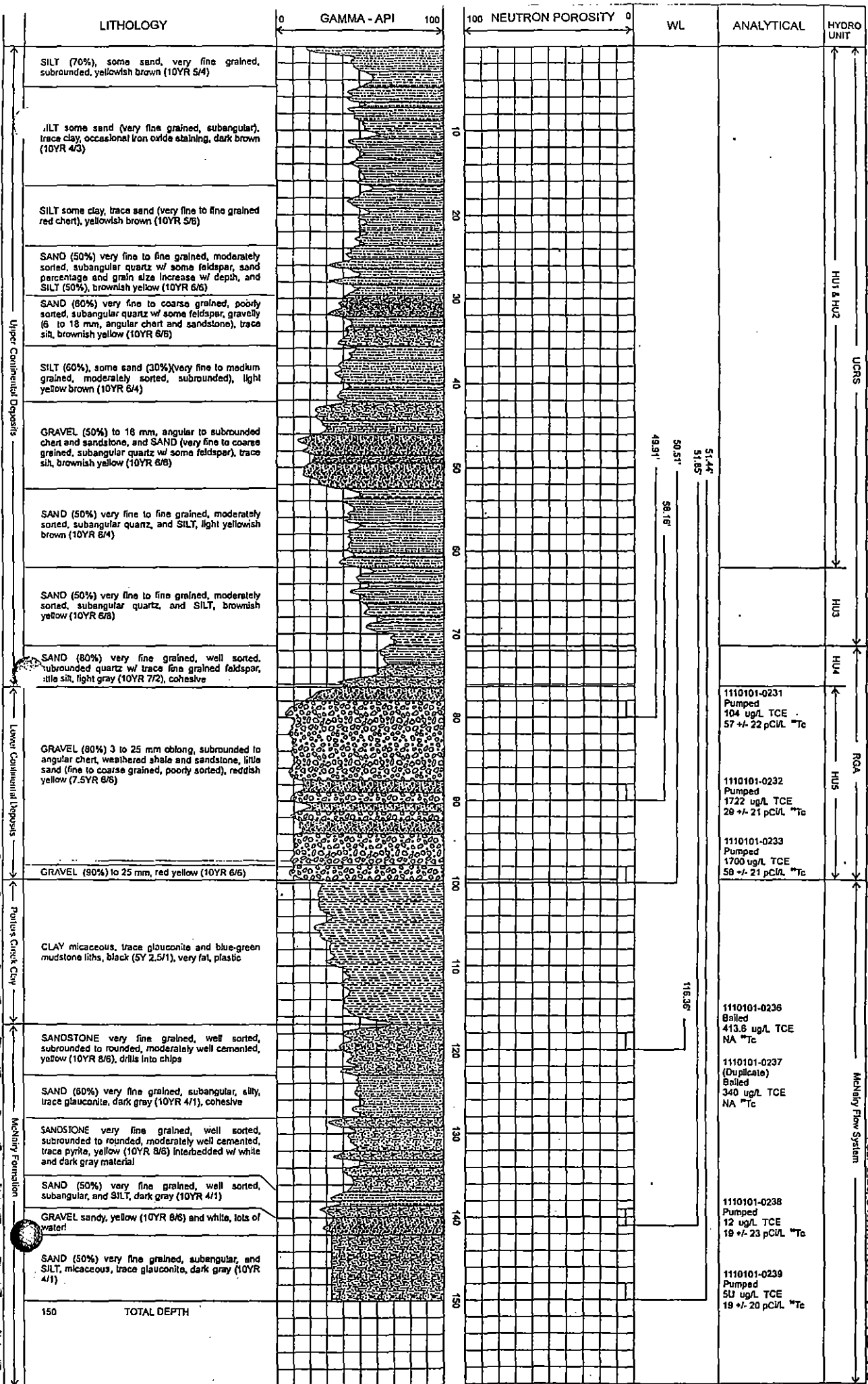
Elevation: 380.12
Euler Coord: S 684.1, W 686.1

P4D8



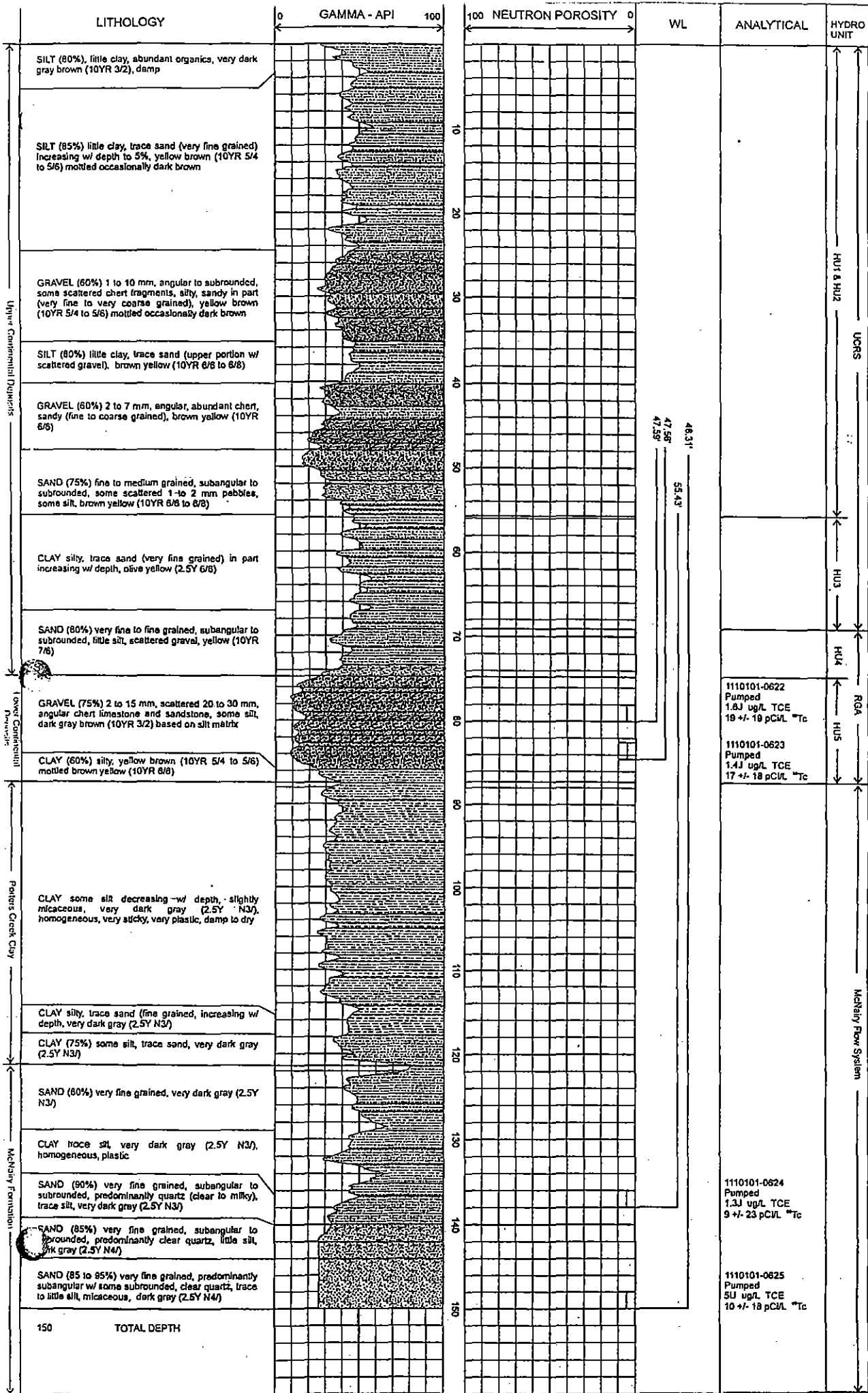
Elevation: 361.99
 PGDD Doc# S 1221.1 W639.8

P4D9



Elevation: 380.84
 PDDP Coord: S 1555.1 W 733.4

P4D10



48.31'
47.58'
47.59'

1110101-0622
Pumped
1.6J ug/L TCE
19 +/- 18 pCvL ^{**Tc}

1110101-0623
Pumped
1.4J ug/L TCE
17 +/- 18 pCvL ^{**Tc}

1110101-0624
Pumped
1.3J ug/L TCE
9 +/- 23 pCvL ^{**Tc}

1110101-0625
Pumped
5U ug/L TCE
10 +/- 18 pCvL ^{**Tc}

Elevation: 379.1
PDDP Core ID: S-2007/S-W7208

P4D11

LITHOLOGY

GAMMA - API

100 NEUTRON POROSITY

WL

ANALYTICAL

HYDRO UNIT

Upper Continental Deposits

Lower Continental Deposits

Purvis Creek Clay

McNary Formation

SILT (70%), some sand, very fine grained, subangular, yellowish brown (10YR 5/4), cohesive

SAND (60%) very fine to medium grained, poor sorting, subrounded to angular, sand percentage increases to 80% by 30', silty, yellow brown (10YR 5/4)

GRAVEL (80%) up to 9 mm, sandy (30%) very fine to coarse grained, poorly sorted, subrounded, trace silt, yellow brown (10YR 5/4)

GRAVEL (60%) up to 12 mm, sandy (20%) very fine to coarse grained, poorly sorted, subrounded, little silt, yellow brown (10YR 5/4)

SAND very fine grained, well sorted, subrounded quartz, yellow brown (10YR 5/4), very loose, non-cohesive, flows readily

SAND (50%) very fine to fine grained, moderately sorted, subangular quartz, and SILT, light yellowish brown (10YR 6/4), cohesive, moderately dense

SAND (70%) very fine to fine grained, moderately sorted, subangular quartz, little silt, trace gravel, light yellowish brown (10YR 6/4)

SILT (70%) little clay, trace sand (very fine grained, subrounded), brownish yellow (10YR 6/8), moderately cohesive

GRAVEL (80%) 3 to 38 mm, subrounded to angular chert, weathered shale and sandstone, little sand (fine to coarse grained, poorly sorted, subangular to subrounded), reddish yellow (7.5YR 6/8)

CLAY micaceous, trace glauconite and blue-green mudstone liths, black (5Y 2.5/1), very fat, plastic

SAND (60%) very fine grained, subrounded, silty, micaceous, trace glauconite, occasional pyrite nodules, black (5Y 2.5/1)

SAND (80%) very fine grained, subangular, little silt, black (5Y 2.5/1), common pyrite nodules 132' to 133', 120' to 140' is upward fining sequence

SAND (80%) very fine grained, subangular, little silt, micaceous, trace glauconite, trace lignite, dark gray (5YR 5/1)

150 TOTAL DEPTH

10
20
30
40
50
60
70
80
90
100
110
120
130
140
150

27.12

40.13'

51.97'

65.0'

119.08'

1110101-0258
Bailed
1U ug/L TCE
NA ⁹⁰Tc

1110101-0259
Bailed
1U ug/L TCE
NA ⁹⁰Tc

1110101-0260
Bailed
5U ug/L TCE
NA ⁹⁰Tc
(Field GC)

1110101-0261
Bailed, Duplicate
1 ug/L TCE
NA ⁹⁰Tc
(Fixed lab)

1110101-0262
Pumped
1U ug/L TCE
4 +/- pCi/L ⁹⁰Tc
(Fixed lab)

1110101-0263
Pumped, Duplicate
5U ug/L TCE
NA ⁹⁰Tc
(Field GC)

1110101-0264
Pumped
1U ug/L TCE
0 +/- 0 pCi/L ⁹⁰Tc
(Fixed lab)

1110101-0265
Bailed, Duplicate
5U ug/L TCE
NA ⁹⁰Tc
(Field GC)

HU1 & HU2

UCR8

HU3

HU4

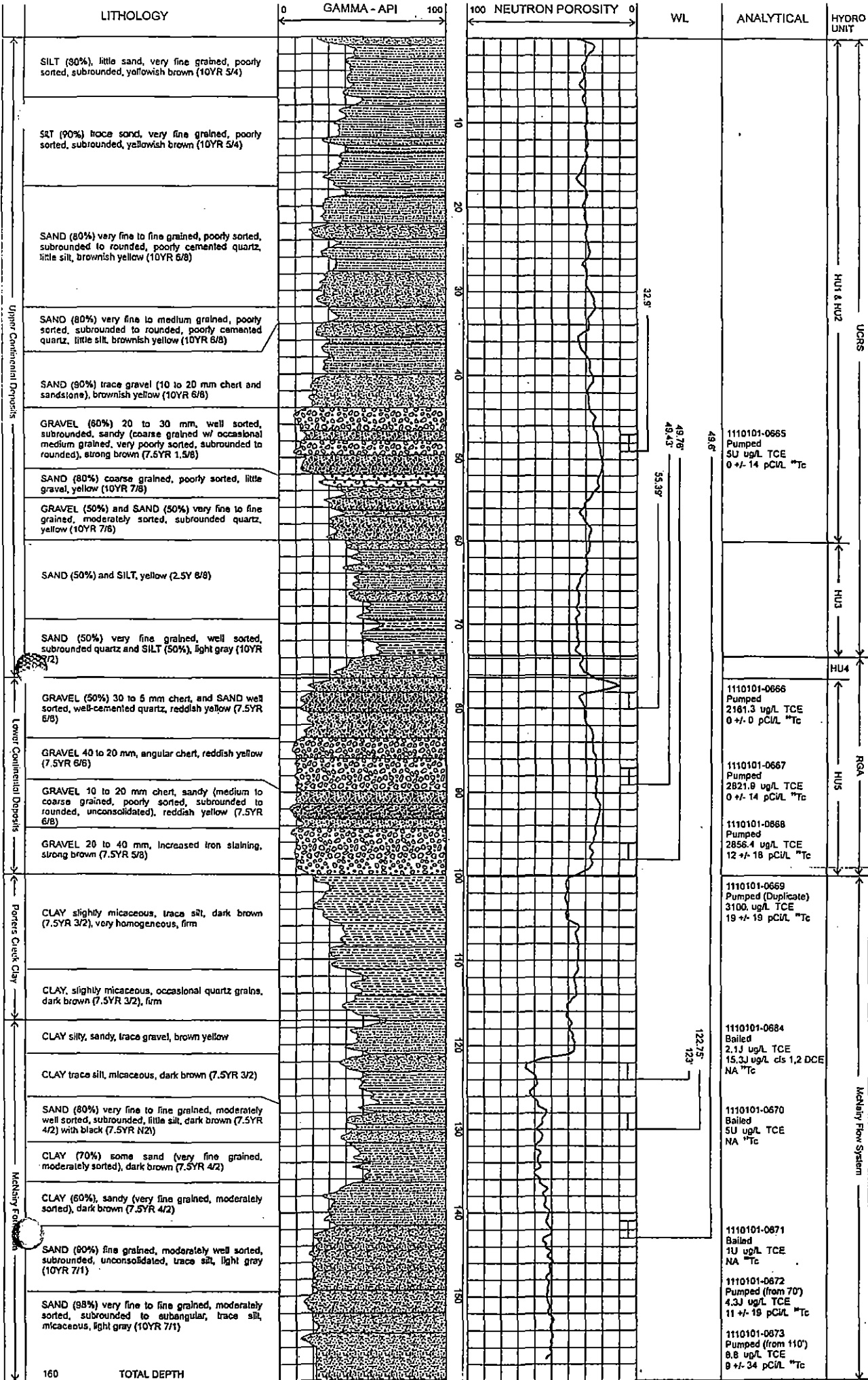
RGA

HU5

McNary Flow System

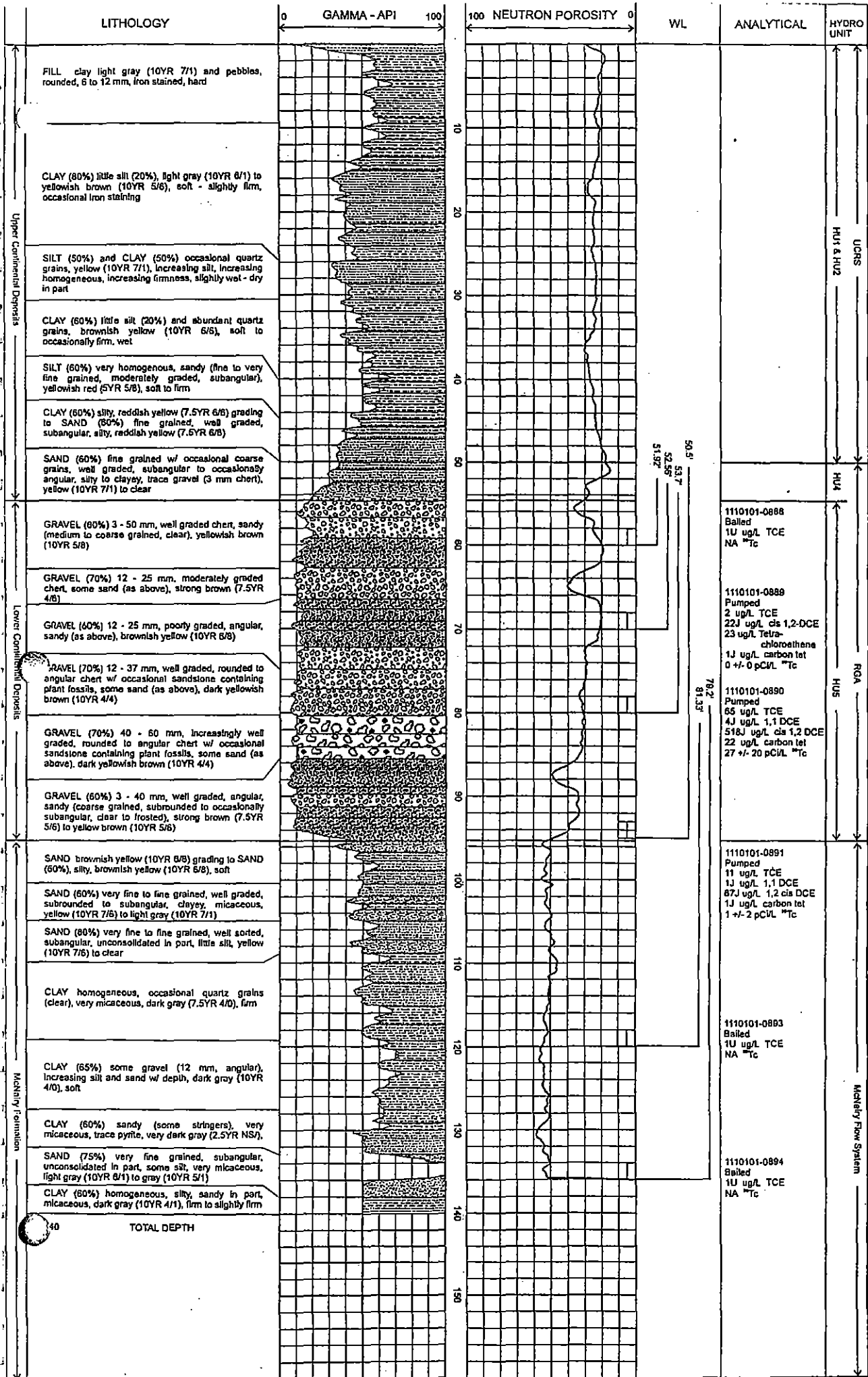
Elevation: 380.23
EGDP Coord: S 1645.6, W 693.0

P4D12



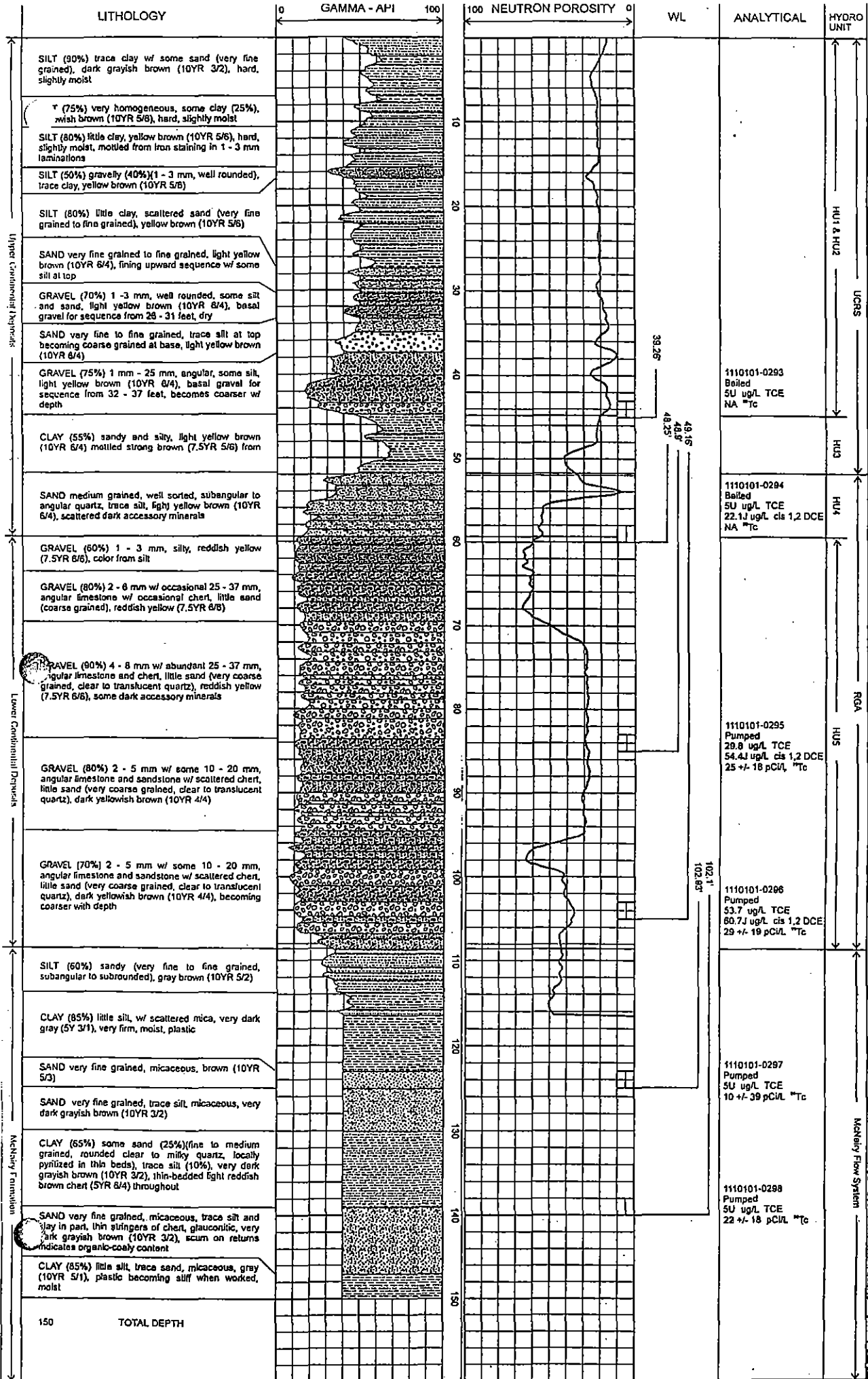
Elevation: 381.4
 PDDP Coord: S1051.8, W755.1

P4D12A



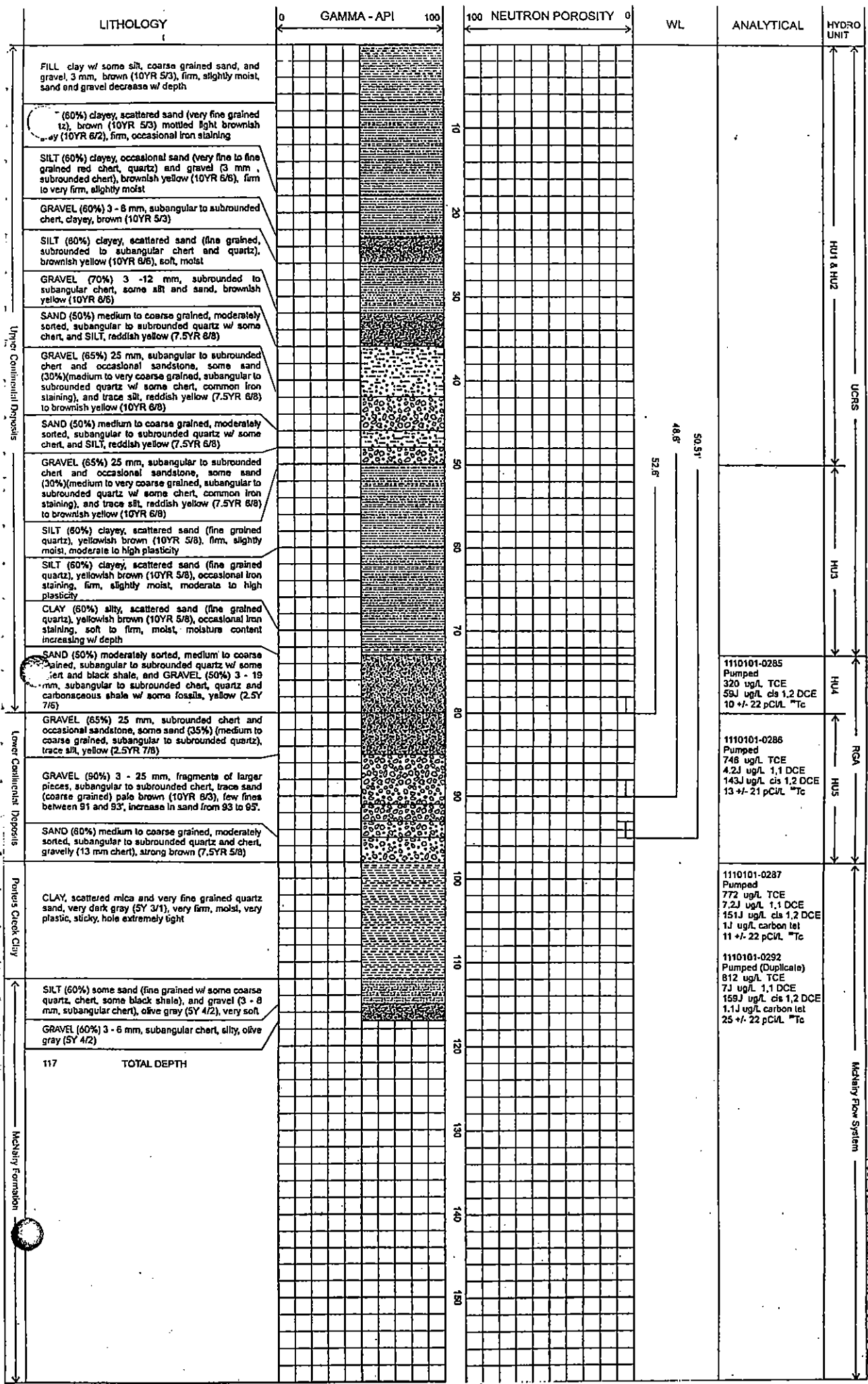
Revision: 3/7/78
 RSD/CGP/ML/KAL/M/28809

P4E1

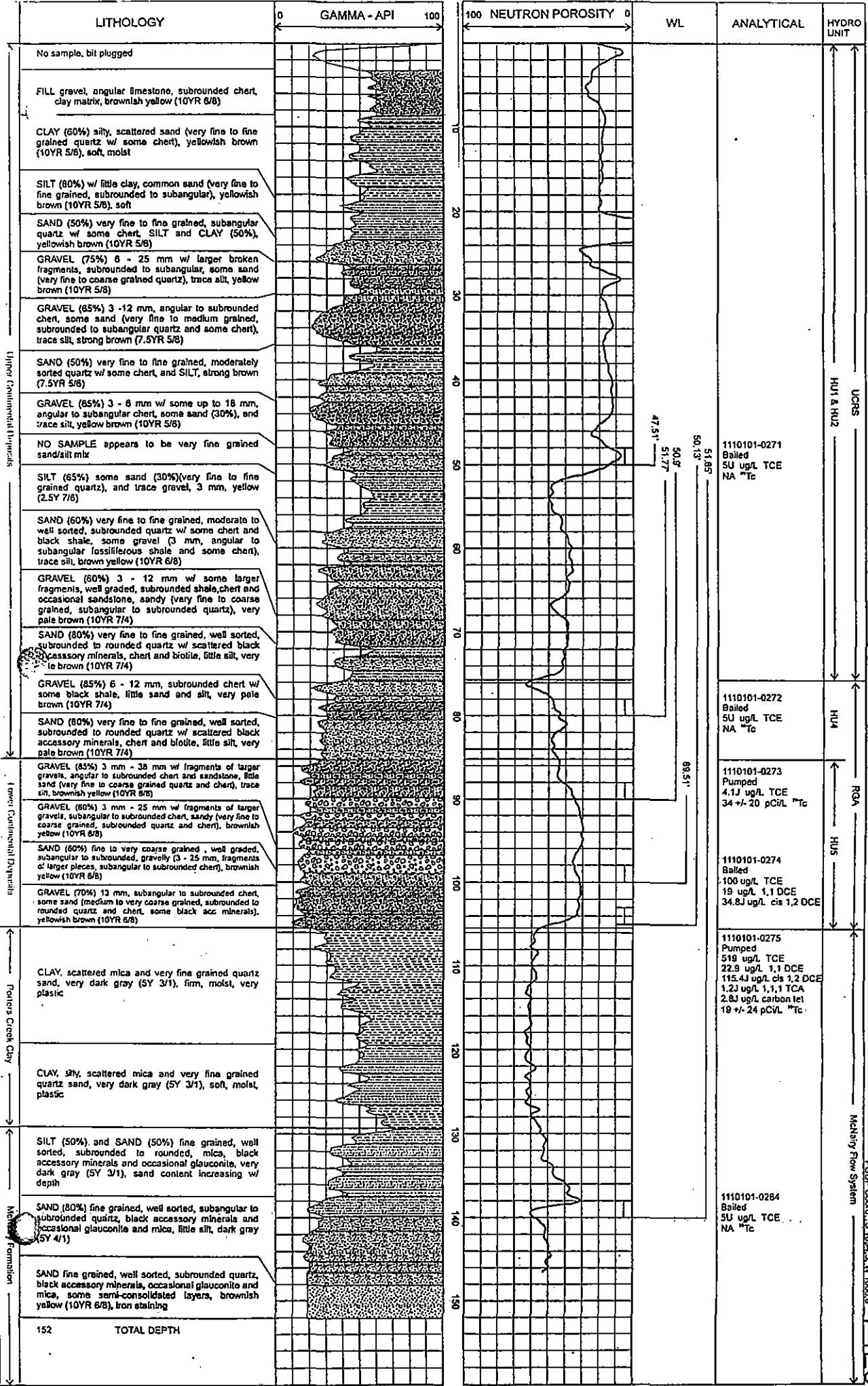


Elevation: 370.06
 GCP Coord: N 295.0 W 2327.5
 Mchley Flow System

P4E2



Revision: 361108
 RSDP Report S.782.4.V.1979.6
 Mchalyi Flow System
 P4E4



Elevation: 381.99
 RDP Coord: S 1824 E, W 160818
 McNary Flow System

PAE6

LITHOLOGY

GAMMA - AFI 100

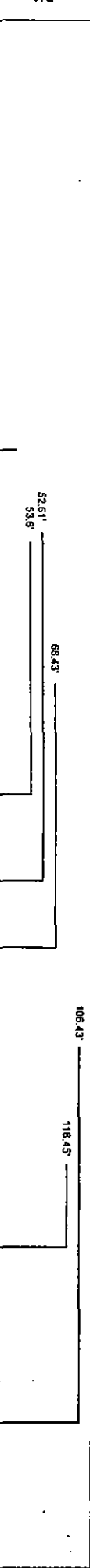
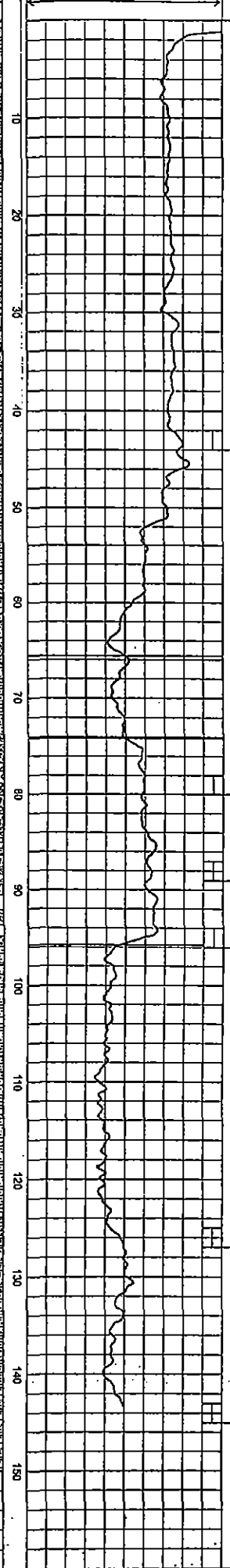
100 NEUTRON POROSITY U

WL

ANALYTICAL

HYDRO UNIT

CLAY (80%) little silt (20%), reddish yellow (7.5YR 7/6), firm, iron staining	
CLAY (80%) little silt (20%), occasional sand grains (quartz and chert), reddish yellow (7.5YR 7/6), and w/ gray (10YR 8/1), firm to soft	
CLAY (70%) some silt, homogeneous, brownish yellow (10YR 8/6), soft, damp	
CLAY (80%) w/ little silt, trace biotite, pebbles, brownish yellow (10YR 8/6) mottled w/ light gray (10YR 7/1), soft, damp	
CLAY (60%) silty, occasional sand grains (chert), light gray (10YR 7/1), firm, occasional iron staining	
GRAVEL (50%) 3 - 8 mm, chert, sandy (40%) (medium to coarse grained, poorly sorted, clear to brownish yellow (10YR 8/6)), trace silt, yellowish brown (10YR 5/8) to brown (7.5YR 5/8)	
GRAVEL (60%) 3 - 8 mm, chert, some sand (medium to coarse grained, poorly sorted, clear to brownish yellow (10YR 8/6)), trace silt, yellowish brown (10YR 5/8) to brown (7.5YR 5/8), decrease in sand and silt	
CLAY (40%) some sand (30%) (very fine to fine grained), and gravel (30%) (18 - 25 mm, chert), yellow (2.5YR 7/6)	
GRAVEL (65%) very rounded chert w/ some quartz, some sand (35%), white (2.5Y 8/2)	
CLAY (90%) trace silt, light gray (2.5Y N7/7), firm, homogeneous	
CLAY (70%) some sand (30%) (fine grained, moderately well sorted, subrounded, clear quartz), light gray (10YR 7/1), soft, some mottled iron staining	
CLAY (60%) sandy (fine grained, moderately well sorted, subrounded, clear quartz), white (10YR 8/2), homogeneous	
CLAY (90%) trace sand (fine grained, moderately well sorted, subrounded, clear quartz), white (10YR 8/2), homogeneous	
CLAY (60%) sandy (fine grained, moderately sorted, subrounded, multicolor quartz and chert), white (10YR 8/2), soft, moist	
GRAVEL (90%) 2 to 25 mm w/ some larger fragments, rounded to angular chert, trace sand and silt, white (10YR 8/2) to brownish yellow (10YR 6/8) to light gray (10YR 7/1)	
GRAVEL (80%) 2 to 25 mm w/ some larger fragments, rounded to angular chert, little sand (coarse to very coarse grained, poorly sorted, subrounded to rounded quartz), yellow (10YR 7/8)	
GRAVEL (85%) 2 to 50 mm w/ some larger fragments, rounded to angular chert, little sand (very coarse grained, poorly sorted, subrounded to rounded quartz), yellow (10YR 7/8)	
CLAY little silt, scattered very fine grained quartz sand, very dark gray (2.5Y 3/1), soft to firm	
CLAY (95%) trace silt, very dark gray (2.5Y N/3), firm to very firm, very homogeneous	
CLAY (95%) trace silt, trace gravel (5 mm), very dark gray (2.5Y N/3), firm, very homogeneous	
SAND (80%) very fine to fine grained, moderately well sorted, subrounded to subangular, abundant biotite, trace pyrite, clayey, gray (2.5Y NS) to dark gray	
SAND (50%) quartz, and CLAY (50%), trace biotite, dark gray (2.5Y N4/4), soft	
SAND (70%) fine to very fine grained, well sorted, subrounded, moderately cemented quartz, mica, some clay, light gray (2.5Y N6/ to 10YR 8/1)	
150 TOTAL DEPTH	

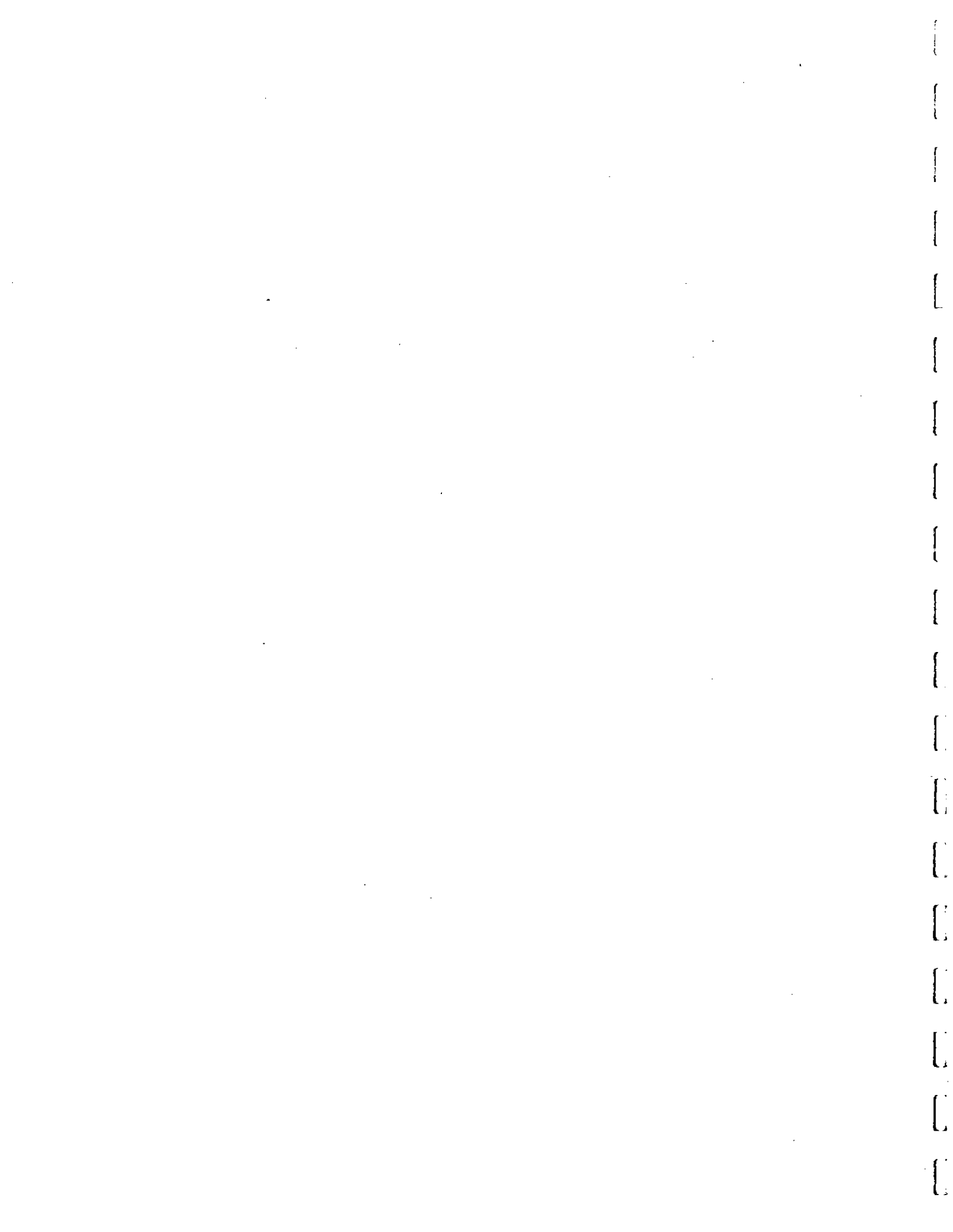


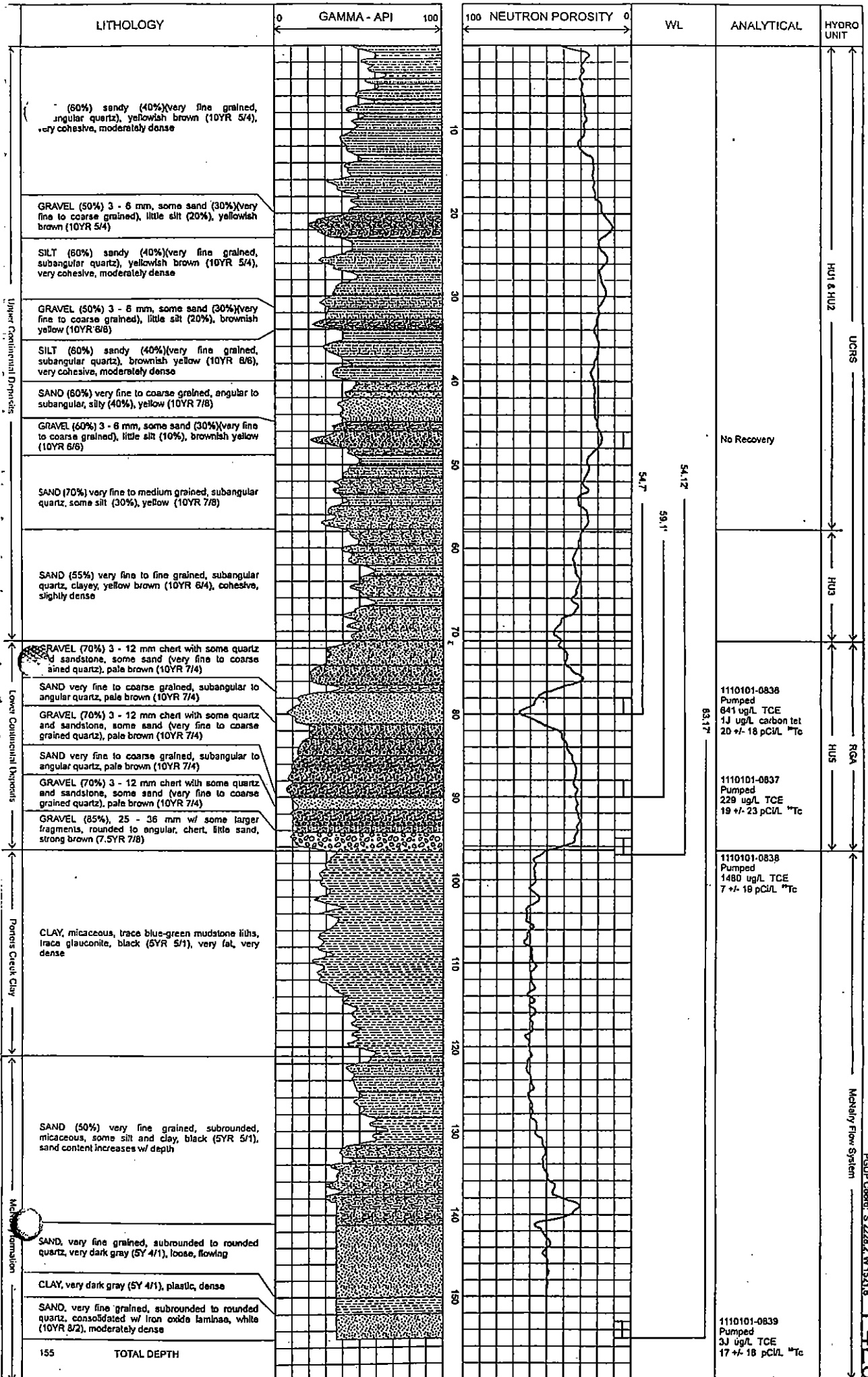
1110101-0759 Bailed 0.1J ug/L TCE 18J ug/L cis 1,2 DCE NA **Tc
1110101-0760 Pumped 1331 ug/L TCE NA **Tc
1110101-0781 Pumped 2385 ug/L TCE 12 +/- 23 pCi/L **Tc
1110101-0762 Pumped 2284 ug/L TCE 3 +/- 32 pCi/L **Tc
1110101-0763 Bailed 1.6J ug/L TCE 28J ug/L cis 1,2 DCE NA **Tc
1110101-0764 Pumped 0.3J ug/L TCE 10 +/- 8 pCi/L **Tc

HUT & HUZ	UCRS
HU3	HUS
HUS	RGA
McNairy Flow System	

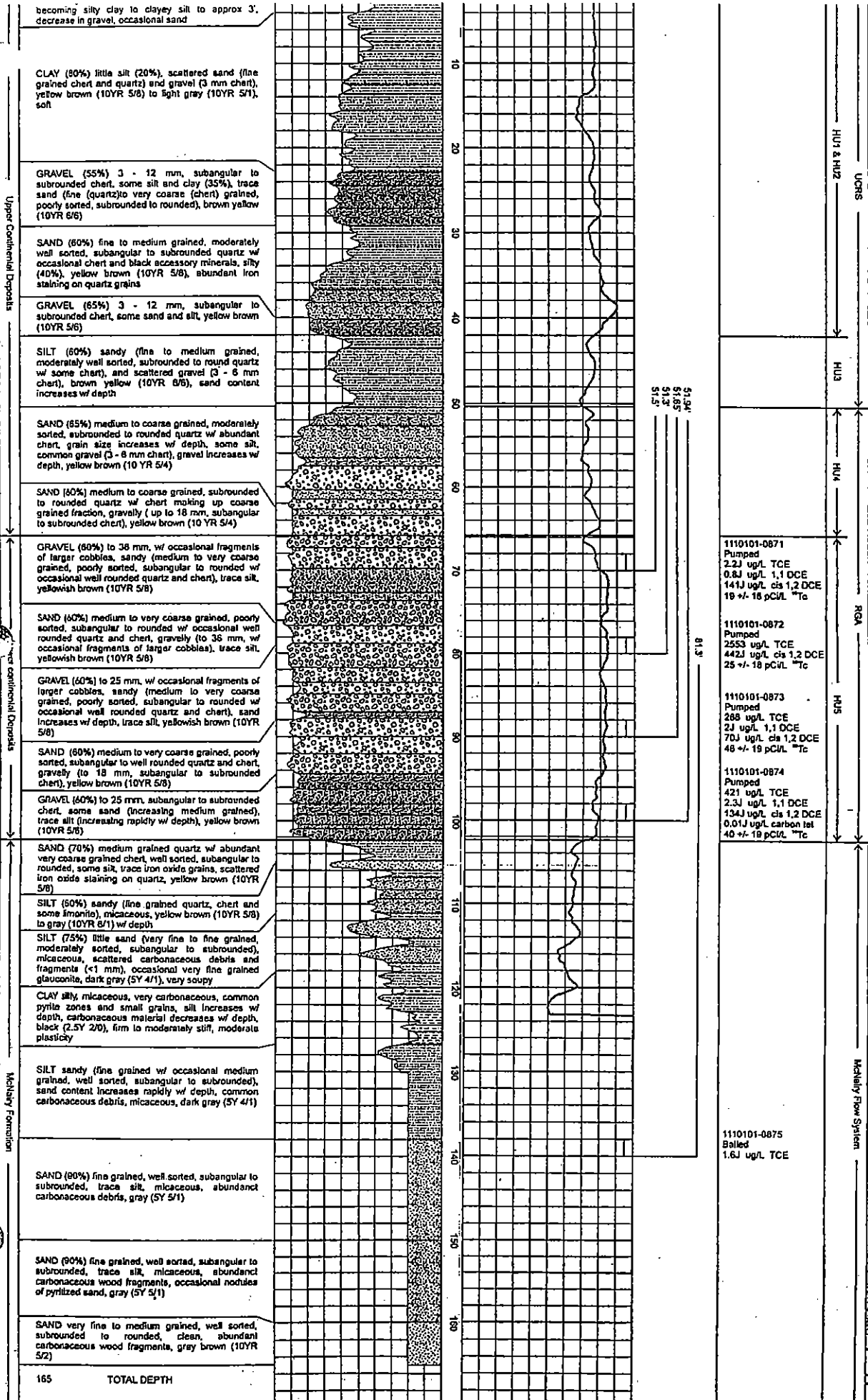
Elevation: 390.42
PCOP Control: S-1914.8, V-931.3

P4E7

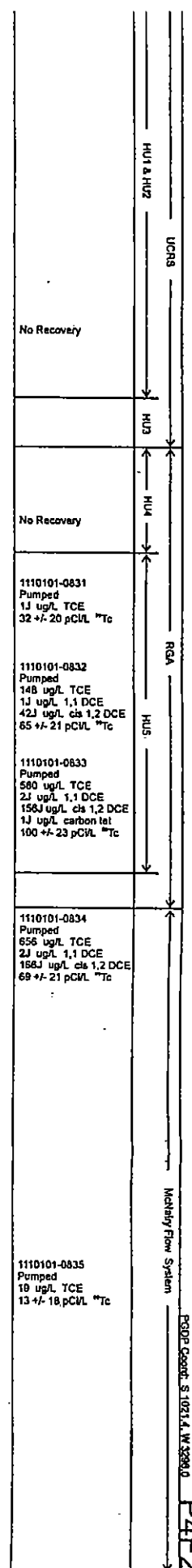
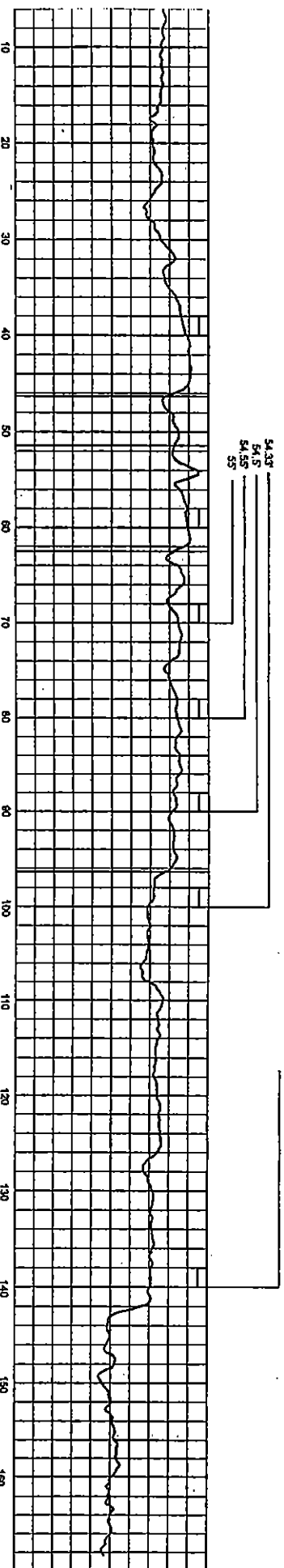
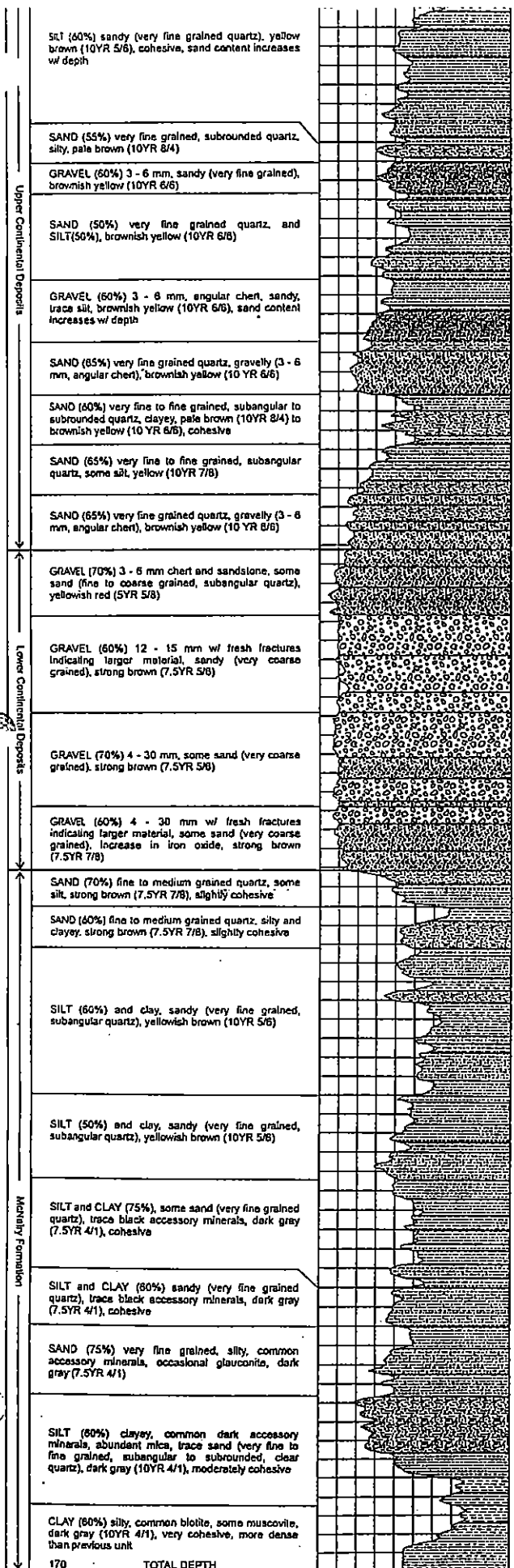




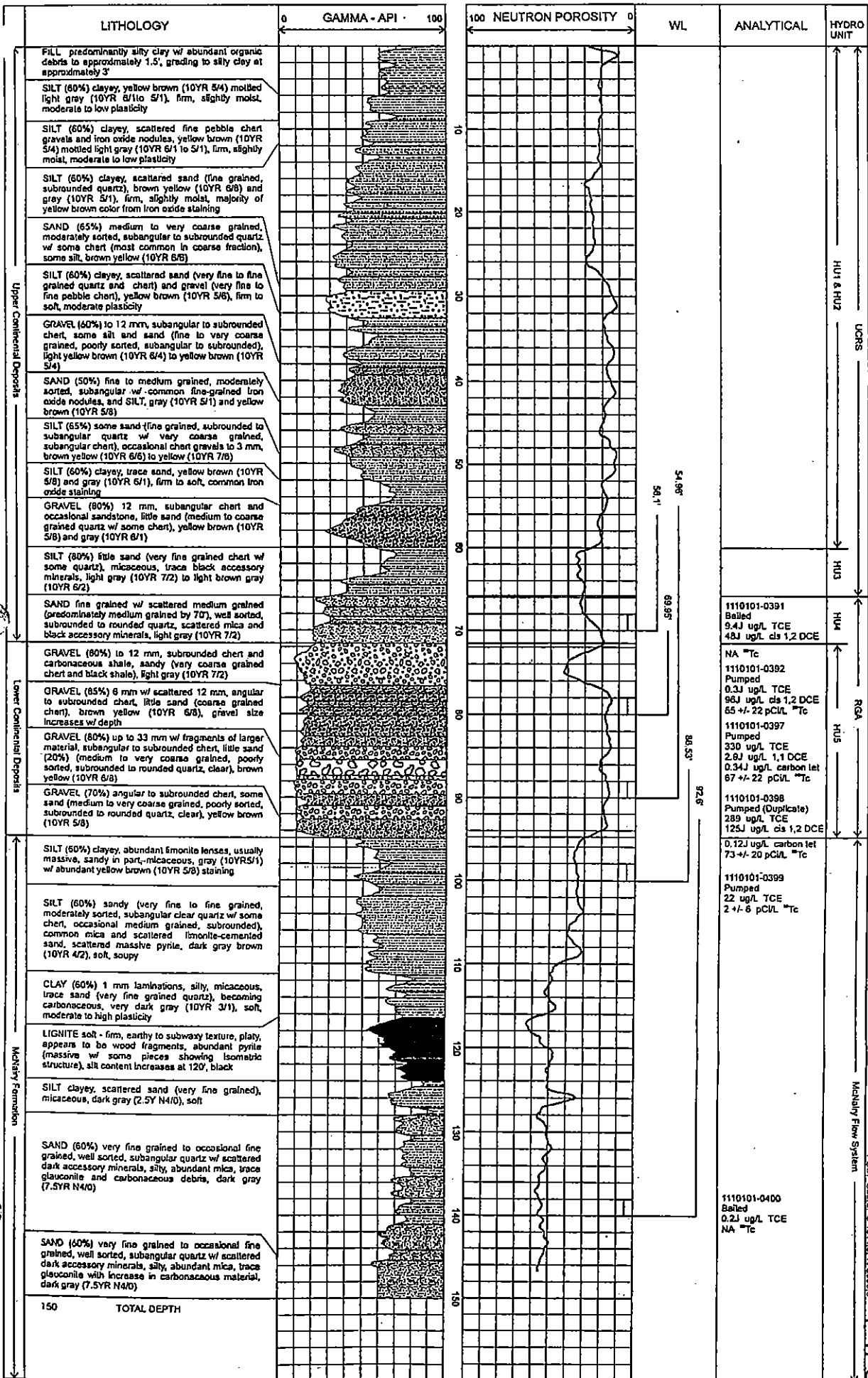
PAE8



Borehole 37718
 RSP Core: 3641Z W222A
P4E1

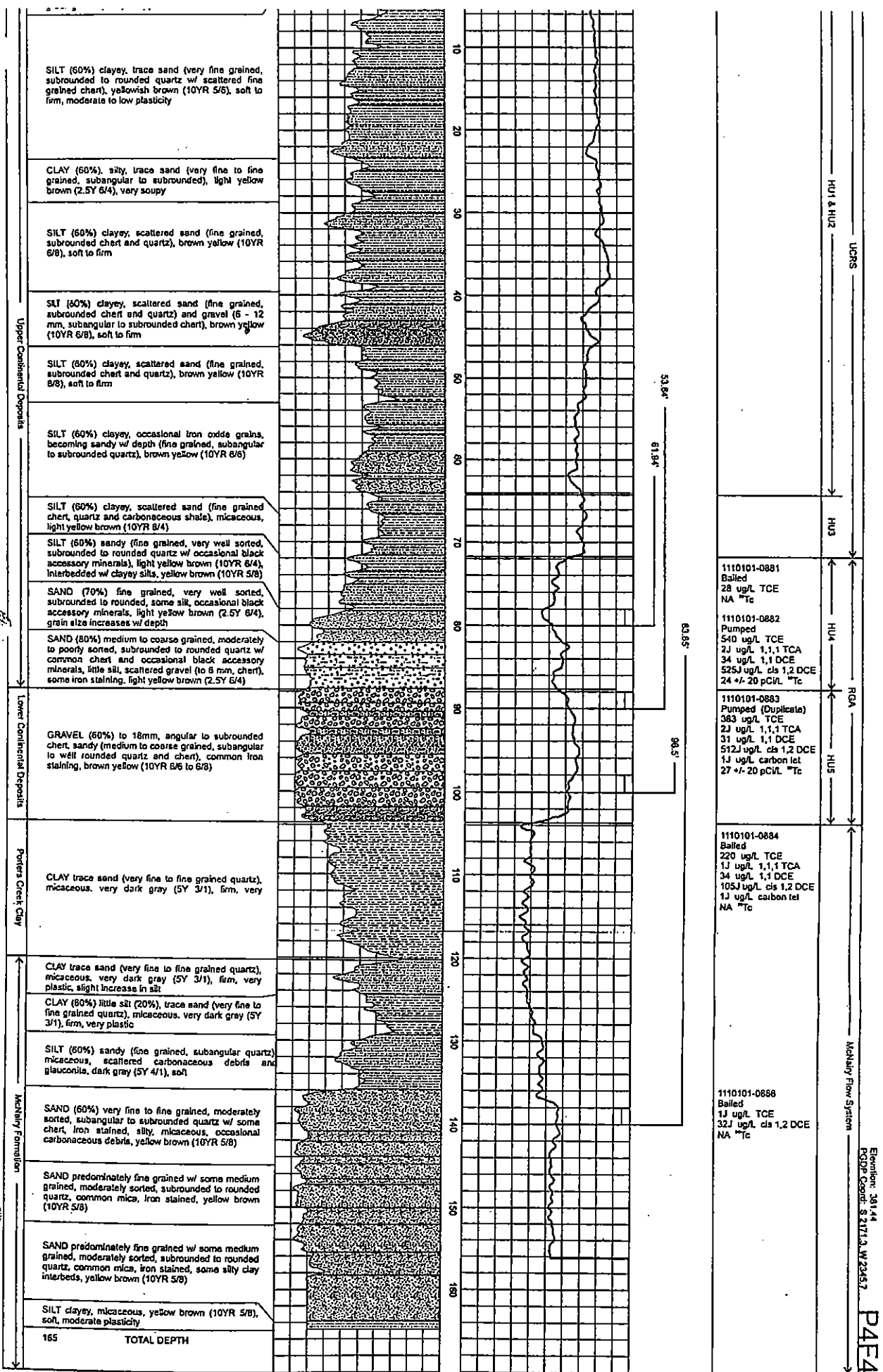


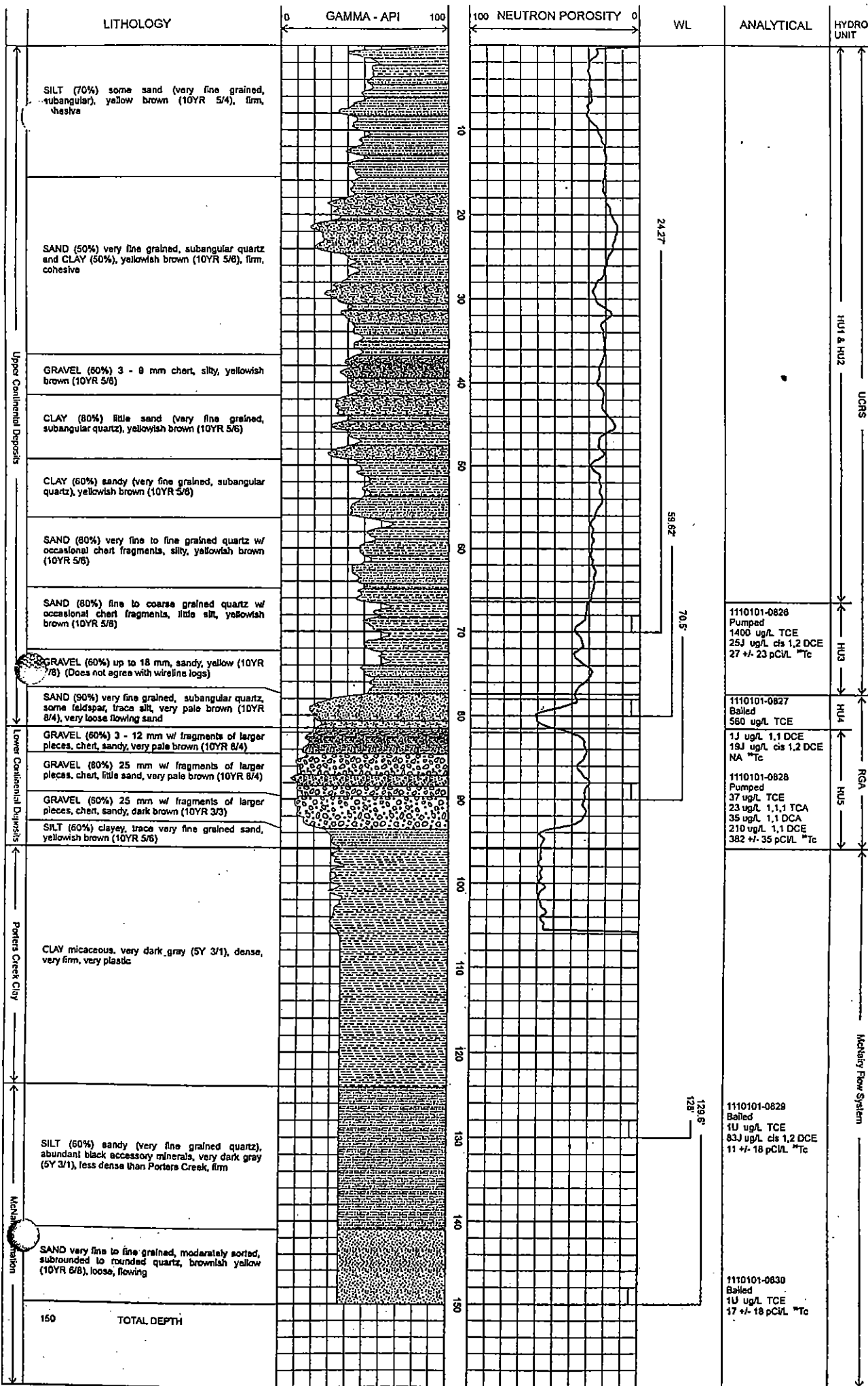
P4E2



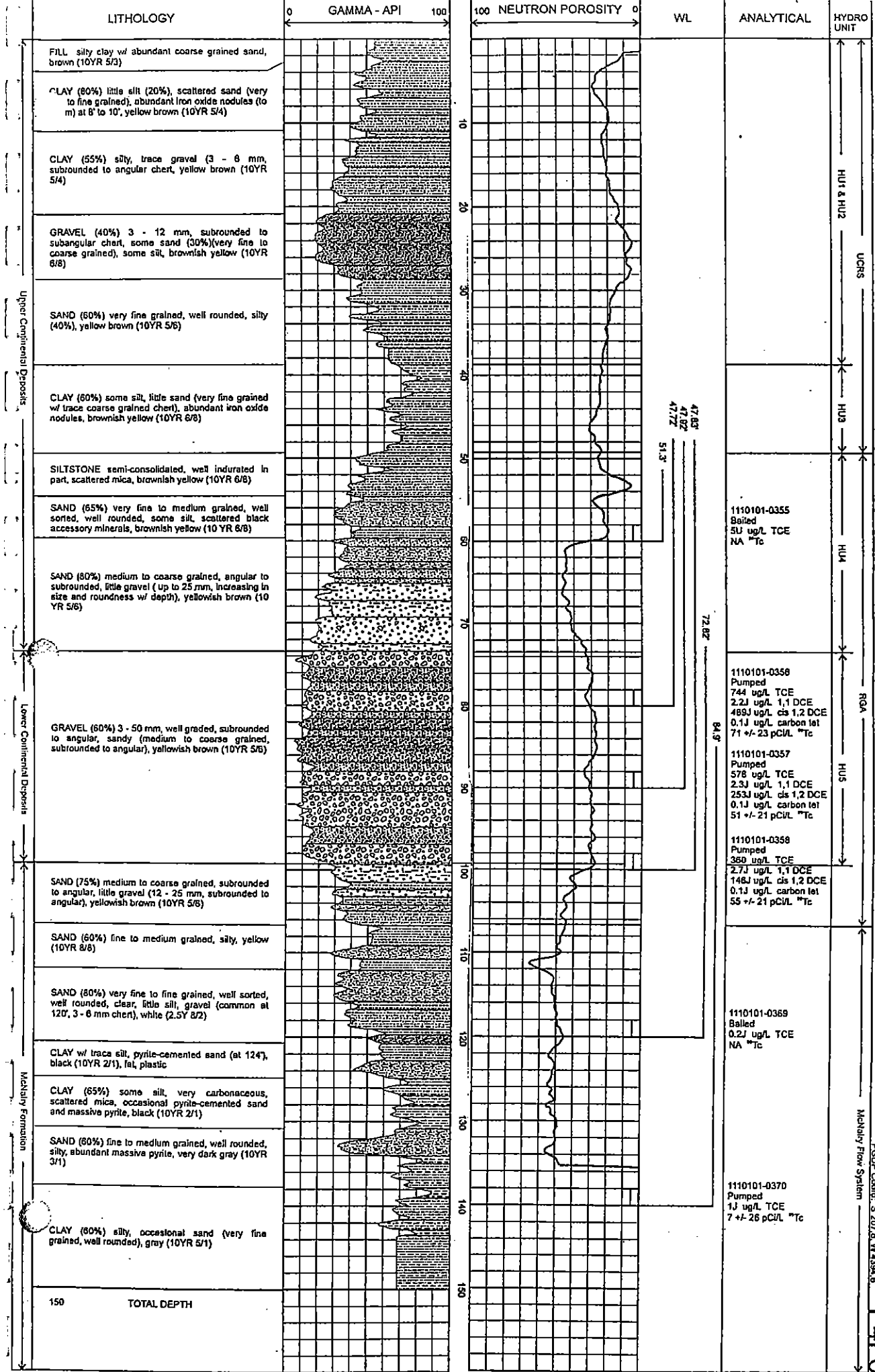
Environ: 38228
F03P Oahai S 1614 S.W. 3059.0

P4F3



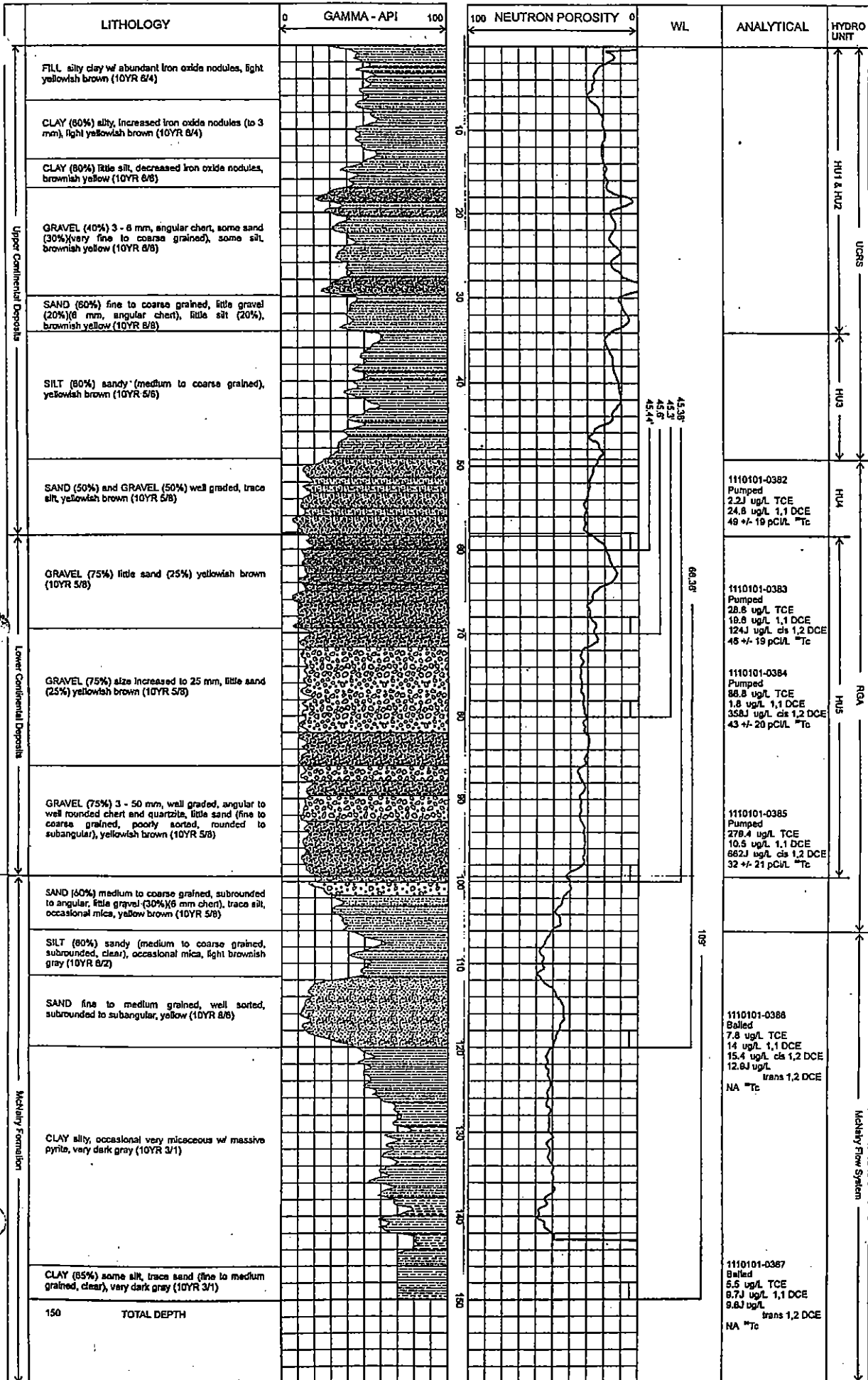


Elevation: 381.88
 FGDF Coord: S 2868.5, W 2095.8



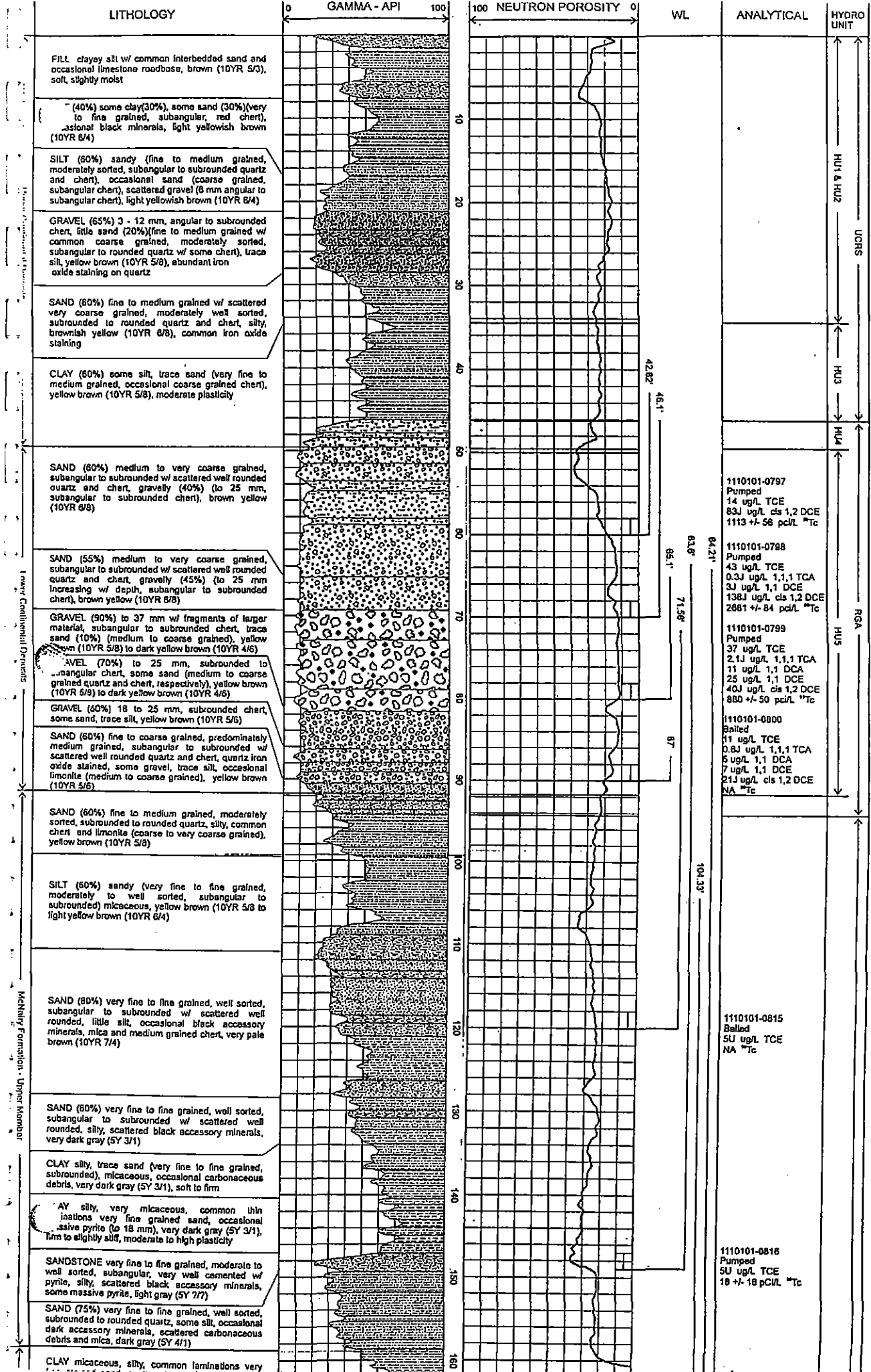
Elevation: 375.97
 PSDP Count: S-207.8 W-4394.8
 Mandary Flow System

P4F6



Elevation: 572.96
 FSDP Core#: N1002.W4812.3

PAF7



SANDSTONE very fine to fine grained, moderate to well sorted, subangular, very well cemented w/ pyrite, silty, scattered black accessory minerals, some massive pyrite, light gray (SY 7/7)

SAND (75%) very fine to fine grained, well sorted, subrounded to rounded quartz, some silt, occasional dark accessory minerals, scattered carbonaceous debris and mica, dark gray (SY 4/1)

Y micaceous, silty, common laminations very grained sand, scattered carbonaceous debris, dark gray (SY 4/1)

SILT (80%) little sand (20%) (very fine to fine grained, well sorted, subangular to subrounded), micaceous, common carbonaceous debris, scattered black accessory minerals, dark gray (SY 4/1), sand increases w/ depth

SAND (70%) very fine to fine grained, well sorted, subangular to subrounded, occasional well rounded, some silt, micaceous, trace black accessory minerals, scattered carbonaceous debris, dark gray (SY 4/1)

SAND (85%) very fine to fine grained, well sorted, subangular to subrounded, trace silt, micaceous, scattered carbonaceous debris, occasional black accessory minerals, gray (SY 5/1) to dark gray (SY 4/1)

SAND (70%) fine grained, well sorted, subrounded to rounded, little silt, micaceous, common carbonaceous debris, dark gray (SY 4/1)

SAND (85%) fine grained, well sorted, subrounded to rounded, trace silt, micaceous, common carbonaceous debris, dark gray (SY 4/1)

SILT (60%) sandy (40%) (fine grained w/ occasional medium grained, well sorted, subangular to well rounded), micaceous, abundant wood fragments up to 12 mm, gray brown (2.5YR 5/2)

SILT (60%) sandy (40%) (fine grained w/ occasional medium grained, well sorted, subangular to well rounded), micaceous, decreasing wood fragments becoming absent by 235', gray brown (2.5YR 5/2)

SILT (60%) clayey (30%), slightly micaceous, common sand (very fine- to fine-grained), common carbonaceous debris, scattered siltstone (slightly sandy, micaceous, occasional carbonaceous debris, light brown), siltstone decreasing by 245', dark gray (SY 4/1)

SILT (75%) some sand (25%) (very fine- to fine-grained w/ occasional medium-grained, subangular to well-rounded, moderately sorted), micaceous, scattered siltstone fragments, dark gray (SY 4/1)

CLAY (60%) silty (40%), common thin laminations <1 mm sand (very fine grained quartz, slightly micaceous), scattered carbonaceous debris, dark gray (SY 4/1), firm to slightly stiff, moderate to high plasticity

SILT clayey, micaceous, scattered carbonaceous debris, increasing sand (very fine grained, subrounded), occasional fragments pyrite-cemented sandstone, very dark gray (SY 3/1)

SILT (70%) some sand (30%), micaceous, common carbonaceous debris, occasional siltstone gravel (12 mm, carbonaceous, slightly micaceous, tan), dark gray (SY 4/1)

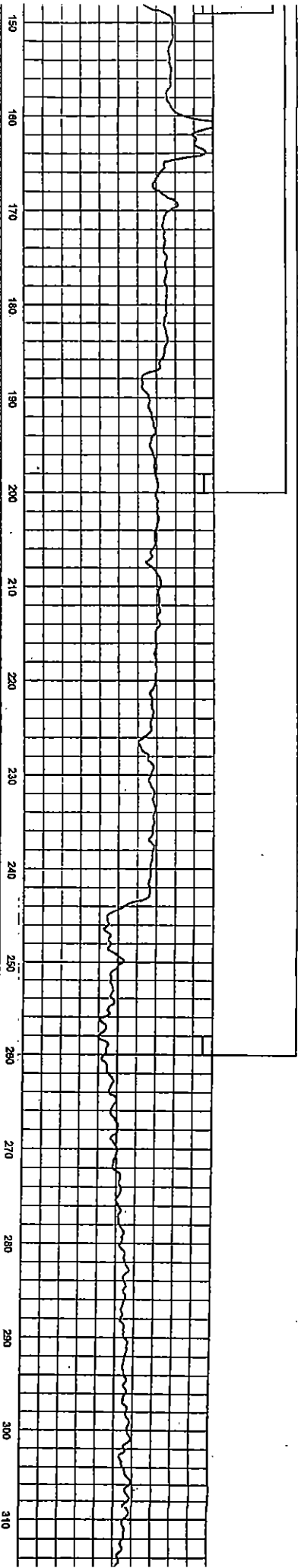
SAND (70%) very fine to fine-grained (predominant) w/ some medium-grained, well sorted, subrounded to rounded, some silt (30%), scattered carbonaceous debris, common siltstone fragments (very sandy, carbonaceous, tan) olive gray (SY 5/2)

SAND (85%) very fine to fine-grained, well sorted, subrounded to rounded, micaceous, common carbonaceous debris, scattered siltstone gravels (very sandy, tan), occasional pyrite-cemented sandstone nodules, gray (SY 5/1)

SAND (90%) very fine to fine-grained, well sorted, rounded to rounded, little silt (10%), scattered thin sandstone (fine grained, pyrite cement, very micaceous, occasional pyritized wood fragments), gray (SY 5/1)

SAND (90%) fine to medium-grained, moderately well sorted, subrounded to rounded, abundant pyrite-cemented sand nodules (3 - 25 mm), common carbonaceous wood fragments (occasionally pyritized), slightly micaceous, dark gray (SY 4/1)

SAND (90%) fine to medium-grained, moderately well sorted, subrounded to rounded, decreasing pyrite-



SU ug/L TCE
18 +/- 16 pCi/L ¹³⁷Cs

1110101-0817
Bailed
SU ug/L TCE
NA ¹³⁷Cs

1110101-0818
Bailed
SU ug/L TCE
17J ug/L cis 1,2 DCE
NA ¹³⁷Cs

Machery Foundation - 1 meter Monitor

Machery Foundation - 1 meter Monitor

Machery Flow System

to weathered, micaceous, silty, shaly, scattered siltstone fragments, dark gray (5Y 4/1)

CLAY (60%) silty (40%), common thin laminations <1 mm sand (very fine grained quartz, slightly micaceous), scattered carbonaceous debris, dark gray (5Y 4/1), firm to slightly stiff, moderate to high plasticity

clayey, micaceous, scattered carbonaceous s, increasing sand (very fine grained, subrounded), occasional fragments pyrite-cemented sandstone, very dark gray (5Y 3/1)

SILT (70%) some sand (30%), micaceous, common carbonaceous debris, occasional siltstone gravel (12 mm, carbonaceous, slightly micaceous, tan), dark gray (5Y 4/1)

SAND (70%) very fine to fine-grained (predominant) w/ some medium-grained, well sorted, subrounded to rounded, some silt (30%), scattered carbonaceous debris, common siltstone fragments (very sandy, carbonaceous, tan) olive gray (5Y 5/2)

SAND (85%) very fine to fine-grained, well sorted, subrounded to rounded, micaceous, common carbonaceous debris, scattered siltstone gravels (very sandy, tan), occasional pyrite-cemented sandstone nodules, gray (5Y 5/1)

SAND (90%) very fine to fine-grained, well sorted, subrounded to rounded, little silt (10%), scattered nodules sandstone (fine grained, pyrite cement, very carbonaceous, occasional pyritized wood fragments), gray (5Y 5/1)

SAND (90%) fine to medium-grained, moderately well sorted, subrounded to rounded, abundant pyrite-cemented sand nodules (3 - 25 mm), common carbonaceous wood fragments (occasionally pyritized), slightly micaceous, dark gray (5Y 4/1)

SAND (90%) fine to medium-grained, moderately well sorted, subrounded to rounded, decreasing pyrite-cemented sand nodules (3 - 25 mm, gone by 315), common carbonaceous wood fragments (occasionally pyritized), slightly micaceous, dark gray (5Y 4/1)

SAND (85%) fine-grained, well sorted, clean, subangular to subrounded, occasional carbonaceous debris and mica, abundant pyritized sand nodules at 330', light gray (5Y 7/1)

SAND medium to coarse-grained, moderately sorted, clean, well rounded, abundant pyritized sand nodules, common black carbonaceous wood fragments, trace siliceous limestone gravels (3 mm), dark gray (5Y 4/1)

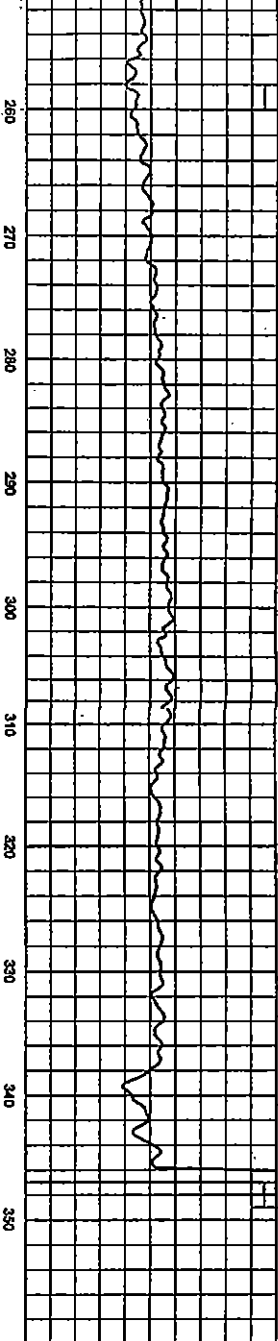
GRAVEL 12 mm, clean, silicified limestone, occasional sand (coarse grained, decreases w/ depth), trace pyritized sand, gray (5Y 6/1) to very dark gray (5Y 3/1)

LIMESTONE, weathered, clay, limestone fragments, dark grayish brown

LIMESTONE very fine crystalline, hard, no visible porosity, light to medium gray

350 TOTAL DEPTH

Turbidite Zone
Micaschist/limestone

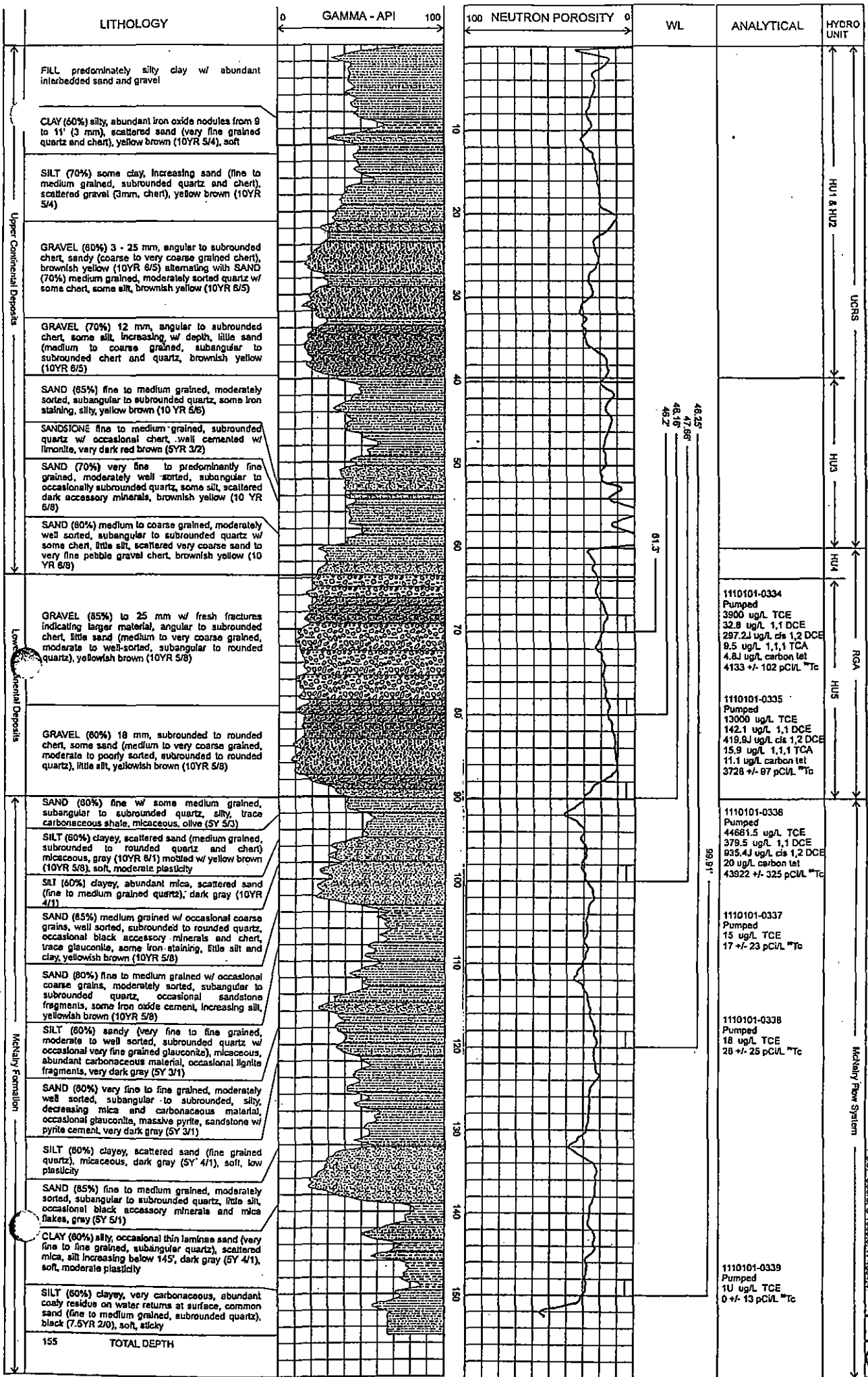


1110101-0818
Bailed
5U ug/L TCE
17J ug/L cis 1,2 DCE
NA Tc

1110101-0819
Bailed
5U ug/L TCE
20 +/- 20 pc/L Tc

Elevation: 371.55
FGDP Coord: N 690, W 4814

PAGE 8



46.25
47.86
48.16
48.2

61.3

99.91

1110101-0334
Pumped
3900 ug/L TCE
32.9 ug/L 1,1 DCE
297.2J ug/L cis 1,2 DCE
8.5 ug/L 1,1,1 TCA
4.8J ug/L carbon tet
4133 +/- 102 pCi/L ²²⁶Rn

1110101-0335
Pumped
13000 ug/L TCE
142.1 ug/L 1,1 DCE
419.8J ug/L cis 1,2 DCE
15.9 ug/L 1,1,1 TCA
11.1 ug/L carbon tet
3728 +/- 87 pCi/L ²²⁶Rn

1110101-0336
Pumped
44681.5 ug/L TCE
379.5 ug/L 1,1 DCE
935.4J ug/L cis 1,2 DCE
20 ug/L carbon tet
43922 +/- 325 pCi/L ²²⁶Rn

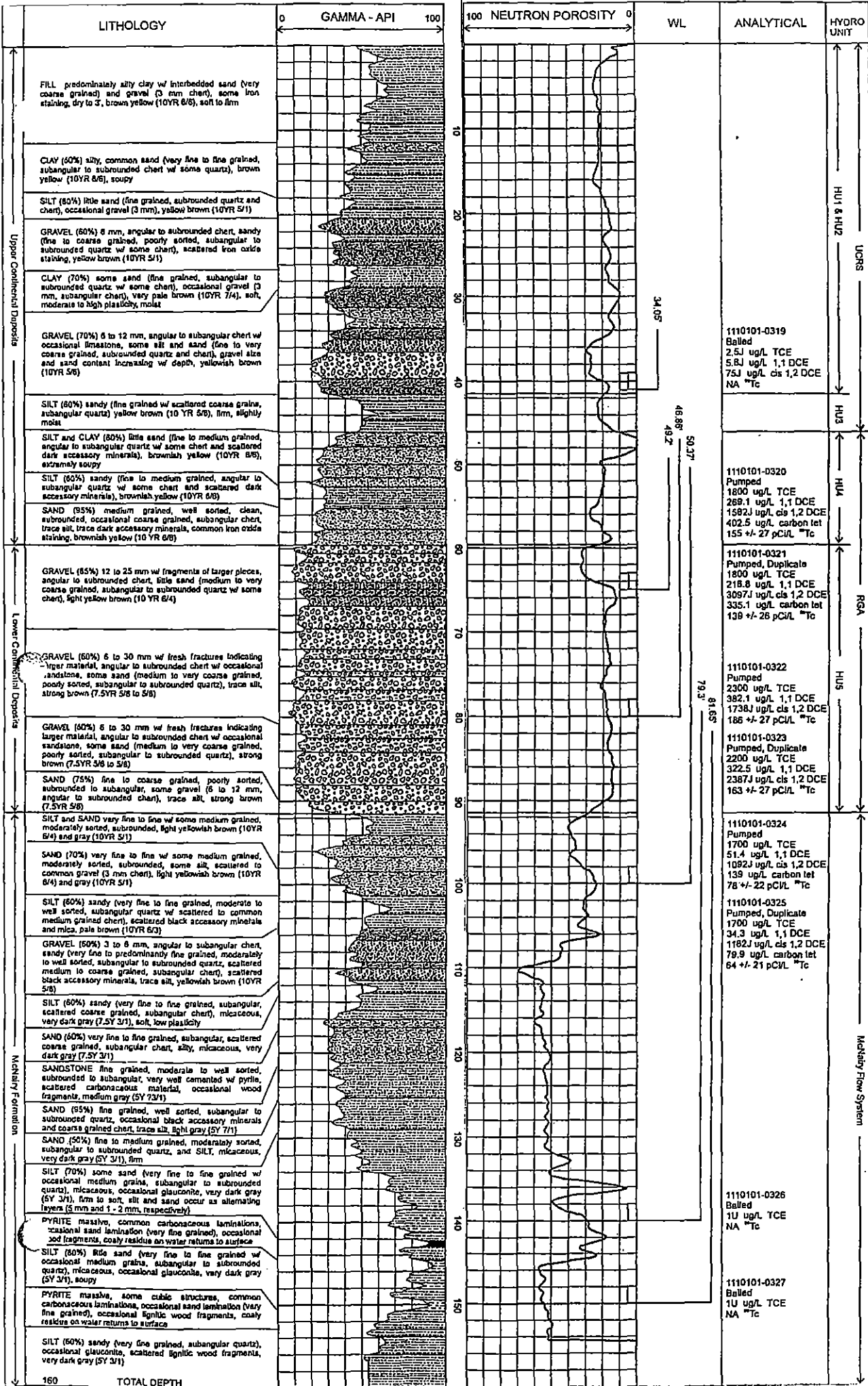
1110101-0337
Pumped
15 ug/L TCE
17 +/- 23 pCi/L ²²⁶Rn

1110101-0338
Pumped
18 ug/L TCE
26 +/- 25 pCi/L ²²⁶Rn

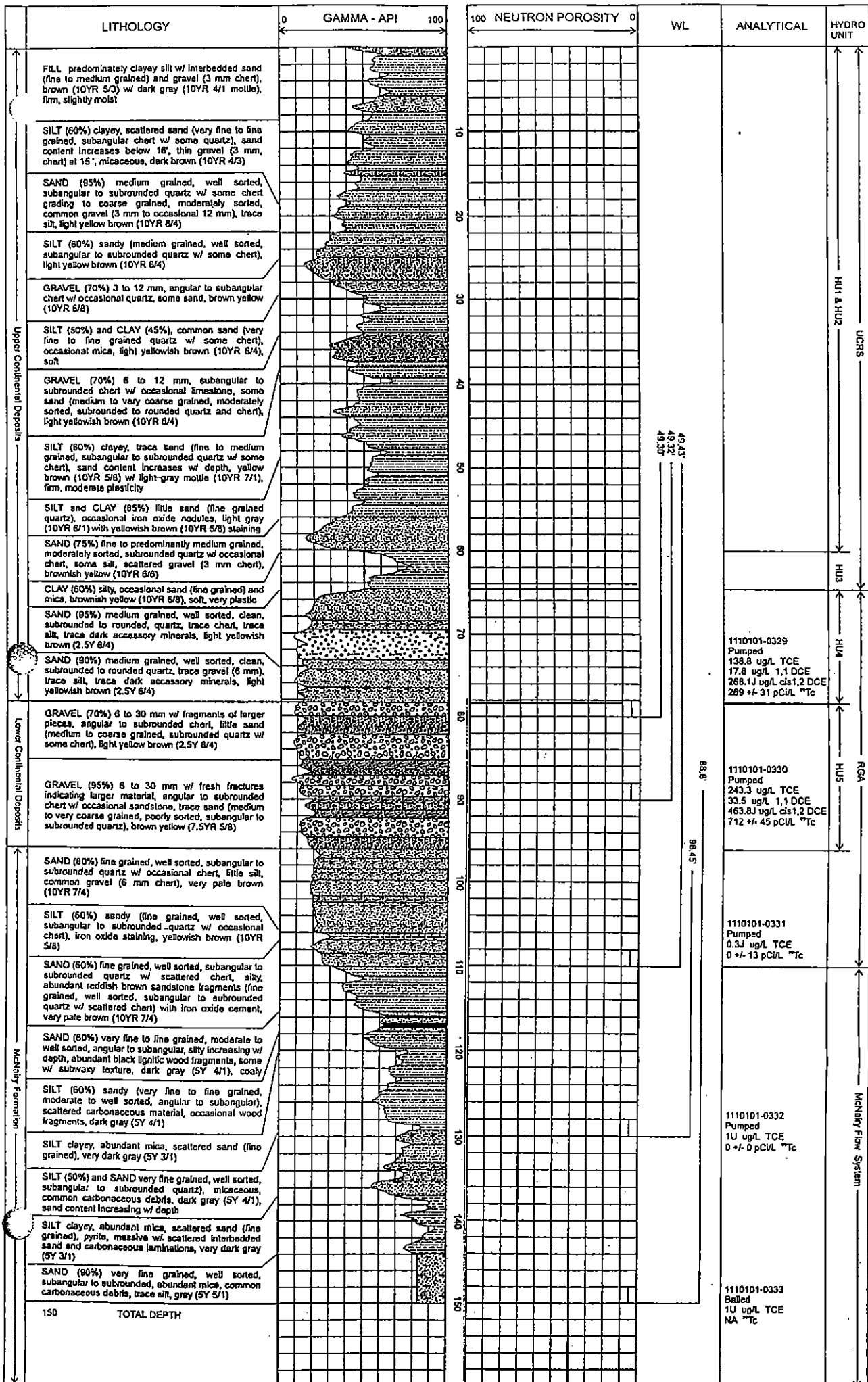
1110101-0339
Pumped
1U ug/L TCE
0 +/- 13 pCi/L ²²⁶Rn

Elevation: 376.19
PGDS Coord: S. 1005.5, W. 455.4

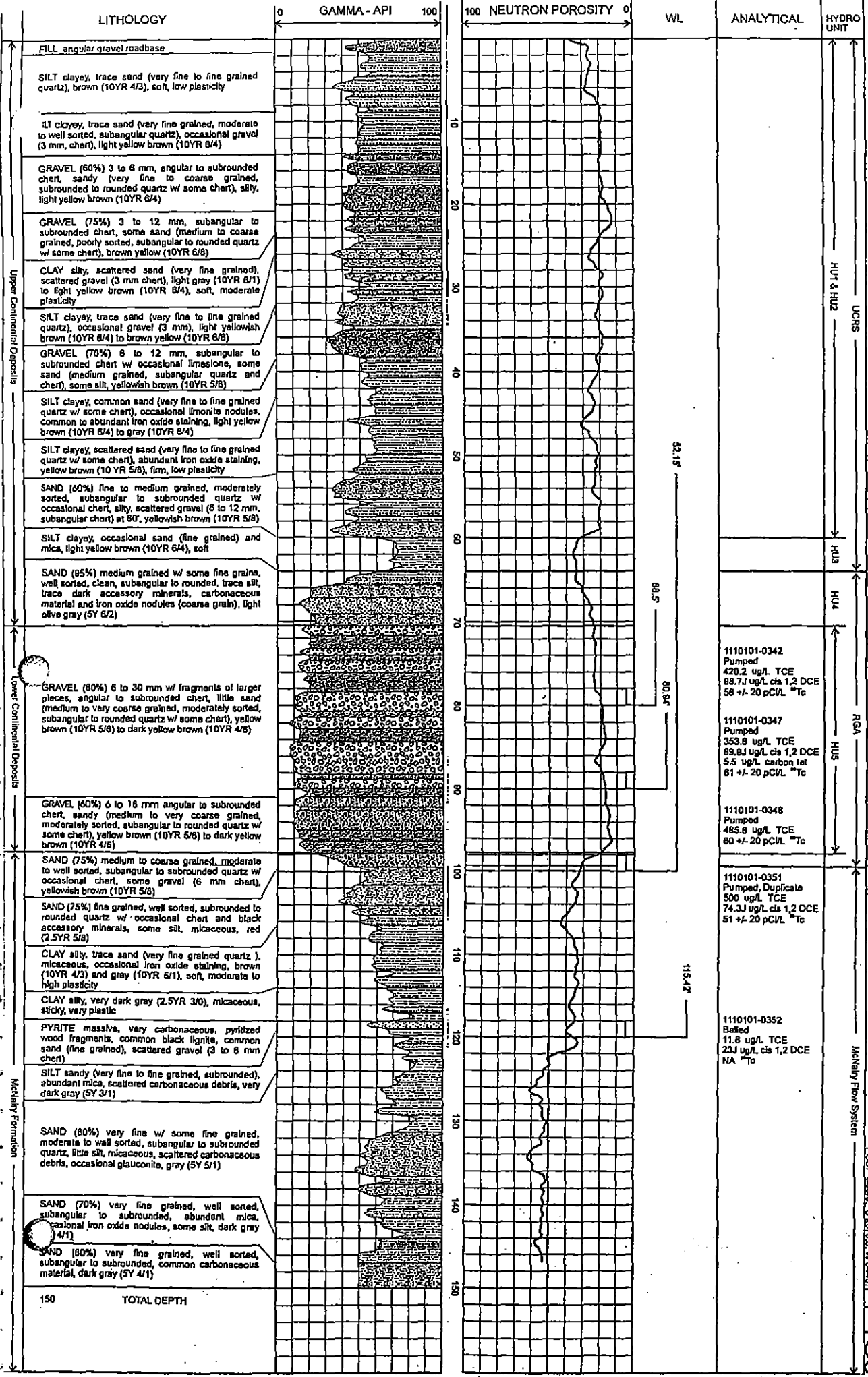
P4G1



Elevation: 318.89
PODP Coord: S 1008.8 W 3913.2



Elevation: 378.20
 Project: 32087.0 W 3871.0



1110101-0342
Pumped
420.2 ug/L TCE
88.7 ug/L cis 1,2 DCE
58 +/- 20 pCVL TMTc

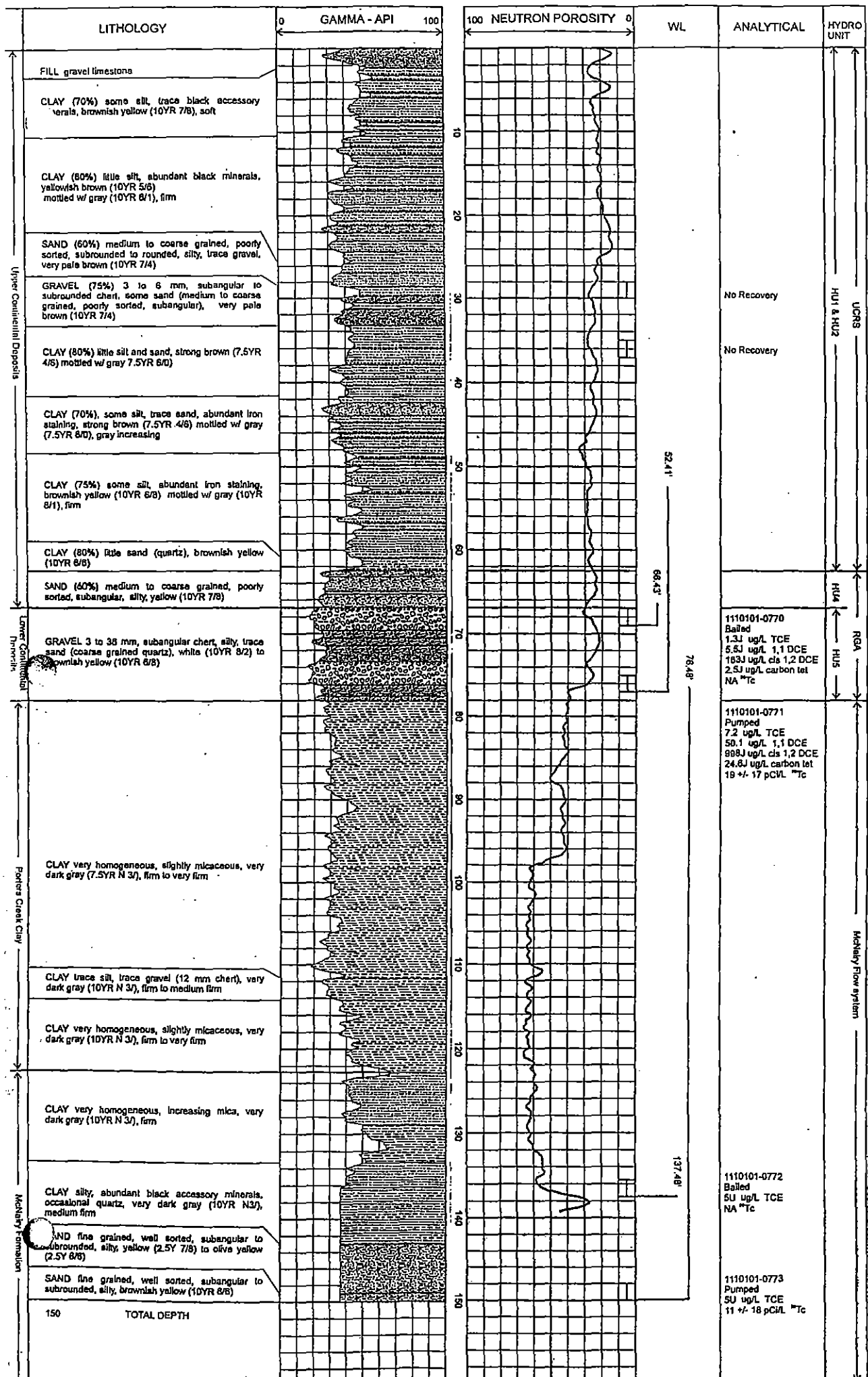
1110101-0347
Pumped
353.8 ug/L TCE
89.8 ug/L cis 1,2 DCE
5.5 ug/L carbon tet
81 +/- 20 pCVL TMTc

1110101-0348
Pumped
485.8 ug/L TCE
60 +/- 20 pCVL TMTc

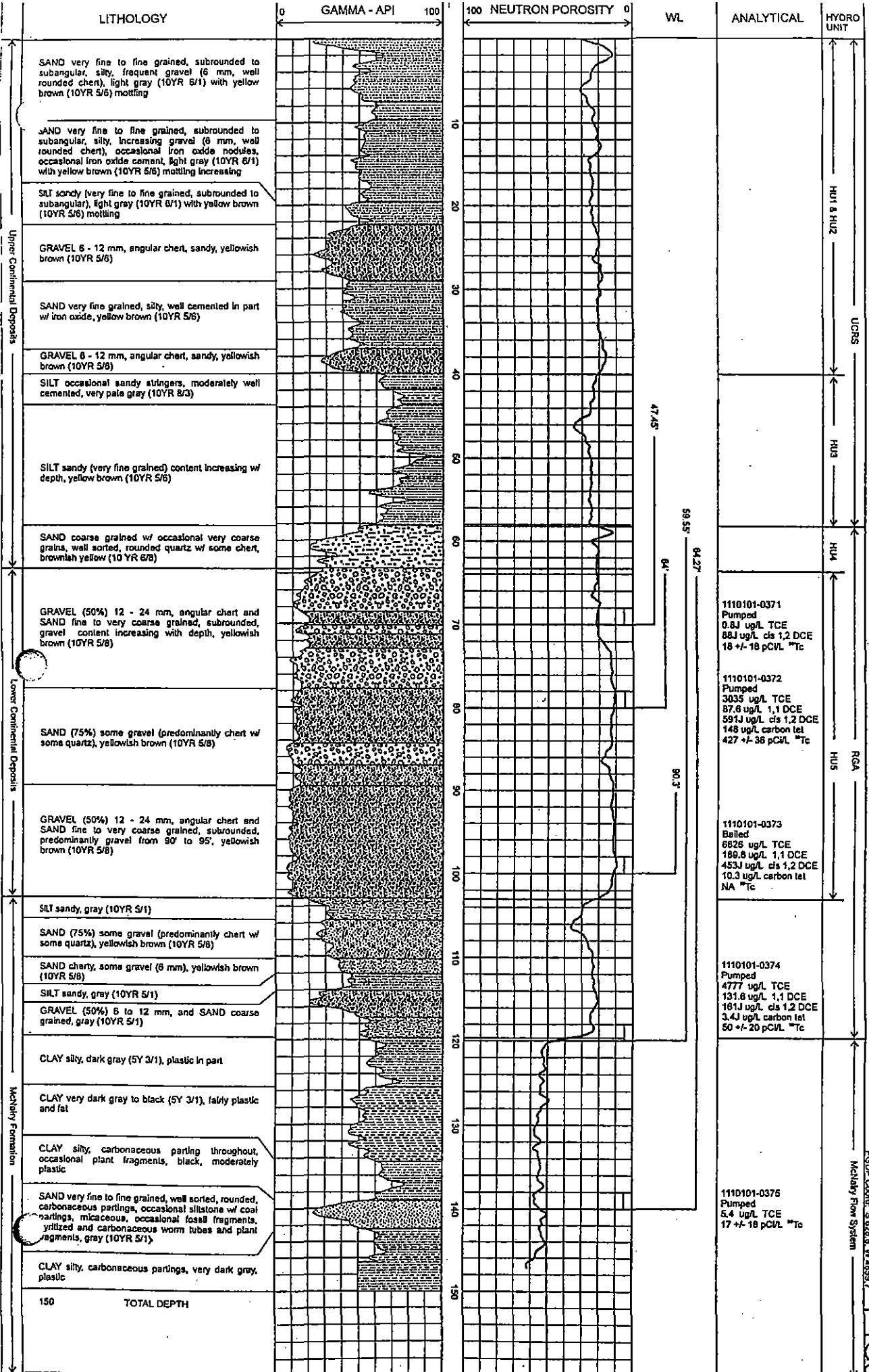
1110101-0351
Pumped, Duplicate
500 ug/L TCE
74.3 ug/L cis 1,2 DCE
51 +/- 20 pCVL TMTc

1110101-0352
Bailed
11.8 ug/L TCE
23J ug/L cis 1,2 DCE
NA TMTc

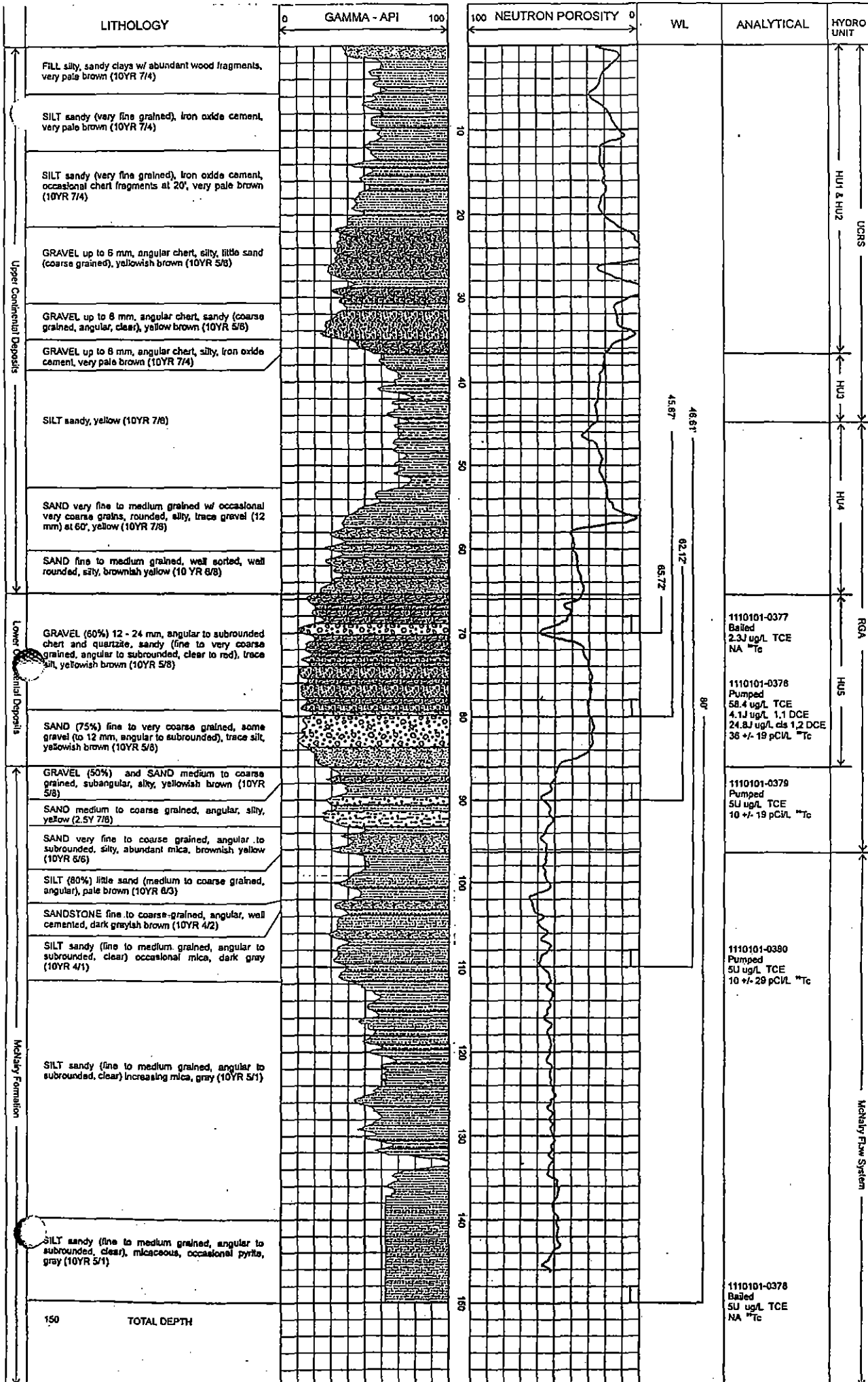
Elevation: 391.96
RSPD Coord: S 2879.3, W 3400.1
PAG5



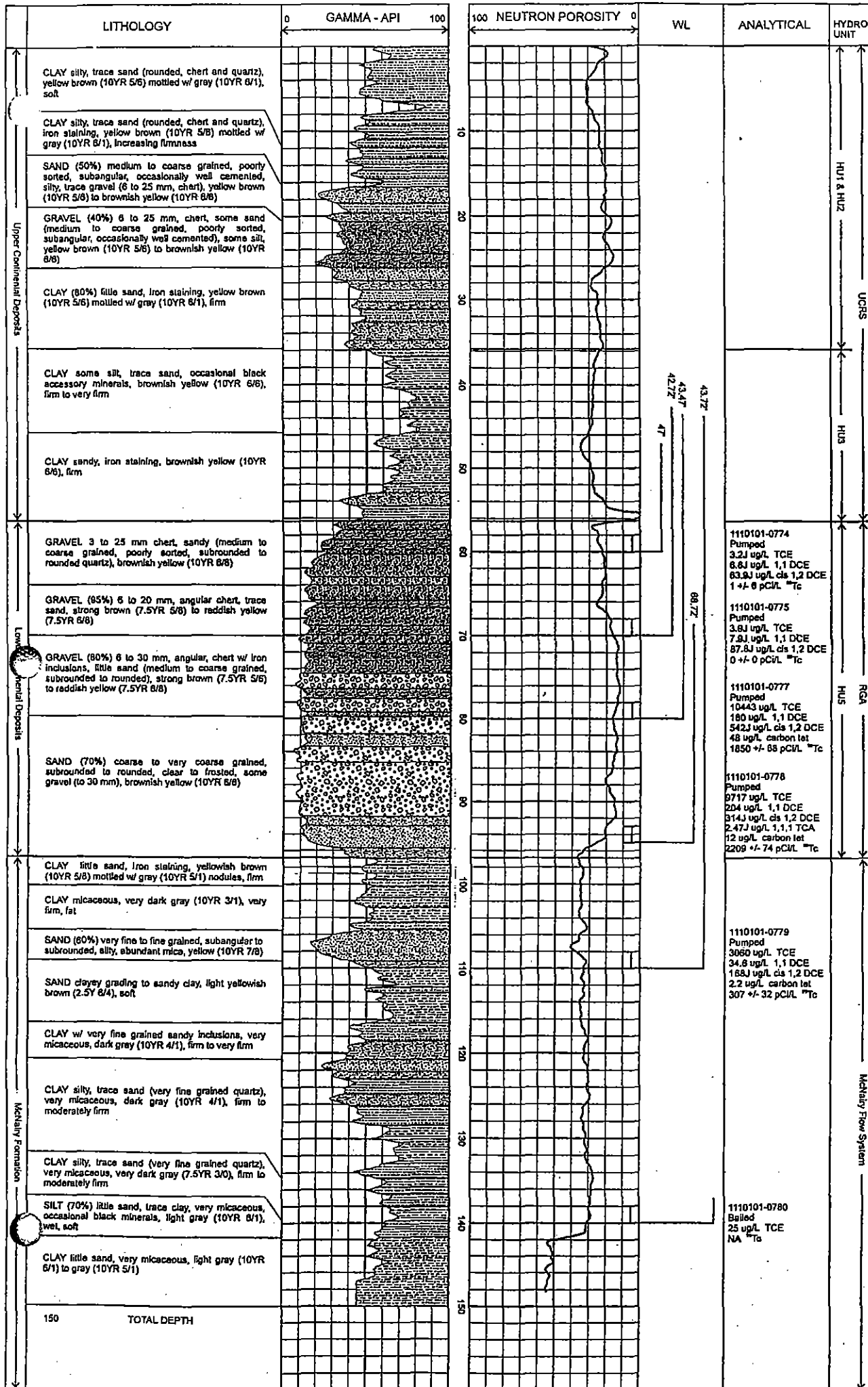
Elevation: 361.68
 PGDP Coord. S. 3079.6, W. 2217.0

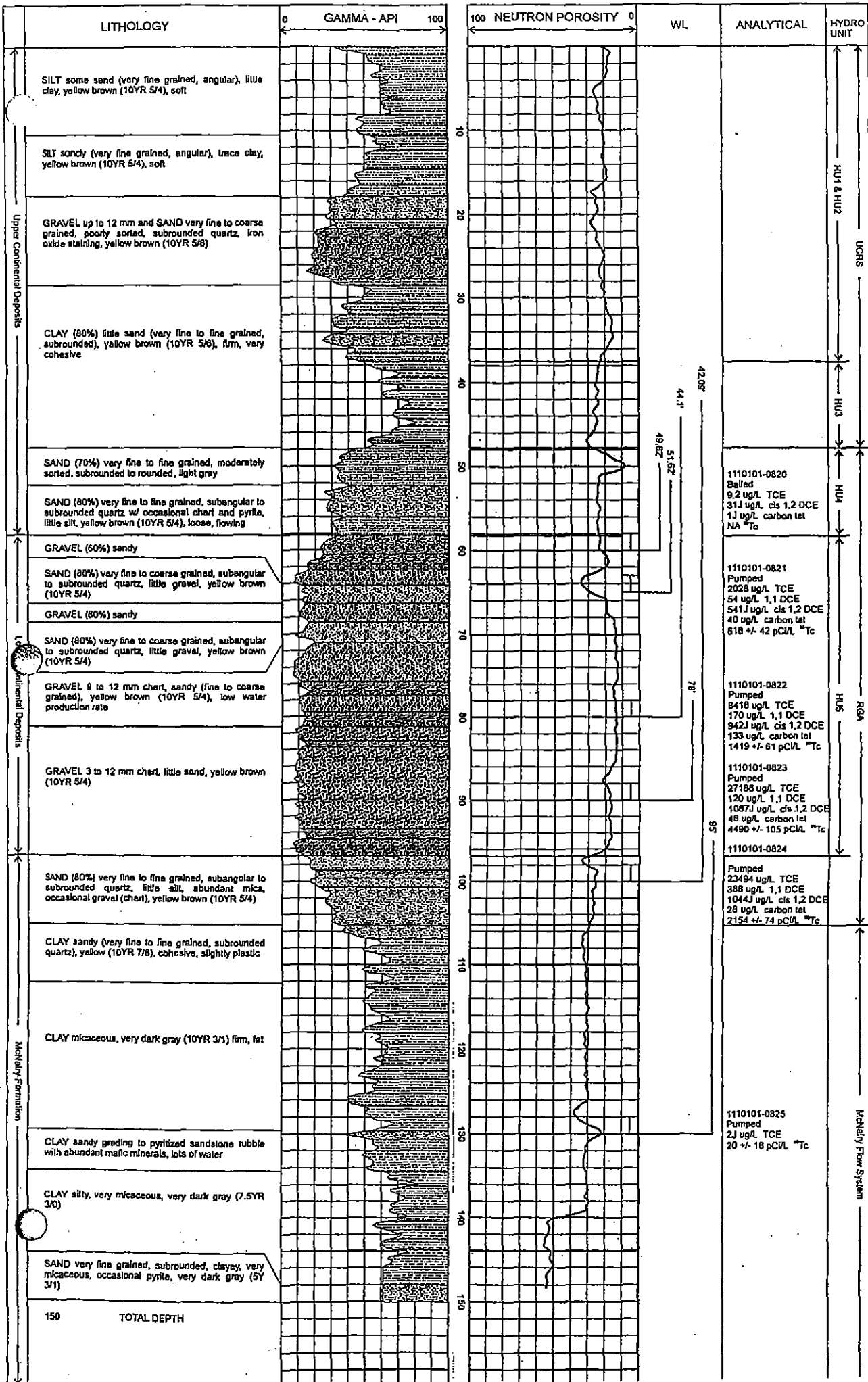


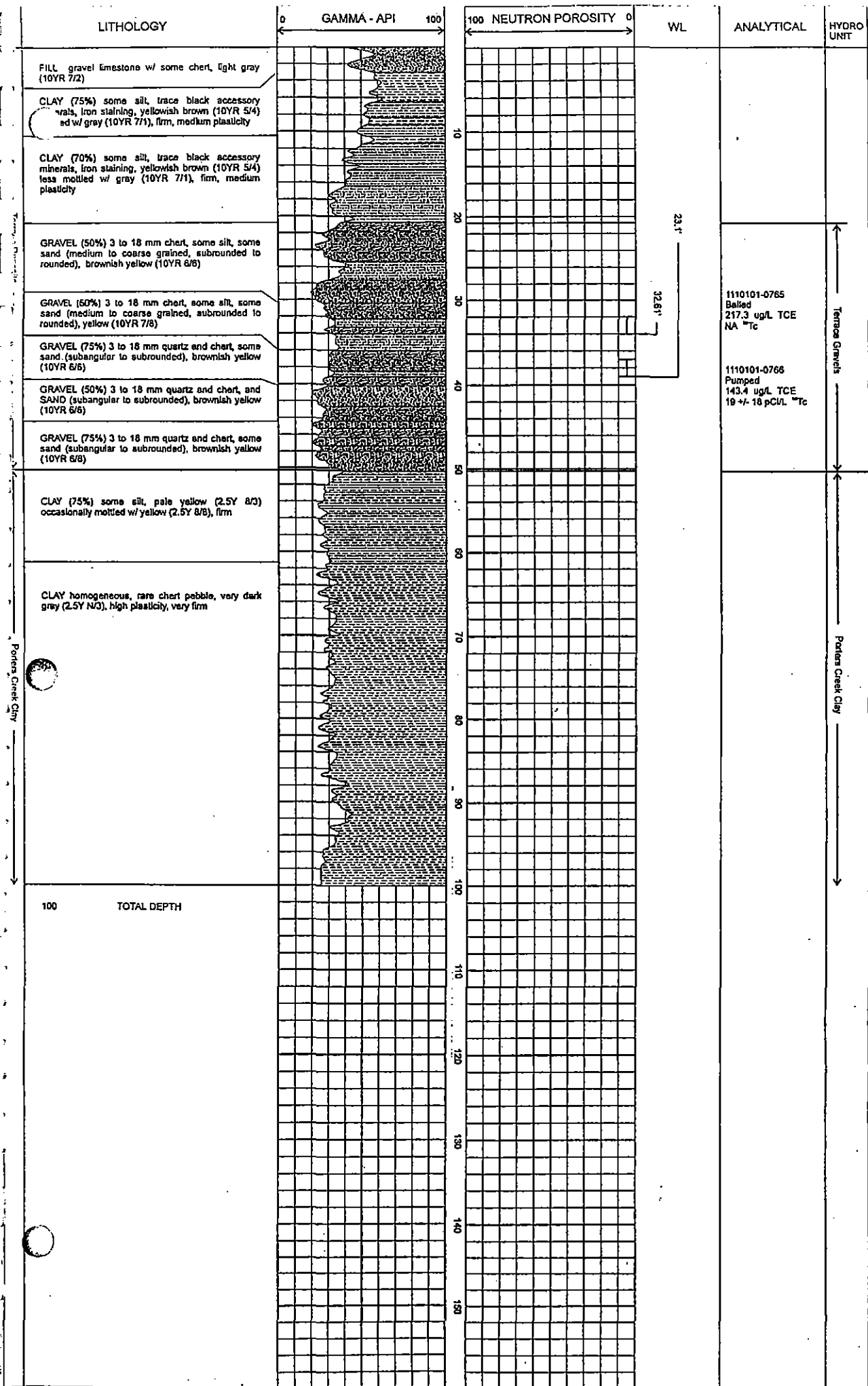
Elevation: 375.13
PCDP Cont. S 628.8 W 489.7
McNelly Flow System



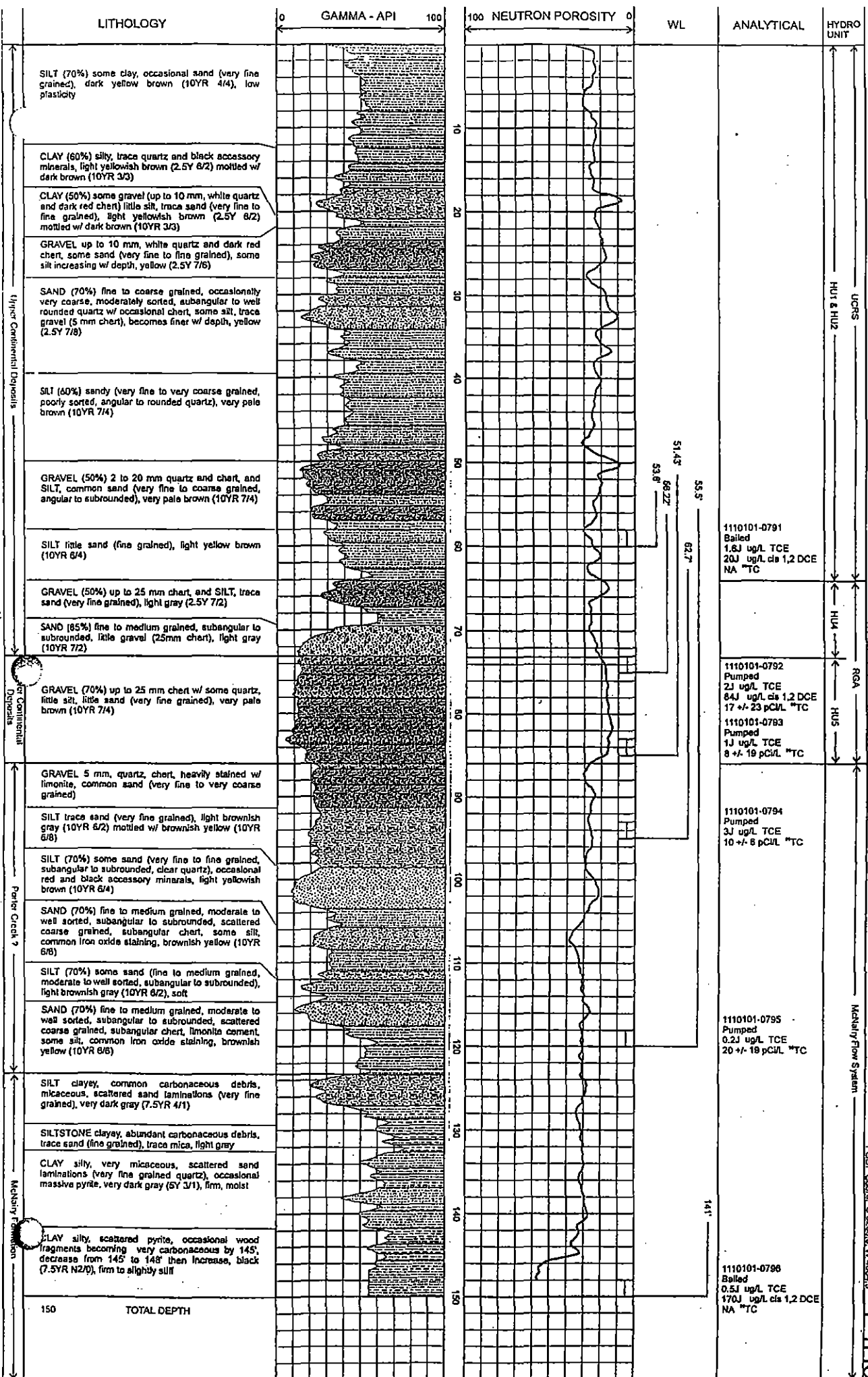
Revised: 3/7/85
 Field Coord: S 873.8, W 5398.1



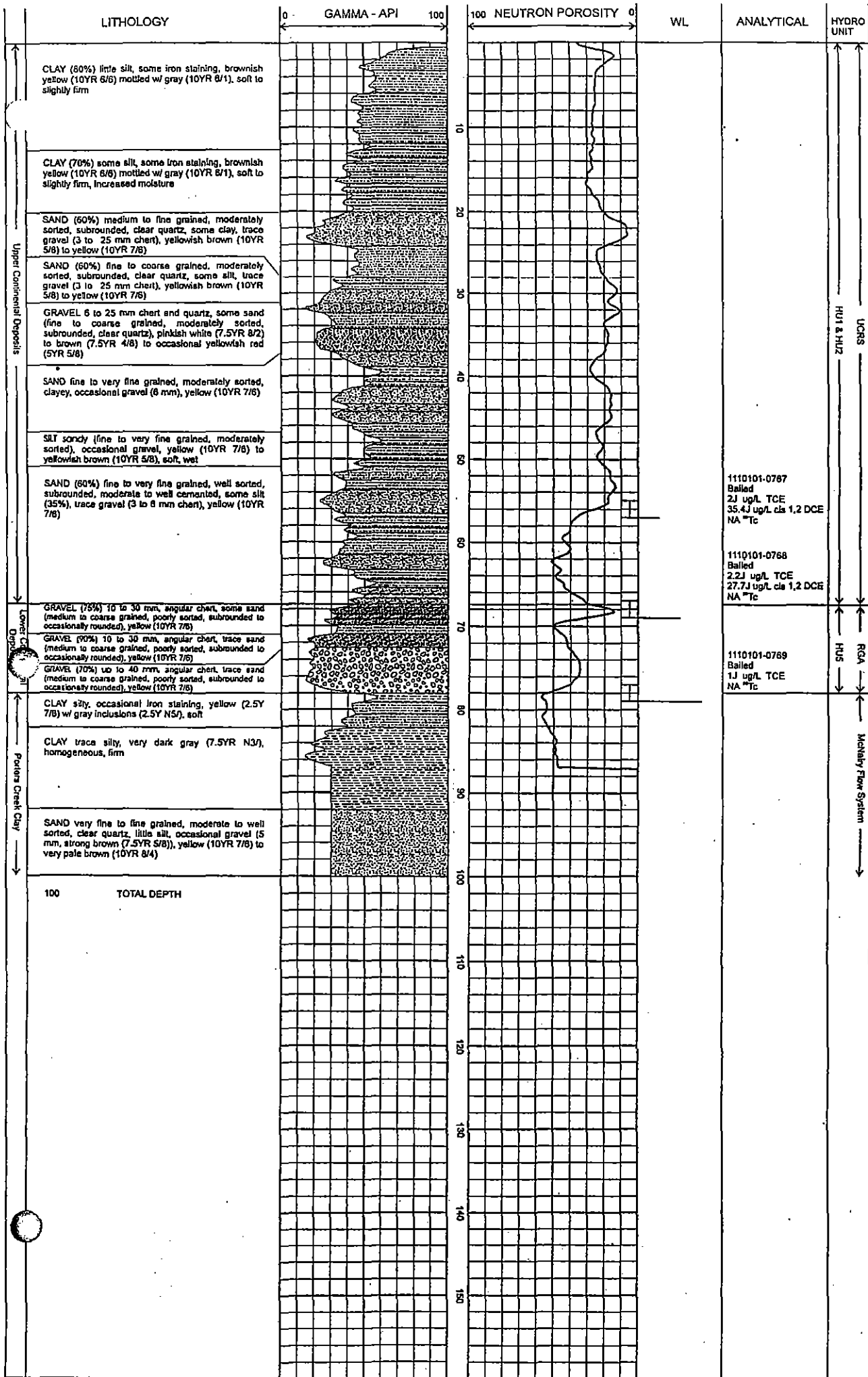




Elevation: 382.4
 PGDP Coord: S 3491.8, W 2356.1
P4H1

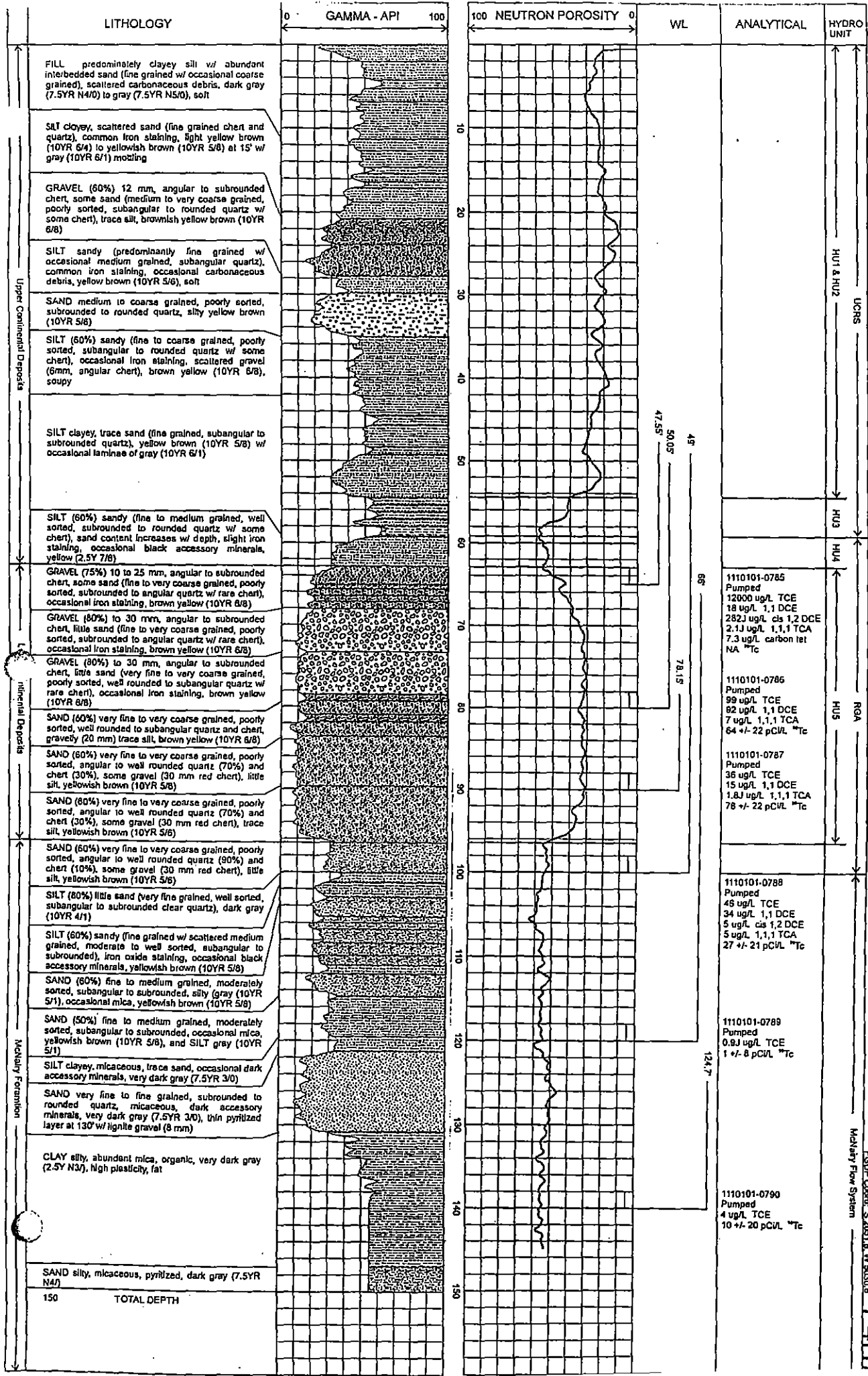


Elevation: 390.06
 P&GP Coord: S 3288.0, W 4094.3
PAHS



Drawn: 363.53
 PGP/Coast S 3481 & W 3731.0

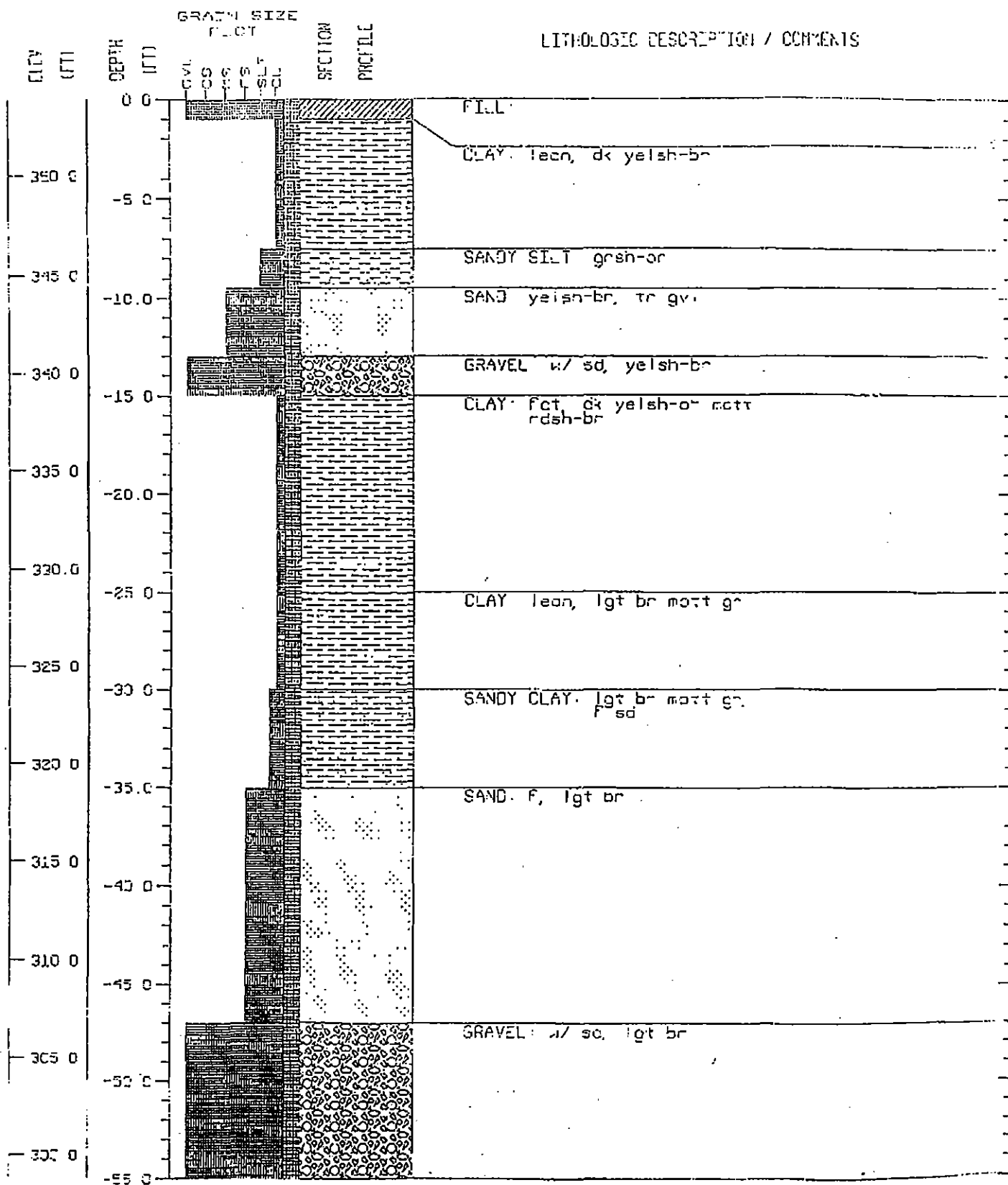
P4H6



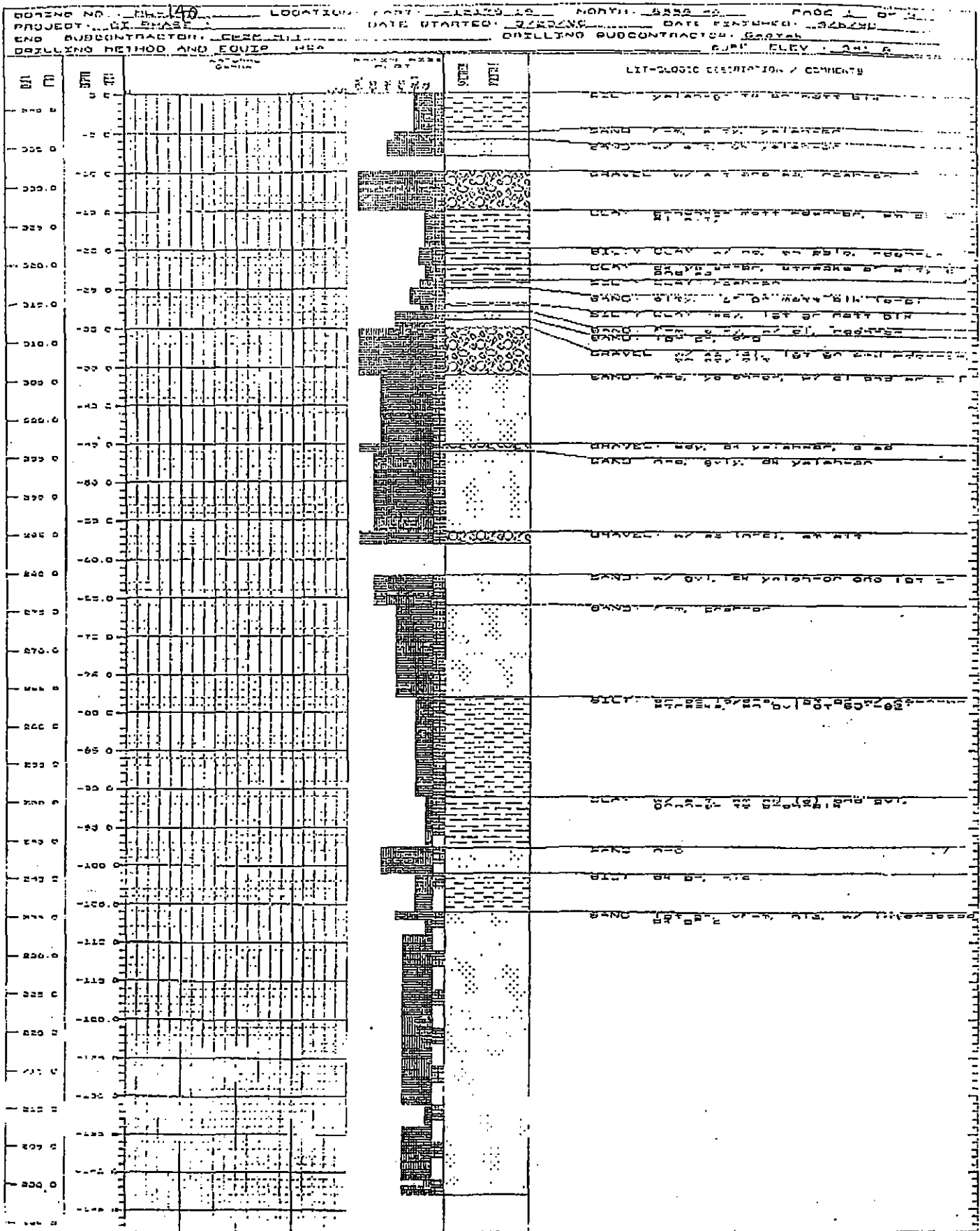
Elevation: 372.81
 PCSP Cont. S.0831.0 W.800.8
 Mainly Flow System
PAH

MW-194

353 8



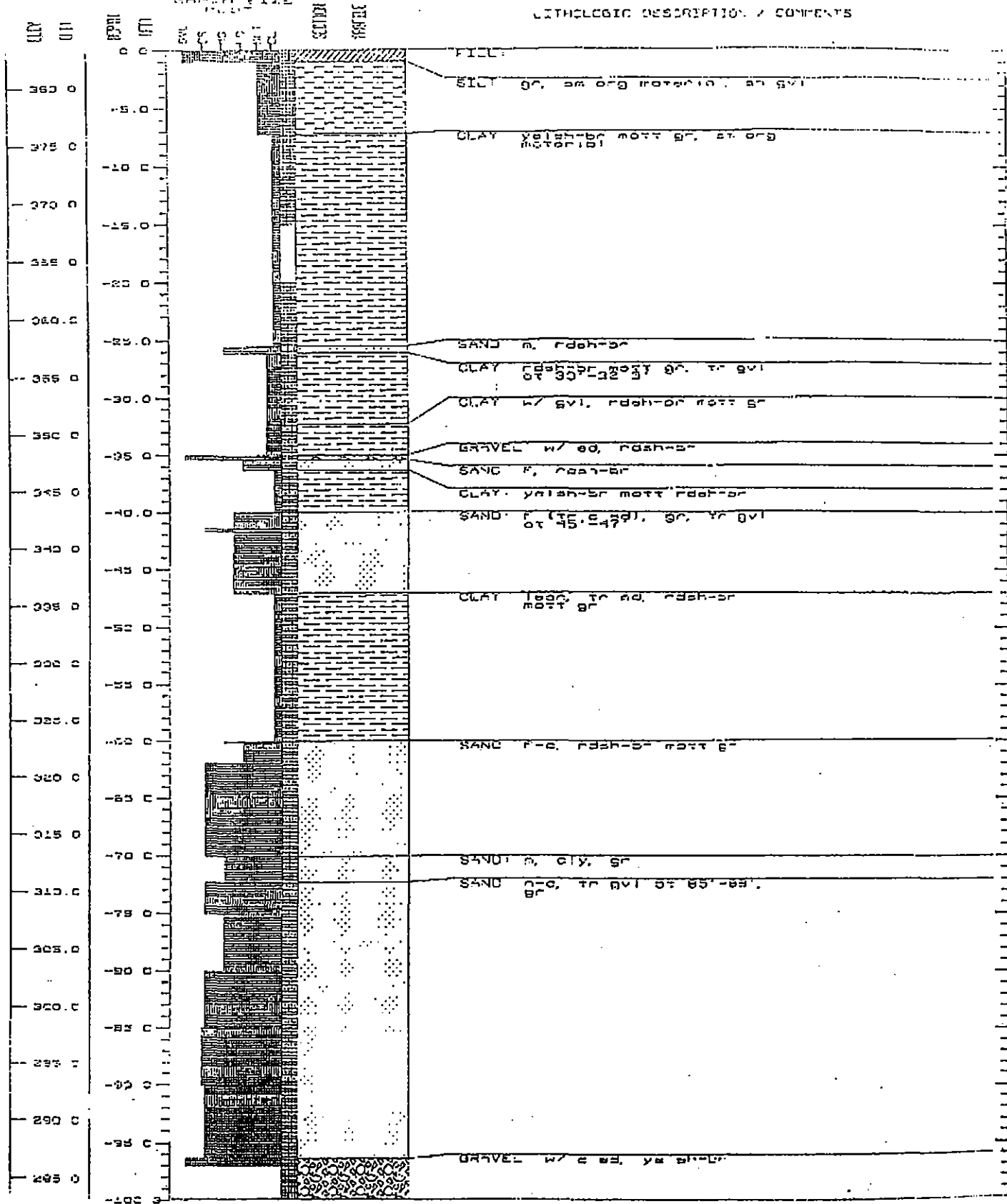
MW-140



MW-163

303 1

LITHOLOGIC DESCRIPTION & COMMENTS

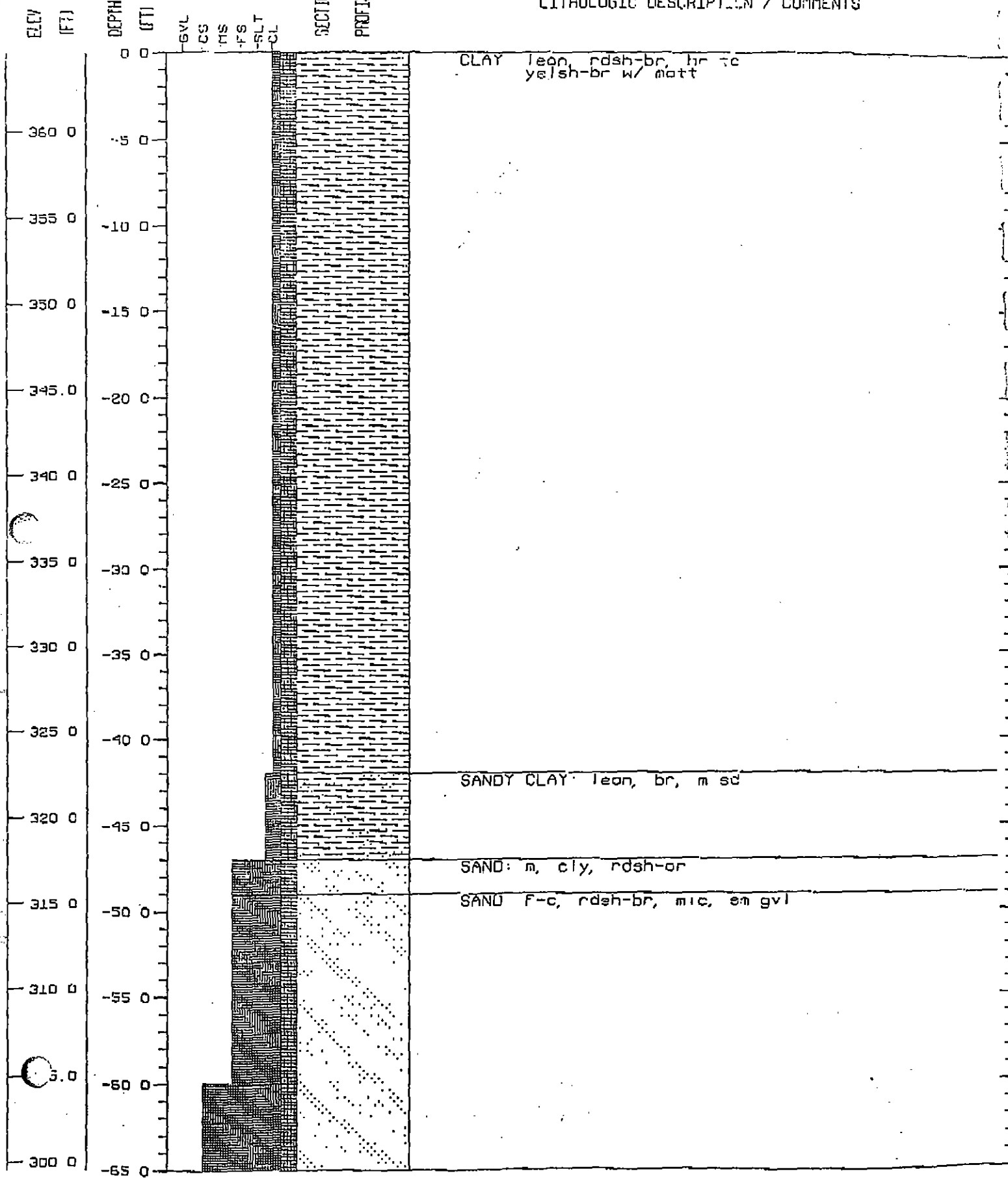


MW-201

364.5

GRAIN SIZE
POINT

LITHOLOGIC DESCRIPTION / COMMENTS



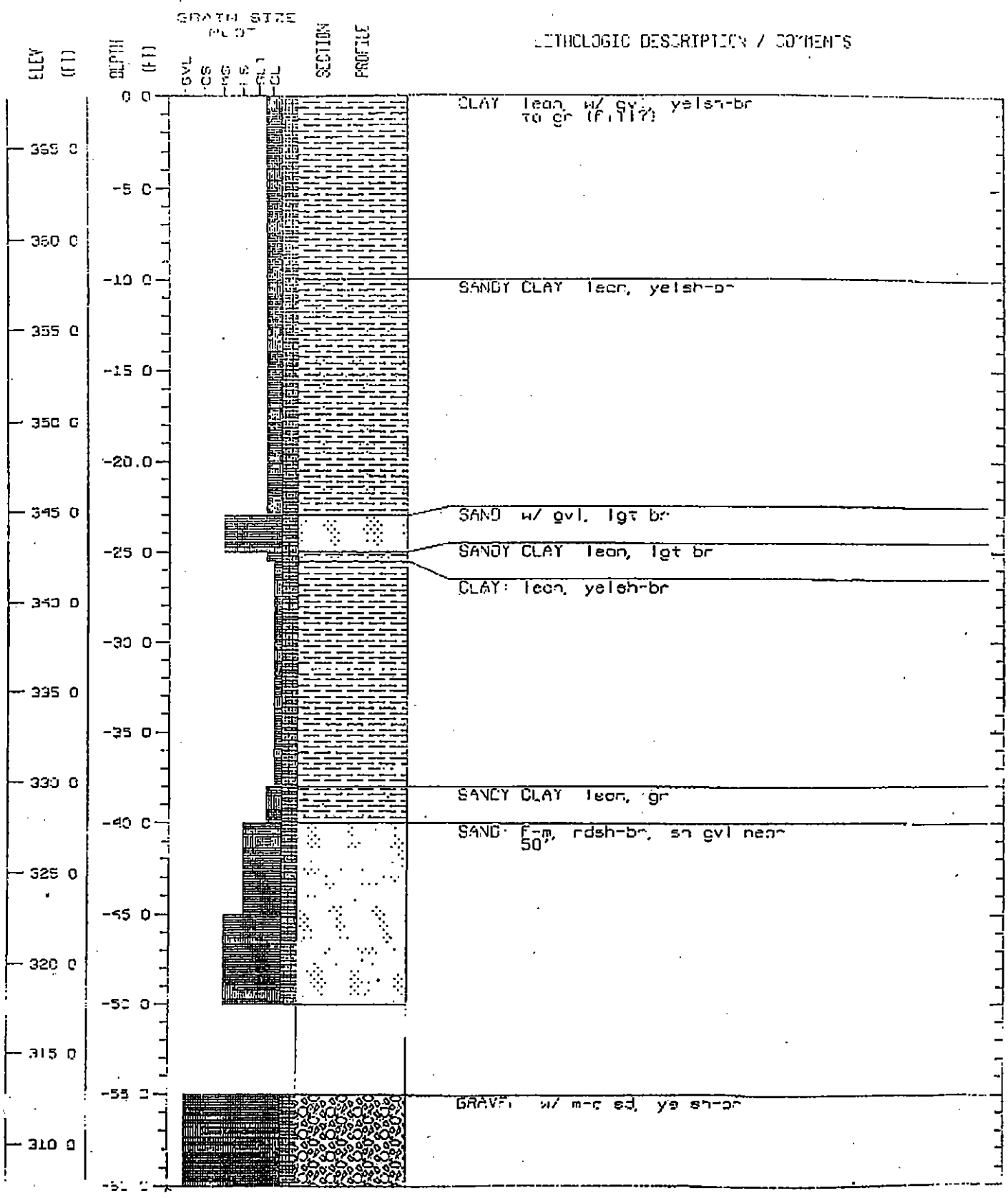
PGDP Boring P4-F08
 Land Surface = 371.95' AMSL

P4-F08

DEPTH (FEET)	GRAPHIC LOG	LITHOLOGY DESCRIPTION	GAMMA LOG
0		<u>Loess & U. Cont. Dep.</u> 0-49'	
50		<u>L. Cont. Dep.</u> 49-90'	
100	UPPER MBR	<u>McNairy Fm.</u> 90-337'	
150		<u>Sand:</u> 90-98' <u>Silt:</u> 98-112' <u>Sand & Silt:</u> 112-134'	
150	LEVINGS	<u>Clay:</u> 134-148', slty <u>Sand:</u> 148-159'	
200		<u>Silt:</u> 159-185', cly <u>Silt:</u> 185-215', sdy.	
250	LOWER MBR	<u>Clay & Sand:</u> 215-263', interbd	
300		<u>Silt:</u> 263-269' <u>Sand:</u> 269-337'	
350		<u>Rubble Zone:</u> 337-347' <u>Mississippian:</u> 347'-TD TD = 350'	

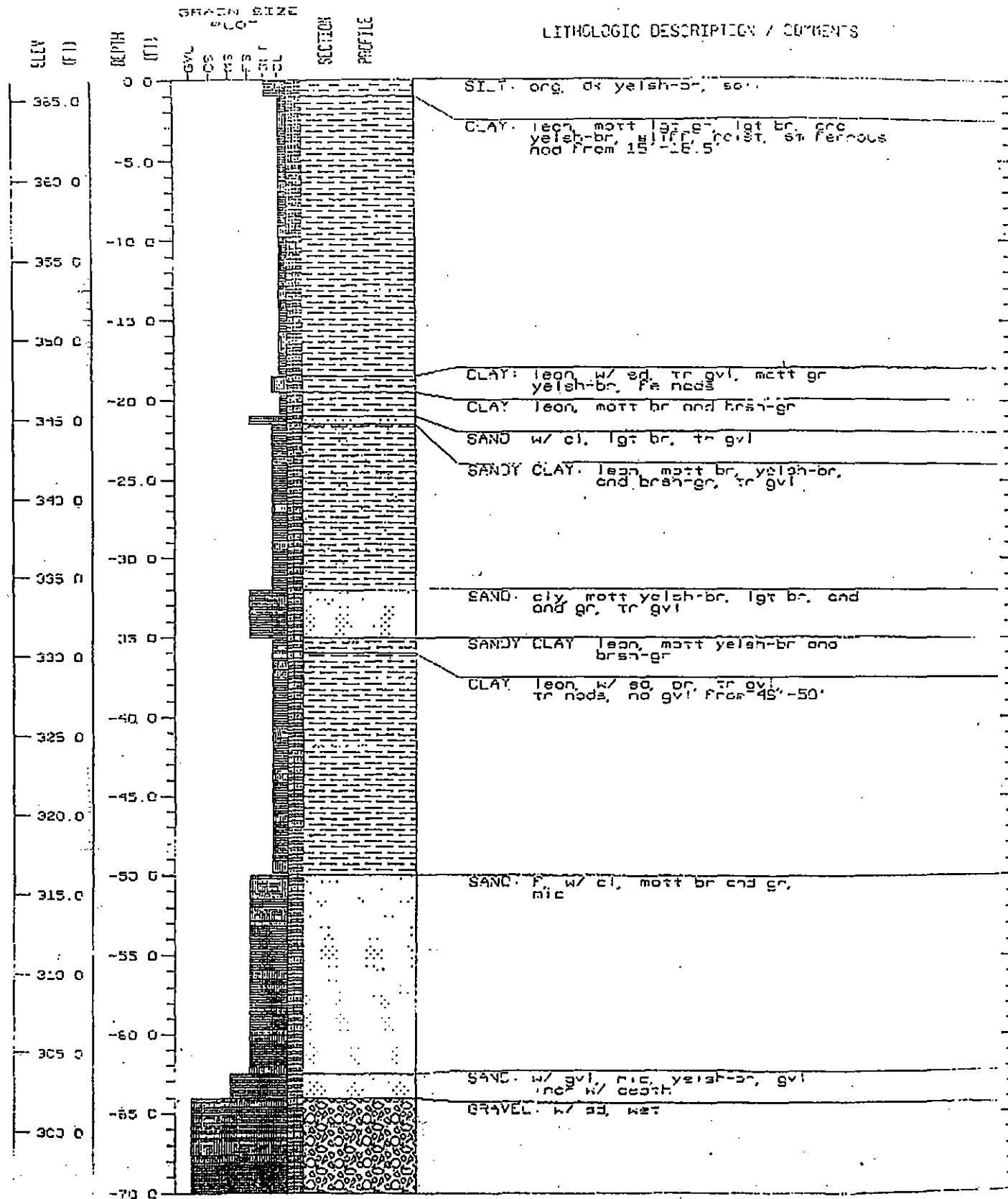
MW-181

367 8

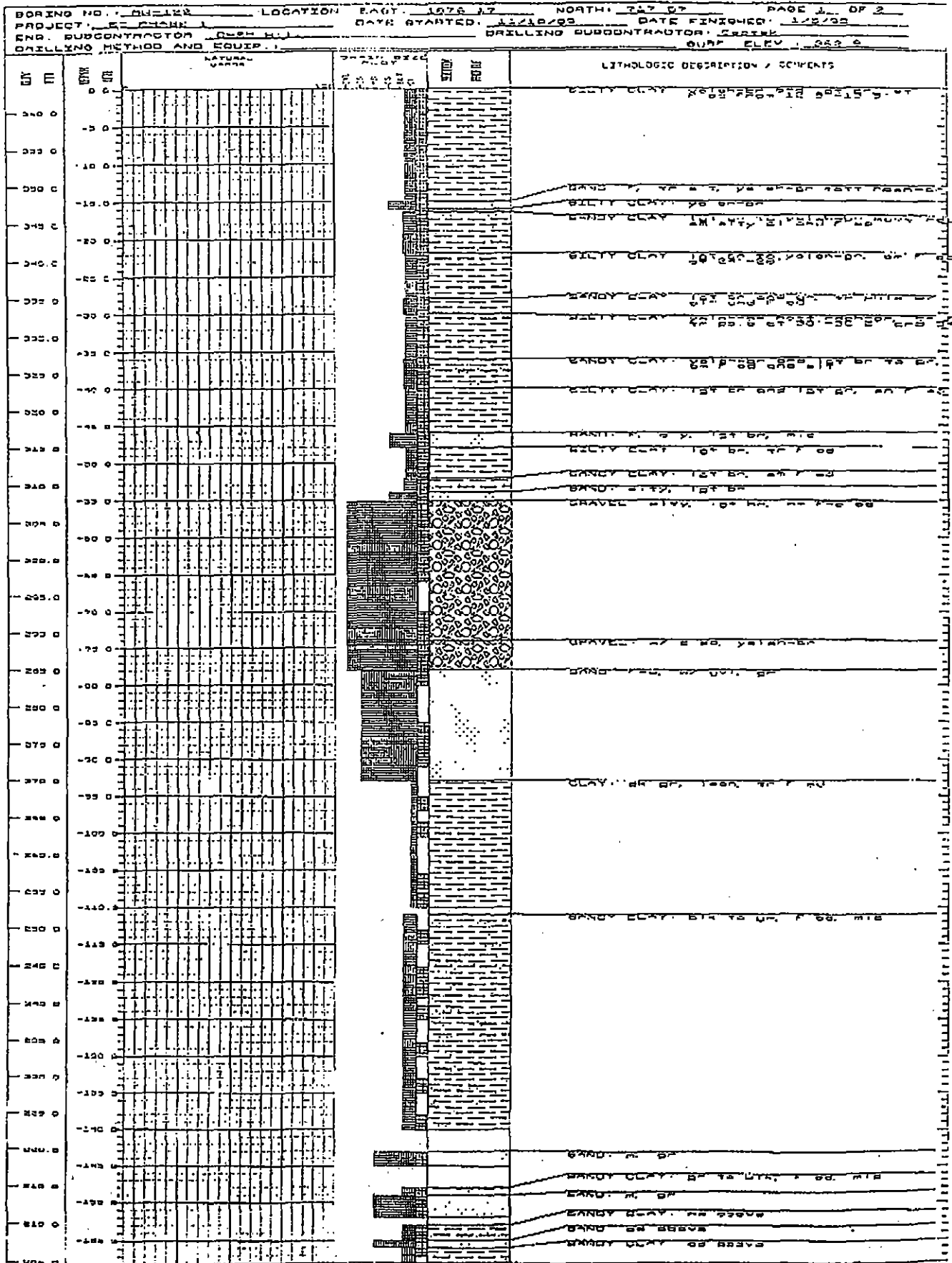


MW-193

366 2

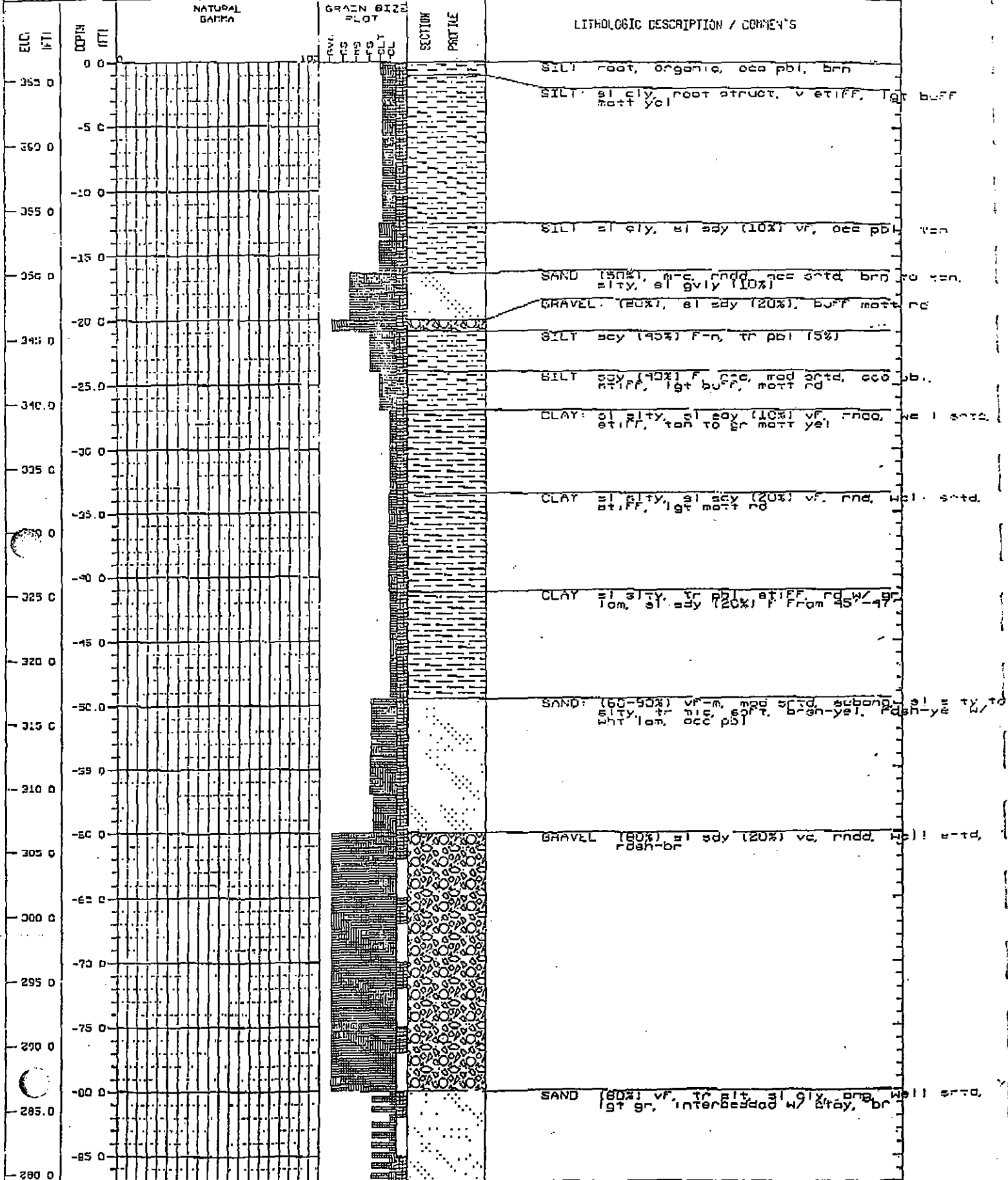


MW-122



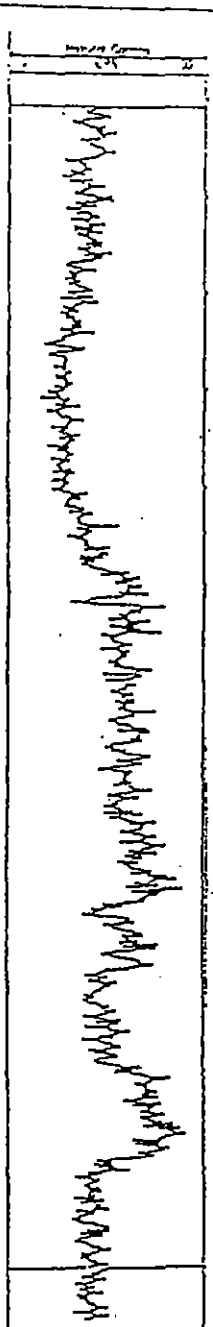
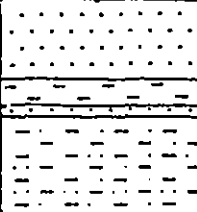
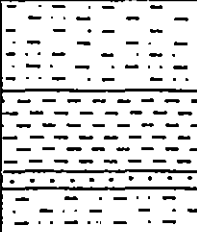
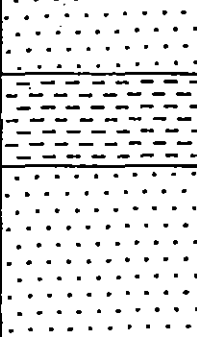
MW-106

BORING NO.: S-22 LOCATION: EAST -0437 7 NORTH: 990.6 PAGE 1 OF 2
 PROJECT: A2-023 GW Monitoring Probate STARTED: 10/29/91 DATE FINISHED: 10/31/91
 ENG. SUBCONTRACTOR: PGDP DRILLING SUBCONTRACTOR: Concrete Well Drilling
 DRILLING METHOD AND EQUIP.: CME-55 HSA to 60' and mud rotary to 95' SURF. ELEV.: 355.4



PGDP Boring Z16
Land Surface = 370.9' AMSL

Z16

DEPTH (FEET)	GRAPHIC LOG	LITHOLOGY DESCRIPTION	GAMMA LOG
0 - - - - - - 50		<u>Loess & U. Cont. Dep. 0-62'</u>	
- - - - - - 100		<u>L. Cont. Dep. 62-101'</u>	
150		<u>McNairy Fm. 101-322'</u> <u>Sand: 101-122'</u> <u>Silt: 122-129'</u> <u>Sand: 129-131', gvly</u> <u>Silt, Sand, & Clay: 131-162' gvly</u>	
200		<u>Silt, Sand, & Clay: 162-186'</u> <u>Clay & Silt: 186-207'</u> <u>Sand: 207-211'</u> <u>Silt & Clay: 211-224'</u>	
250 - - - - - - 300		<u>Sand: 224-248'</u> <u>Clay: 248-272'</u> <u>Sand: 272-322'</u>	
350 - - - - - -		<u>Mississippian : 322'-TD</u> TD = 356.5'	

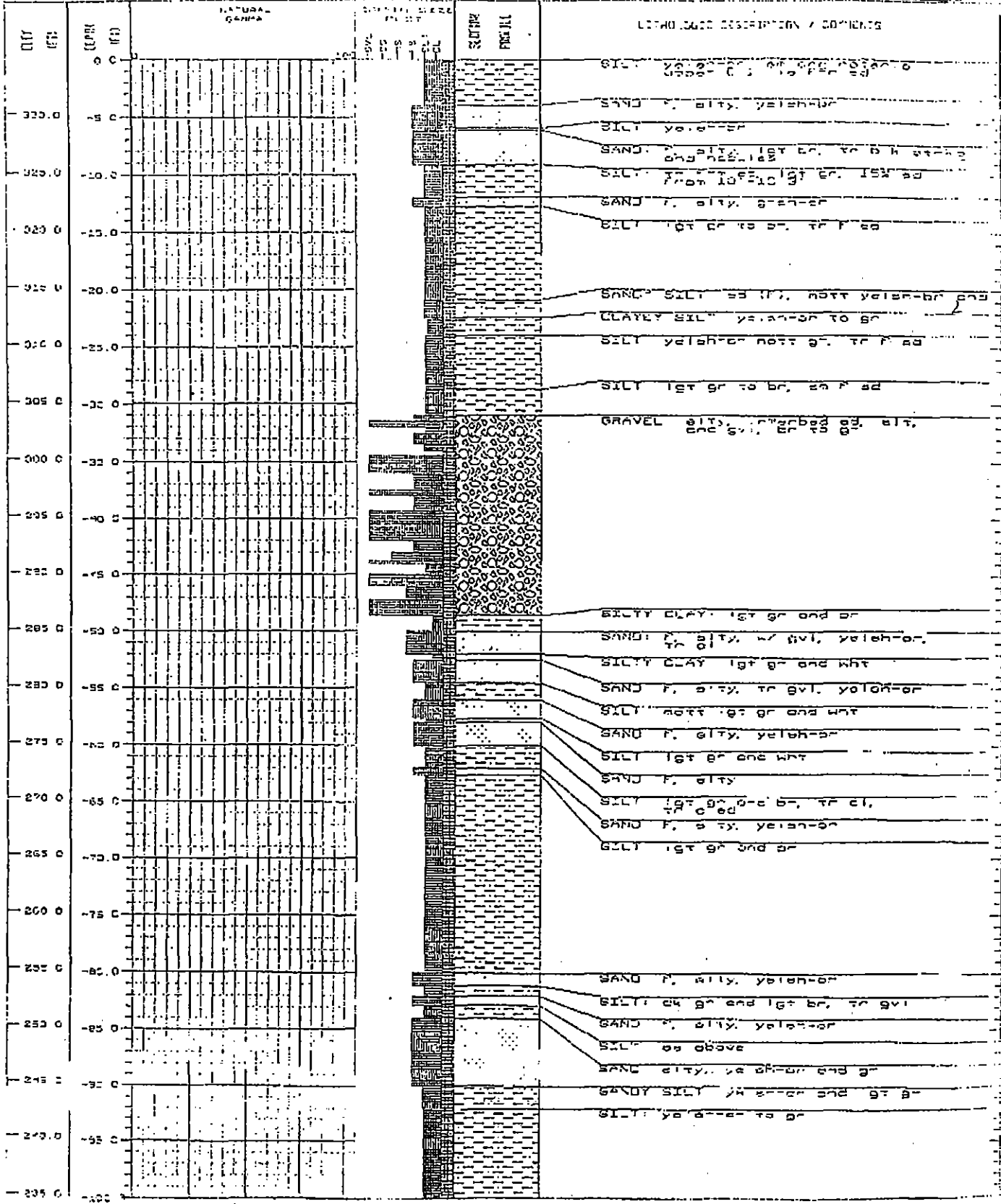
PGDP Boring Z12
Land Surface = 351.1' AMSL

Z12

DEPTH (FEET)	GRAPHIC LOG	LITHOLOGY DESCRIPTION	GAMMA LOG
0 50 100		<u>Loess & U. Cont. Dep. 0-75'</u> <u>L. Cont. Dep. 75-110'</u>	
150		<u>McNairy Fm. 110-333'</u> <u>Sand: 110-129'</u> <u>Silt: 129-140'</u>	
200		<u>Clay: 140-168'</u> <u>Sand: 168-175', gvy</u> <u>Silt: 175-229'</u>	
250		<u>Sand & Silt: 229-283'</u>	
300		<u>Sand: 283-333'</u>	
350		<u>Rubble Zone: 333-348'</u> <u>Mississippian : 348'-TD</u> <u>TD = 369'</u>	

MW-133

BORING NO. MW-133 LOCATION LAKE CHARLES 65 NORTH 51217 PAGE 1 OF 2
 PROJECT SE PHASE DATE STARTED 2/22/93 DATE FINISHED 2/22/93
 ENG. SUBCONTRACTOR CHEN M DRILLING SUBCONTRACTOR UNION
 DRILLING METHOD AND EQUIP. Aug 1 1993 USA SURF. ELEV. 334.7



MW-121

PGDP Well MW121

Land Surface = 372.43 ' AMSL

Drilled by Geotek Engineering in 1989-1990

DEPTH (FEET)	GRAPHIC LOG	LITHOLOGY DESCRIPTION
0		<u>Loess & U. Cont. Dep.</u> 0-52'
50		<u>L. Cont. Dep.</u> 52-88'
100	UPPER MBIR	<u>McNairy Em.</u> 88'-TD Clay: 88-95.5' grysh-pink, intrbd w/ sd. 95.5-110' slty, mic, yellsh-brn Sand: 110-115' cly, yllsh-brn 115-130' well sort, w/slt, yellsh-brn-gry. 130-135' intrbd w/cl
150		<u>Silt:</u> 135-165' olv blk, w/thin sd lens 165-170' intrbd w/f sd, wht 170-200.5' olv blk w/thin sd lens
200	LEVINGS	<u>Sand:</u> 200.5'-TD vf, well sort, slty, lt gry TD = 211.5'

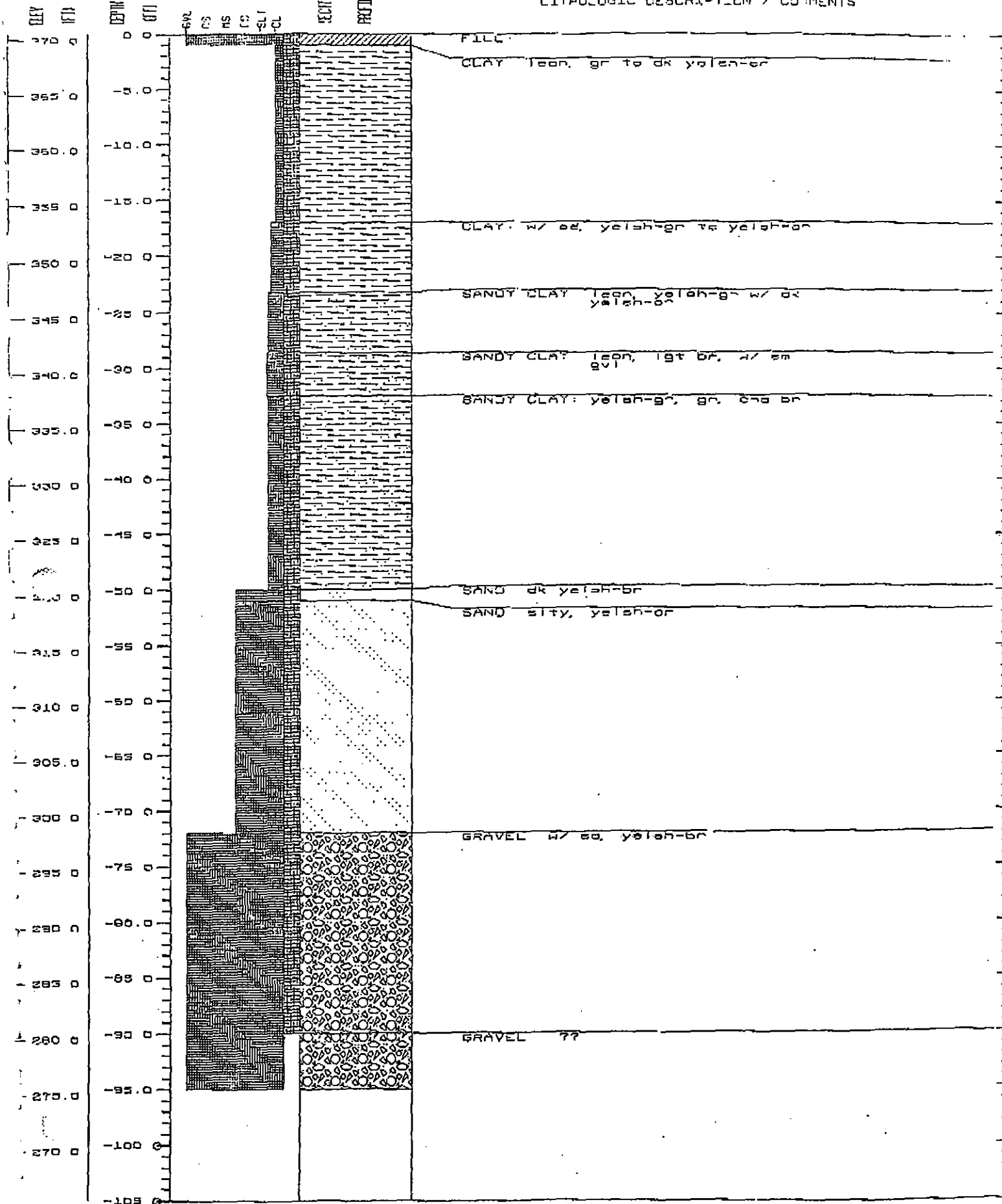
MW-202

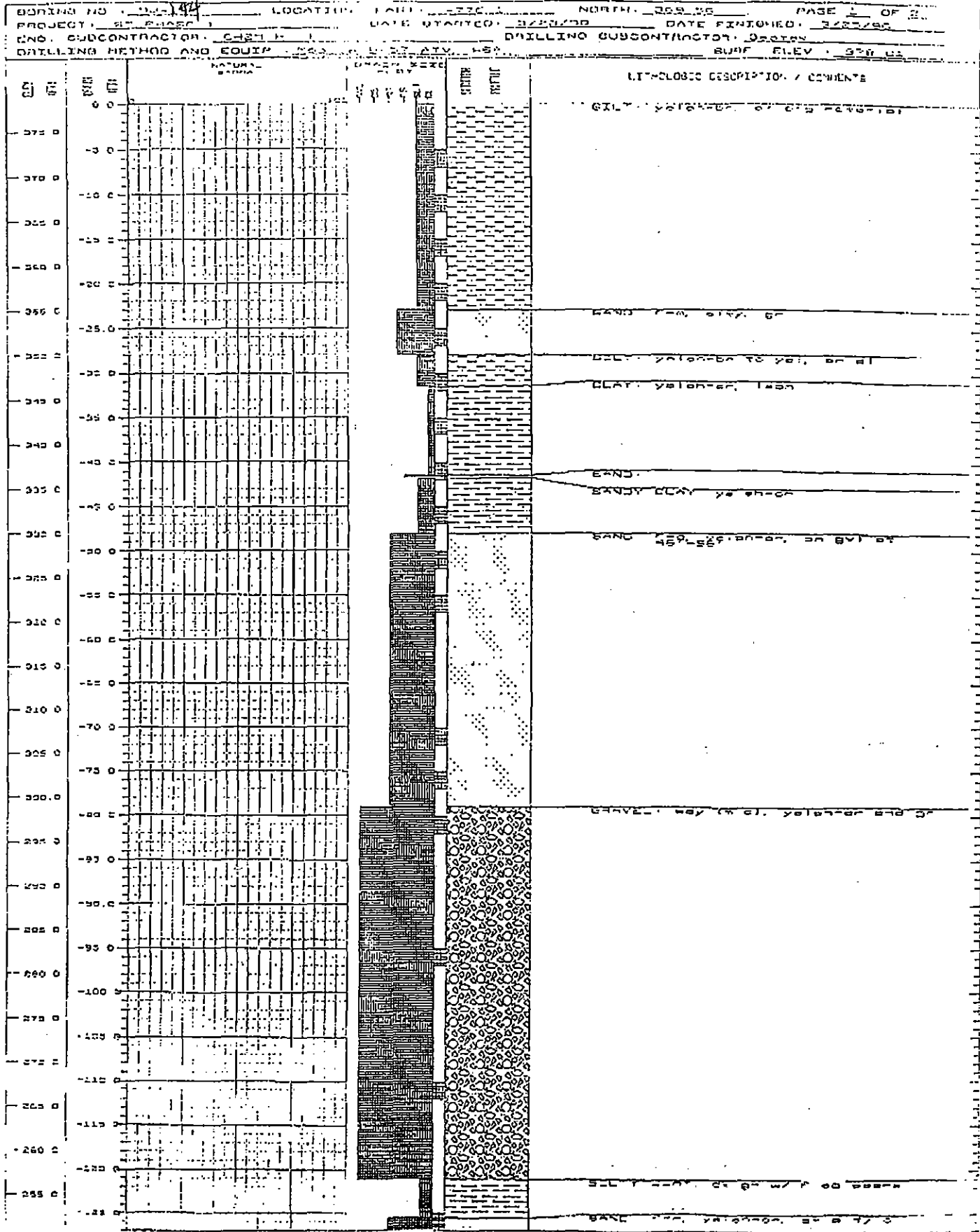
370 0

GR
S
LS
MS
CS
CL

SECTION
PART

LITHOLOGIC DESCRIPTION / COMMENTS





Appendix F

GLOSSARY OF GEOPHYSICAL TERMS

Glossary

(from Sheriff, 1973; Sheriff and Geldart, 1982)

common-depth-point (CDP): having the same midpoint between source and detector.

Also called common-midpoint or common-reflection-point.

common-depth-point stack: a sum of the traces corresponding to the same midpoint. The traces from different profiles having different offset distances are gathered together, corrected for statics and normal moveout, and then summed (or stacked). The objective is to attenuate random effects and events whose dependence on offset is different from that of primary reflections.

filter: A part of a system that discriminates against some of the information entering it. Band pass filters are often specified by listing their low-cut and high-cut component filters. Filter characteristics are often specified by the frequencies at which the amplitude is down by 3 dB (70 percent or half power) and by the slope of the cutoff.

f-k plot: A frequency-wavenumber plot, which displays how data sort into distinguishable sets in the frequency-wavenumber domain. The energy density within a given time interval is usually contoured. Used to examine the direction and apparent velocity of seismic waves.

normal moveout: Differences in the arrival time of reflections because of the distance between source and receiver.

velocity analysis: Calculation of stacking or NMO velocity from measurements of normal moveout. In current usage, generally involves common-midpoint data but includes also $T-\Delta T$ analysis and X^2-T^2 analysis. Most analysis schemes assume a normal moveout, measure the coherency at that normal moveout, and then vary the normal moveout in order to maximize the coherency. The stacking velocity value depends somewhat on the amount of data included in the analysis, that is, on the range of offsets and locations analyzed. Where all reflectors are horizontal and where velocity varies only with depth, the stacking velocity is approximately the rms velocity.

stack: A composite record made by combining traces from different records. Stacking involves filtering because of timing errors or waveshape differences among the elements being stacked.

stacking velocity: Velocity calculated from normal-moveout measurements and a constant-velocity model. Used to maximize events in common-midpoint stacking. Sometimes erroneously called "rms velocity". Usually calculated for the best-fit hyperbola to gather data, the value thus depending somewhat on the range of offsets involved. Fitting an NMO equation to CDP data is equivalent to assuming an ellipsoidal wavefront, yielding the stacking velocity of the horizontal component.

